INFORMATION TO USERS

This manuscript has been reproduced from the microfilm master. UMI films the text directly from the original or copy submitted. Thus, some thesis and dissertation copies are in typewriter face, while others may be from any type of computer printer.

The quality of this reproduction is dependent upon the quality of the copy submitted. Broken or indistinct print, colored or poor quality illustrations and photographs, print bleedthrough, substandard margins, and improper alignment can adversely affect reproduction.

In the unlikely event that the author did not send UMI a complete manuscript and there are missing pages, these will be noted. Also, if unauthorized copyright material had to be removed, a note will indicate the deletion.

Oversize materials (e.g., maps, drawings, charts) are reproduced by sectioning the original, beginning at the upper left-hand corner and continuing from left to right in equal sections with small overlaps. Each original is also photographed in one exposure and is included in reduced form at the back of the book.

Photographs included in the original manuscript have been reproduced xerographically in this copy. Higher quality 6" x 9" black and white photographic prints are available for any photographs or illustrations appearing in this copy for an additional charge. Contact UMI directly to order.

UMI

A Bell & Howell Information Company
300 North Zeeb Road, Ann Arbor MI 48106-1346 USA
313/761-4700 800/521-0600

THE BEHAVIOUR OF STEEL-FREE CONCRETE BRIDGE DECK SLABS UNDER STATIC LOADING CONDITIONS

by

John Patrick Newhook

A Thesis Submitted to the
Faculty of Engineering
in Partial Fulfilment of the Requirements
for the Degree of

DOCTOR OF PHILOSOPHY

Major Subject: Civil Engineering

APPROVED:

[redacted]
Dr. Aftab A. Mufti, Supervisor

[redacted]
Dr. Leslie G. Jaeger

[redacted]
Dr. Alex Kalamkarov

[redacted]
Dr. Alan Watson, External Examiner

TECHNICAL UNIVERSITY OF NOVA SCOTIA

Halifax, Nova Scotia 1997

TECHNICAL UNIVERSITY OF NOVA SCOTIA

"AUTHORITY TO DISTRIBUTE MANUSCRIPT THESIS"

TITLE:

THE BEHAVIOUR OF STEEL-FREE CONCRETE BRIDGE DECK SLABS UNDER STATIC LOADING CONDITIONS

The above library may make available or authorize another library to make available individual photo/microfilm copies of this thesis without restrictions.

Full Name of Author: John Patrick Newhook

Signature of Author: [redacted]

Date: Feb/15/97

TABLE OF CONTENTS

LIST OF TABLES

LIST OF FIGURES

LIST OF SYMBOLS AND ABBREVIATIONS

CHBDC	Canadian Highway Bridge Design Code
TUNS	Technical University of Nova Scotia
OHBDC	Ontario Highway Bridge Design Code
FRC	Fibre Reinforced Concrete
CSA	Canadian Standards Association
ACI	American Concrete Institute
BS	British Standard

f'_c	concrete compressive strength (MPa)
P	load (kN)
d	depth of concrete slab (mm)
b_0	perimeter of shear area (mm)
ρ	density of concrete reinforcement
c	punch shear formula
u	punch shear formula
f_{cu}	punch shear formula
f_{ck}	punch shear formula
λ	density of concrete (kg/m^3)
ϕ_c	materialresistance factor for concrete
C	outer diameter of idealized concrete crack pattern (mm)
B	diameter of idealized load area (mm)
c_1	base of conical shell (mm)
c_2	depth of compressive stress block (mm)
α	angle of shear crack
Δ	deflection of deck (mm)
ψ	angle of rotation of wedge
Δ_L	lateral deflection (mm)

y	location of neutral axis or centre of rotation of wedges (mm)
V	vertical load at support of wedge (kN)
T	oblique compressive force (kN)
T_h	horizontal component of T (kN)
T_v	vertical component of T (kN)
K	lateral restraint stiffness per length of slab (N/mm/mm)
F	lateral restraining force per length of slab (kN/m)
F_w	lateral restraining force on a wedge (kN)
E_s	modulus of elasticity of steel (MPa)
E_c	modulus of elasticity of concrete (Mpa)
A_s	area of steel strap (mm^2)
A_c	area of concrete (mm^2)
δ	deflection (mm)
ϵ	strain
ϵ_{ct}	circumferential strain
ϵ_s	strain in steel straps
ϵ_y	yield strain of steel
r	radius (mm)
z	distance above center of rotation (mm)
R	circumferential compressive force (kN/m)
R_r	circumferential compressive force acting on a wedge component (kN)
σ_{cty}	circumferential stress at y from edge of load (MPa)
σ_r	radial concrete stress (Mpa)
σ_z	vertical concrete stress (MPa)
σ_θ	circumferential concrete stress (MPa)
σ_1	major principle stress (MPa)
σ_2	intermediate principle stress (MPa)
σ_3	minor principle stress (MPa)
σ_{cube}	compressive strength of concrete cube (Mpa)

W	force variable (kN)
β_1	concrete stress block variable
A_p	tire print area (mm^2)
k	concrete confinement constant
a	constant for equation (40)
b	constant for equation (40)
S_s	spacing of straps (mm)
S_g	spacing of girders (mm)
S_l	effective length of straps (mm)
K'	spring constant for a strap (N/mm)
I	moment of inertia (mm^4)
S_w	spacing of wheel loads (mm)
P_u	punching failure load (kN)
P'_u	total punching failure for multiple wheel loads (kN)
t	thickness of slab (mm)
t_s	projection of shear connectors into the deck slab (mm)
t_e	effective thickness of slab (mm)
t_h	height of haunch (mm)
L_u	unsupported length of edge beam (mm)
F_c	strength of strap connection (kN)
f_y	yield stress of straps (MPa)
k_g	lateral restraint reduction factor for support system stiffness

ACKNOWLEDGEMENTS

The author wishes to express sincere gratitude to both Dr. Aftab A. Mufti and Dr. Leslie G. Jaeger for their professional encouragement, technical guidance and personal friendship throughout this endeavour. The author also expresses appreciation to Dr. Baidar Bakht and Dr. Gamil Tadros for their valued technical input.

The laboratory assistance of Mr. Richard Sarty and Mr. Blair Nickerson is thankfully acknowledged.

The author gratefully acknowledges the funding which made this possible. Student and project funding was received from the following sources: Natural Sciences and Engineering Research Council of Canada, Vaughan Engineering Associates Limited, ISIS Canada Network of Centres of Excellence, and the Technical University of Nova Scotia.

ABSTRACT

It has been successfully demonstrated that the removal of all internal reinforcing steel from the deck slab of concrete slab on steel girder bridges is possible. The internal steel reinforcement is not replaced with another synthetic or non-ferrous reinforcement; but, rather the whole bridge deck structural system is modified with the addition of external steel straps. Such a system is now being referred to as a steel-free concrete bridge deck system. Experimental testing has demonstrated the feasibility of the concept and the substantial ultimate load capacity of the system. A highway bridge utilizing this technology has been in operation since December, 1995. This thesis examines in detail the behaviour of the steel-free concrete bridge deck system under static load conditions. A rational model is developed which reliably predicts the behaviour of the system. Verification of the model is demonstrated through analysis of previous experimental works. An experimental program is undertaken to access many of the serviceability and ultimate load characteristics of the system. Using the rational model, a parametric study is undertaken to establish the effect of the various key geometric and material parameters on the behaviour of the system. Finally, design recommendation are presented and discussed in light of the findings of this thesis as well as the current draft recommendations of the new Canadian Highway Bridge Design Code.

1 INTRODUCTION

1.1 General

It has been successfully demonstrated that the removal of all internal reinforcing steel from the deck slab of concrete slab on steel girder bridges is possible. The internal steel reinforcement is not replaced with another synthetic or non-ferrous reinforcement; but, rather the whole bridge deck system is modified with a system of external steel straps. Such a system is now being referred to as a steel-free bridge deck system. Previous experimental testing has demonstrated the feasibility of the concept and the substantial ultimate load capacity of the system.

The thesis undertook to investigate in detail the fundamental behaviour of the steel-free bridge deck system. A theoretical model for predicting the behaviour and the ultimate load capacity is developed. The model is verified using the results of previous experimental tests. A series of tests were conducted to experimentally investigate a number of behavioural characteristics. The experimentation was also used to verify the design safety of the first steel-free bridge deck constructed in the field. The key parameters which influence the performance of the system were identified and the relative sensitivity of behaviour to changes in these parameters were determined using the theoretical model. Finally, design guidelines are presented based on the current state-of-the-art of steel-free bridge decks.

The thesis undertook to investigate the structural behaviour of the system under static loading only. Response of the structure to cyclic, dynamic and impact loadings is beyond the scope of this work. As well, the fatigue performance of the system and material durability of the concrete is not included. The experimental work is limited to simple span structures; however, the theoretical work is applicable to both simple and continuous spans.

1.2 Steel-Free Deck Concept

1.2.1 History

Originally concrete bridge deck slabs were designed as reinforced concrete with the level of reinforcement determined from assumptions of flexural bending and failure. The slab was assumed to be a transverse bending member between a series of supporting girders. This method, commonly called the flexural design method, led to high levels of steel reinforcement in the slab. Continuing research revealed that the mode of failure of bridge decks was not flexure. In fact, deck slabs failed at concentrated load values that were several times higher than predicted by flexural theory. It was determined that compressive membrane forces, sometimes referred to as internal arching forces, were being developed within the slabs and leading to a punching failure mode. These membrane forces gave the bridge deck substantial reserve capacity beyond its flexural design capacity. By taking advantage of this arching behaviour, a substantial reduction in the amount of reinforcing steel required can be realized. Empirically it was shown that for many situations 0.3% reinforcing steel in each direction, in a top and bottom layer, was sufficient. In 1979, the Ontario Highway Bridge Design Code (OHBDC) was developed which included design provisions for this empirical method. Bakht and Markovic (1985) provide a state-of-the art report on the research that led up to this code development.

In 1988, researchers at the Technical University of Nova Scotia began further investigations into the punching failure of concrete deck slabs. Mufti et al. (1993) demonstrated that the entire removal of all internal steel reinforcement from a concrete slab on girder bridge deck was possible. The key to the system was to provide adequate transverse lateral restraint such that sufficient compressive membrane forces could be developed and the deck failed in punching. This lateral restraint was provided by transverse steel straps, external to the deck slab, which tied adjacent girders together. Recently, this concept has led to the construction of the world's first steel-free concrete bridge deck over Salmon River on the Trans-Canada Highway in Nova Scotia.

1.2.2 Steel-Free Bridge Deck Concept

To understand the behaviour that led to the development of the steel-free bridge deck technology we consider a section of bridge deck shown in Figure 1.1. The concrete deck is made composite with the steel girders through the use of shear connectors. If a concentrated load is applied directly between two girders, the concrete deck will deform and stresses will develop according to flexural theory. Ideally, the highest tensile stresses will develop in the bottom of the slab directly under the load point and in the top of the slab directly over the centerline of each girder. The applied load will eventually reach a magnitude where the tensile stresses will cause the concrete to crack in these zones. If the slab has no internal reinforcement to carry these tensile forces after cracking, and the girders are not sufficiently stiff in the transverse direction, the deck will fail in flexure. It is observed that the top flanges of the girders displace outward, moving away from the point of load application. If transverse steel straps are welded to the top flanges of adjacent girders, as shown in Figure 1.2, then this outward displacement is prevented. The steel straps develop tensile stresses and provide a lateral restraining force to the concrete deck. In turn, compressive membrane forces develop within the deck slab. After cracking of the concrete has occurred, these forces enable the slab to sustain loads through arching action even though it has no remaining flexural capacity. The degree of lateral restraint provided will determine the ultimate load at which the deck fails in punching. This load value can be several times greater than both the load which causes flexural cracking of the deck and the failure load of a reinforced concrete deck.

An isometric view of the steel-free concrete bridge deck system is shown in Figure 1.3. The transverse steel straps are spaced at regular interval, typically 1000 to 1200 mm. The girders, the straps and the deck act as one structural system; therefore, proper connection of the straps is important. Force transfer between all three elements must be possible for the system to function as described. Typically the strap is welded to the top flange of the girder and the

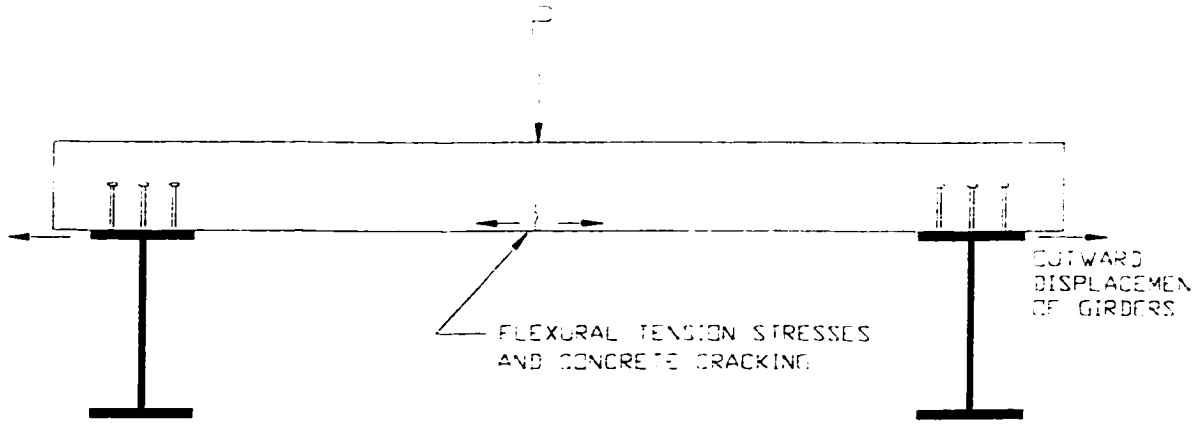

Figure 1.1 Cross-section of a typical bridge deck slab in flexure

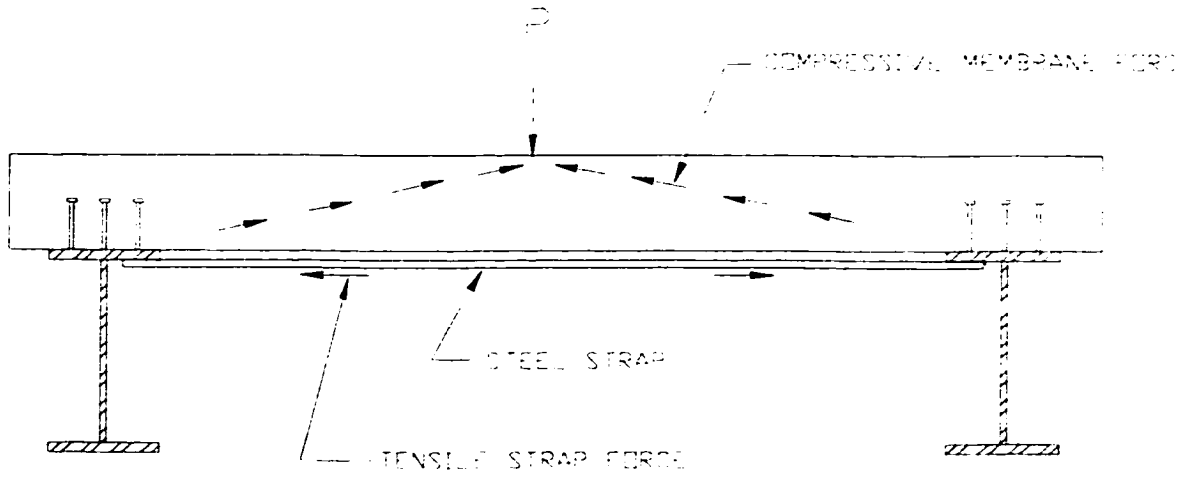

Figure 1.2 Cross-section of a steel-free bridge deck slab

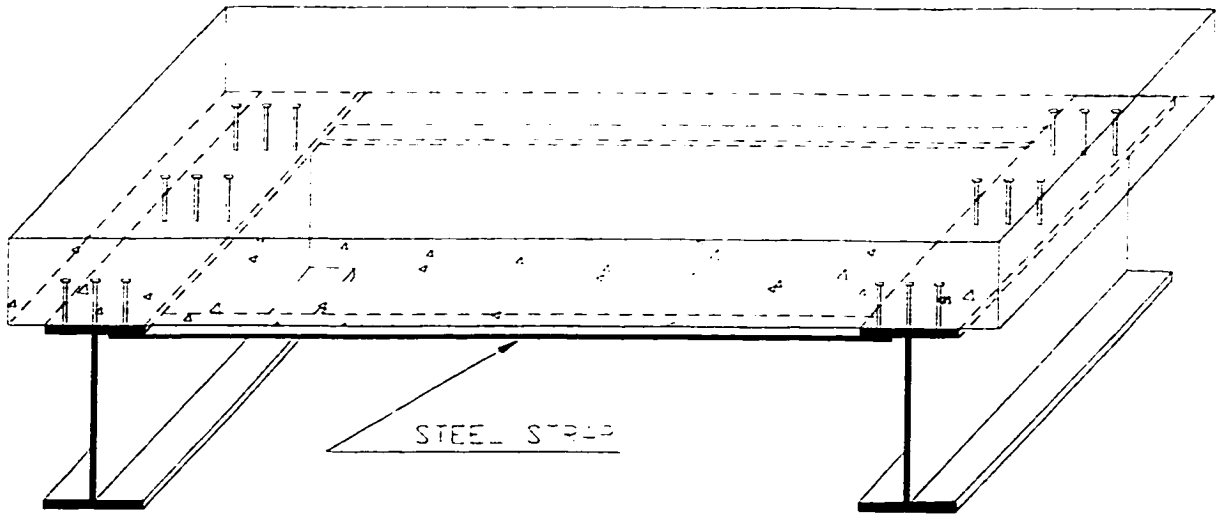

Figure 1.3 Isometric view of steel-free bridge deck slab system

concrete slab is connected to the girders through shear connectors. This detail has performed well; however, Bakht et al. (1996) present a number of alternate straps connection designs which do not have the same fatigue stress limitations as welded connections.

Concrete itself is a brittle material and cracks under low tensile stresses. Two common sources of these tensile stresses in bridge decks, other than stresses from vehicle loads, are the plastic shrinkage of concrete during curing and the thermal expansion/contraction of concrete due to environmental conditions. Plain concrete without any reinforcing steel is especially susceptible to these effects. In the steel-free deck low modulus polypropylene fibres are added to act as a plastic crack control device and to provide some post-crack ductility to the hardened concrete slab. It should be noted that the fibres are secondary reinforcement and do not enhance the strength properties of the concrete.

The reinforcing steel, not being necessary as a primary structural element nor as a secondary crack control element, is removed. The system shown in Figure 1.3 is known as a *steel-free concrete bridge deck*; or in other references as a *fibre reinforced concrete (FRC) bridge deck*, due to the use of fibres in the concrete.

1.2.3 Significance and Benefits of Technology

In North America, most bridge infrastructure is deteriorated or undergoing rapid deterioration. Several studies have produced the following statistics:

- "... in the province of Alberta alone, there are over 500 bridges that will require some sort of rehabilitation" (Alexander and Cheng, 1996)
- More than 200,000 bridges in the United States are structurally or functionally deficient with an estimated repair cost of US $90 billion (Dunker and Rabbit, 1993).
- In the province of Ontario the estimated cost of bridge deck repair and replacement from 1993 to 2003 is over $60 million (Bickley et al., 1993).

While many of these structures are suffering because they are reaching the end of their design life, a significant number of structures are showing premature deterioration due to corrosion of reinforcing steel, particularly in concrete bridge decks. In eastern and north-eastern North America, the corrosion problem is made worse by the heavy use of de-icing salts during winter months. Damage has reached a point where the cost of maintenance and repair is far exceeding the original cost of construction. Attempts have been made to alleviate the problem of corroding reinforcement through the use of increased concrete cover, waterproofing membranes and epoxy-coated rebar. These solutions have been only moderately successful, even in Ontario where the OHBDC empirical method allows for a substantial reduction in the amount of reinforcing steel used, the problem still exists.

The steel-free concrete bridge deck allows for the removal of all reinforcing steel and thereby removes the source of the corrosion entirely. The durability of the deck is increased and the operation and maintenance cost is substantially reduced. It is predicted that the service life span of the deck will increase. In addition, the real costs of traffic delays and re-routing during repairs will also be reduced. The chief benefit of the steel-free deck is reduced long-term infrastructure costs.

The technology does have two other significant benefits. Firstly, with further optimization it can be shown that the steel-free deck will be cheaper than reinforced concrete decks based on capital cost considerations (Newhook and Mufti, 1996). Secondly, the technology leads to a better understanding of bridge deck behaviour in general.

1.3 Previous Research on Steel-Free Bridge Deck Technology

Work on the steel-free concrete bridge deck began in 1988 with pioneering credit belonging to Dr. Aftab A. Mufti of the Technical University of Nova Scotia, Dr. Leslie G. Jaeger of Vaughan International Consultants and Dr. Baidar Bakht of the Ministry of Transportation of Ontario. Numerous publications have been produced either jointly or separately by these individuals but only the key works will be referenced here. Mufti et al. (1993) first reported the work on four half-scale bridge deck models which demonstrated that the concept was possible. The test setups had two and three girders spaced 1000 mm apart with a 100 mm thick fibre reinforced concrete deck. The successful test models had transverse steel straps 64 x 10 mm in cross-section welded to the top flanges of the girders at a spacing of 457 mm. The fibre was a low modulus polypropylene fibre added to the concrete at 0.88% volume fraction. The girders and the deck were made composite by shear connectors. These test decks failed in punching shear. While further research has led to optimization and investigation of new parameters, the fundamental system of the steel-free bridge deck has remained unchanged from this original work.

While the work of Mufti et al. (1993) demonstrated the concept for rectangular bridge decks, Bakht and Agarwal (1993) demonstrated that the concept is also valid for skewed bridge decks. To complement the experimental work, Wegner (1992) undertook a non-linear finite element analysis approach to developing a theoretical design tool for this system. Wegner and Mufti (1994a) report some success with the method, particularly in guiding further experimental work; however, the finite element model was found to be too cumbersome and sensitive to modelling parameters to be of practical use in design. Wegner and Mufti (1994b)

also proposed that a rational model developed for reinforced concrete slabs by Kinnunen and Nylander (1960) may be able to be adapted to the steel-free bridge deck system. A thorough investigation of this model was undertaken in this thesis.

Additional experimental work on a fifth half-scale model tested at TUNS is reported in Newhook et al. (1995). The fifth half-scale model was important in providing direction for further work in five key areas. Firstly, it demonstrated that the concept of an edge beam (Mufti et al., 1993) at the free edge of a slab promoted punching failure in this region of the slab. Secondly, it demonstrated that changing the spacing of the transverse steel straps altered the failure load. Thirdly, it indicated that the diaphragms between girders did not have a significant effect on the restraint stiffness. Fourthly, it indicated that the proximity of the straps to the point of load application and the location of the load relative to the girder span has an effect on restraint stiffness and failure loads. Finally, it indicated that a reduction in the thickness of the concrete deck was possible.

Thorburn and Mufti (1995) reported research on the optimization of the system. Their experimental work demonstrated that a reduction in deck thickness to 175 mm on a 2000 mm girder spacing was possible. This represents a depth to span ratio of 11.4 which is an increase from the previous ratio of 10. They also demonstrated that a reduction in the amount of steel in the straps to 0.37% of the deck cross-sectional area was possible. Thorburn and Newhook collaborated in a joint test (Thorburn and Mufti, 1995 and Newhook and Mufti, 1995) to demonstrated a simple repair technique for the steel-free deck.

In a complementary investigation, Mahue and Bakht (1995) developed a design detail for a concrete barrier wall which could be safely connected to a steel-free deck. As well, Selvedurai and Bakht (1995) performed tests to verify the performance of the steel-free deck under millions of cycles of moving wheel loads. Finally, Bakht et al. (1996) report on alternative strap connection details and strap configurations for the system.

1.4 Original Work of This Author

1.4.1 Rational Model

As indicated above, Wegner and Mufti (1994b) proposed using the work of Kinnunen and Nylander (1960) to develop a rational model for the steel-free concrete bridge deck. Some initial work was performed by Wegner (1993) which demonstrated the feasibility of this approach. In this thesis a thorough investigation of the rational model was undertaken and several improvements to the model were developed. The significant contributions of this author to the rational model are categorized into five items.

1. As will be demonstrated in a later section, the concrete surrounding the point of load application is in a state of three-dimensional compressive stress. Characterizing the behaviour of the concrete in this zone is of key importance. Wegner (1993) used a three-dimensional concrete failure criteria employed by ADINA (Wegner, 1993), a non-linear finite element analysis package. In this thesis, a confinement relationship similar to Richart's (Demers and Neale, 1994) relationship for confined concrete cylinders was employed. In addition, it was determined that a new empirical constant was necessary to describe the confinement conditions in a deck slab as opposed to a concrete cylinder.

2. A fundamental component of the steel-free deck is the lateral restraint which leads to development of the internal arching forces. An experimental and theoretical study was undertaken to develop a method for determining the lateral restraint value to be used in the rational model. The method is able to account for the restraint stiffness provided by both the straps and the girders as well as the variation in restraint stiffness due to the proximity of the individual straps to the applied load.

3. The original model proposed by Wegner (1993) employed only one punching failure criterion that being a failure associated with the attainment of a critical strain value

in the deck slab. This work demonstrated that it is necessary to include a second failure criterion associated with the yielding of the steel straps.

4. Whereas Wegner (1993) used only one experimental model to test his rational model, this work includes experimental verification with all experimental models previously tested. In addition, parameters other than ultimate load comparisons are investigated.

5. While the rational model was developed for steel-free concrete bridge decks, the model is also applied to reinforced concrete bridge decks. Two experimental models are analysed and show favourable comparisons.

1.4.2 Experimental Work

The main experimental work of this thesis was performed on a full-scale model of a bridge deck built in the Heavy Structures Laboratory of TUNS. Testing was performed on the steel frame before the addition of the concrete deck slab and on the completed system with the concrete deck cast in place. A series of tests were performed to investigate parameters which had previously not been studied. The following is a list of the original aspects of this testing program:

- Testing a deck span to thickness ratio of 13.5
- Testing the effect of concrete haunches over the girders
- Testing a strap spacing of 1200 mm
- Testing the capacity of the system in a deteriorated condition
- Testing the effects of multiple wheel loads
- Testing the effects of diaphragms on restraint stiffness
- Testing the lateral restraint stiffness of the straps and girders
- Investigating service load behaviour
- Investigating load sharing between girders
- Investigating composite section behaviour

1.4.3 Parametric Investigations

A parametric investigation was undertaken using the rational model to assess the effects of the various key parameters on the failure load of the steel-free deck. The parameters are ranked according to the level of influence and a summary of the influence of each parameter is presented.

1.4.4 Field Application

The author had the distinct privilege of collaborating with Dr. Aftab A. Mufti, Dr. Leslie G. Jaeger, Dr. Baidar Bakht and Dr. Gamil Tadros in the design of the world's first highway bridge using the steel-free concrete bridge deck technology (Newhook et al. , 1996). The structure is located on the Trans-Canada Highway 104 over the Salmon River near Kemptown, Nova Scotia. The full-scale model tested at TUNS is based on the Salmon River Bridge design. The design of the structure is the original work of the five person design team and the experimental work of this thesis serves as verification of its safety.

1.4.5 Design Recommendations

Design recommendations are presented and discussed based on the theoretical and experimental work of this thesis as well as an extensive understanding of the previous work of other researchers. The draft code clauses of the new Canadian Highway Bridge Design Code (CHBDC) are also reviewed and discussed. The author's own design guidelines are presented and differences with the draft code are highlighted.

2 RATIONAL MODEL FOR PREDICTING THE PUNCHING FAILURE BEHAVIOUR OF STEEL-FREE CONCRETE BRIDGE DECK SLABS

2.1 Overview of Existing Models

It has been known for sometime that reinforced concrete bridge decks fail in punching at loads that can far exceed the flexural design load. Many structural concrete building slabs subjected to concentrated loads also exhibit this behaviour. Because the punching failure can not be predicted by flexural theory, researchers have investigated many approaches including empirical formulas, semi-empirical formulas, rational models and non-linear finite element analysis in an attempt to develop a reliable design tool. Some of these models have been calibrated over a wide number of experimental results and have exhibited good results for many situations. However, all available models have one or both of the following problems. Firstly, models developed for bridge decks or structural slabs include forces developed by the reinforcing steel as key parameters. There is an obvious problem when applying these methods to reinforcing steel-free deck slabs. Secondly, almost all models do not account for the effects of lateral restraint on punching behaviour. Hewitt and Batchelor (1975) did include restraint parameters in their work; however, the restraint parameter relied on forces developed by the reinforcing steel in a manner that is inappropriate for steel-free decks. While all the work of other researchers in the field of punching shear models for reinforced concrete will not be outlined in detail in this thesis, representative works will be referenced throughout this chapter under the appropriate topics.

To demonstrate the problem with present punching shear models, let us consider the provisions of several of the existing concrete codes. The four codes under consideration are the Canadian Standards Association CSA A23.3-M95 Design of Concrete Structures, the American Concrete Institute ACI 318-89 or the American Association of State Highway Transportation Officials AASHTO, British Standard Institute BS 8110, and the European Code CEB-FIP. The appropriate requirements are given in equation form for each code in

equations (1) to (4) respectively. The reader is referred to the following references to examine how others have used these equations for reinforced concrete slab results: Ebeido and Kennedy (1996), Ahmad et al. (1994), Azad et al. (1994), Kuang and Morley (1992).

$$P_{CSA} = \left(1 + \frac{2}{\beta}\right) 0.2\ \lambda\ \phi_c\ \sqrt{f_c'}\,(b_o \cdot d) \tag{1}$$

$$P_{ACI} = 1.33\sqrt{f_c'}(c + d)d \tag{2}$$

$$P_{BS8110} = 3.16\ \sqrt{100\rho} \cdot \sqrt{\frac{f_{cu}}{25}} \cdot \sqrt{\frac{400}{d}}\ (c + d)d \tag{3}$$

$$P_{CEB\text{-}FIP} = 0.12\left(1 + \sqrt{\frac{200}{d}}\right)\sqrt{100\rho f_{ck}}ud \tag{4}$$

Equations (3) and (4) have a term, ρ, representing the density of steel reinforcement in the slab. The use of these equations in a slab devoid of steel reinforcement yields 0 kN as the value of punching load. While equations (1) and (2) do not have terms associated with reinforcement, nor do they have terms associated with restraint stiffness. For these equations lets us consider the slab tested by Thorburn and Mufti (1995). This slab was tested to failure at various locations; each location had a different value of restraint stiffness but the same geometry and concrete strength. The punching failure values varied from 576 to 1127 kN. Using either equation (1) or (2) we would get the same theoretical punch value at each location. For the slab tested P_{CSA} = 830 kN and P_{ACI} = 690 kN. Kuang and Morley (1992) came to a similar conclusion regarding equation (2) when investigating restrained reinforced concrete slabs. The equations cannot be used because they do not account for restraint stiffness effects. Other researchers (Siao, 1994; Regan, 1974; Gardner, 1990; Bazant and Cao, 1987) have investigated similar critical section style equations and have calibrated the

equations for reinforced concrete slab test results. The use of the equations developed by theses researchers would again have the same problems as illustrated by the code formulas when applied to steel-free slabs.

Another common method of examining the failure of reinforced concrete slabs is the yield line method (MacGregor, 1992). In simple terms one examines the failure lines or yield lines of the slab. A moment value is associated with the yielding of the reinforcement along these lines. The load to cause yielding along all designated failure lines is then determined and is considered to be the failure load. The application of the yield line model to steel-free slabs has two obvious problems. Firstly, membrane action not flexure is the most significant characteristic of slab behaviour. Secondly, a deck devoid of internal reinforcement cannot form yield lines. If one proposes that the modulus of rupture replace the yield moment then one can still not explain why the deck has two to three times the capacity of its cracking moments. Kuang and Morley (1992) also investigated the yield line model for restrained reinforced concrete slabs and found it to be inappropriate for slabs with either high degrees of restraint or low reinforcement ratios. In both cases the membrane action is the most significant contributor to slab behaviour.

It is necessary then to develop a new model suitable for the behaviour exhibited by the steel-free deck.

2.2 Characteristic Behaviour of Slabs in Punching

2.2.1 Crack Patterns

In order to develop a model we will first examine some characteristic behaviour of the punching failure of slabs. Common to all slabs that fail in punching is a very distinct crack pattern. On the underside of the slab radial cracks grow outward from the centre of the point of load application. On the top surface, circumferential cracks form at a diameter roughly equivalent to the spacing of support points or girders. The radial cracks on the underside

always form first, at relative low loadings compared to the ultimate failure load. The circumferential cracks form next. Subsequently, the radial cracks will migrate to the top surface to form full depth cracks. Before failure a third crack forms at an inclined angle to the point of load application. This inclined crack starts at the bottom surface of the slab and migrates upward and inward towards the load point. This shear crack forms the boundaries of the punch cone, shown in Figure 2.1, which punches out at failure. Two important points should be noted about the crack patterns. The cracks form early in the load history of the slab and the slab has substantial capacity after the formation of cracks. These crack patterns are not unique to steel-free deck slabs but have been reported by Gardner (1990), Ahmad et al.(1994), Shehata (1990), Marzouk and Hussein (1991), Kuang and Morley (1992), Taylor and Hayes (1965) and Kinnunen and Nylander (1960) for reinforced concrete slabs; by Azad et al.(1994) , Ebeido and Kennedy (1996) and Fang et. Al (1986) for reinforced concrete bridge decks and Malvar (1992) for reinforced concrete pier deck slabs.

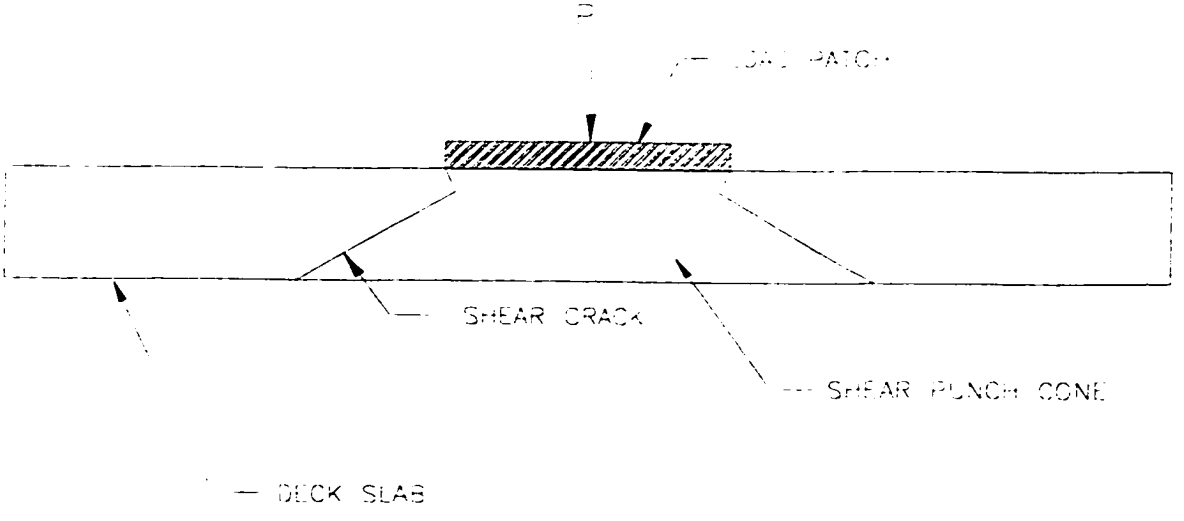

Figure 2.1 Cross-section of deck slab showing shear cracks and punch cone

2.2.2 Flexural Capacity

It has been known that reinforced concrete deck slabs have failure loads that far exceed their flexural capacity (Bakht and Markovic, 1986; Beal, 1982 and Hewitt and Batchelor, 1975). In addition, the above mentioned crack patterns form early in the load history of a deck slab. In the case of reinforced concrete, the reinforcing steel gives the slab moment capacity beyond the cracking moment of the deck. However, in the steel-free deck, the slab has no additional moment capacity beyond its cracking moment. If the slab continues to accept increasing loads after the formation of cracks, then it is obviously not through flexural behaviour.

2.2.3 Lateral Restraint

When investigating the punching failure of slabs, and in particular bridge deck slabs, the effect of the lateral restraint must be considered. Lateral restraint was described in Chapter 1 as the force which resists the outward movement of the concrete, generally by restraining the outward displacement of the girders. This lateral restraint is synonymous with the development of internal compressive membrane action. Ghoneim and MacGregor (1994), Ebeido and Kennedy (1996), Hewitt and Batchelor (1975) Kuang and Morley (1992), Taylor and Hayes(1965) all acknowledge the contribution of lateral restraint or internal arching to increasing the load carrying capacity of slabs. However, only Ghoneim and MacGregor (1994) and Hewitt and Batchelor (1975) made attempts to include this parameter in their respective models. The former included its affect as a constant in-plane force applied at the mid-depth of the slab and the latter used an empirical procedure based on reinforcing steel forces and moments. Both these approaches are inappropriate for the steel-free concrete deck.

The early work of Mufti et al. (1993) clearly illustrates the importance of this restraint to the performance of steel-free slabs. In early testing, no straps were provided between adjacent girders for the model bridge deck slabs. The level of lateral restraint was low and the deck slabs did not fail in a punching mode. The same test configuration was tested again but this time steel straps were added to tie the adjacent girders together. The level of lateral restraint

being significantly higher, the deck slab failed in punching at a load value twice that of the previous tests. In addition, Thorburn and Mufti (1995) clearly demonstrate that by changing only the lateral restraint parameter, a substantially different punching failure load value can be achieved. The internal arching forces and hence the lateral restraint is essential to the performance of the steel-free deck slab system.

2.2.4 Three Dimensional Compression

The concrete zone surrounding the point of load application is in state of a three dimensional stress. This fact has been reported by Kinnunen and Nylander (1960), Jiang and Shen (1986), and Marzouk and Hussein (1991). How these forces are developed will be detailed in a later section; however, the existence of this three dimensional state is important. In effect, it means that the principle compressive stress around the load point can reach values well in excess of the uniaxial compressive stress, f'_c. Therefore, a relatively small area of concrete adjacent to the load point is able to develop compressive forces sufficient to sustain very high applied loads. This compressive stress state is both a key to sustaining high loads and a limiting factor in determining the failure criteria.

Any model of steel-free concrete bridge deck slab behaviour must therefore include at least four parameters which are characteristic to the punching failure of slabs:

1. Consideration of the crack patterns which form before punching failure occurs.
2. Consideration of a mechanism which will allow the continued acceptance of load after flexural capacity has been exceeded.
3. Inclusion of a term to define the lateral restraint stiffness of the system.
4. Inclusion of expressions to account for the increase compressive strength around the load point due to the confinement of concrete.

2.3 Development of a Rational Model

As indicated previously, many different models for punching shear of slabs have been developed. Marzouk and Hussein (1991) state that the rational model developed by Kinnunen and Nylander (1960) still provides the best account of punching behaviour and applied the model to high strength reinforced concrete slabs. Hewitt and Batchelor (1975) incorporated restraining boundary conditions and the compressive membrane action into the Kinnunen and Nylander (1960) model and demonstrated its application to reinforced concrete bridge deck slabs. Although the work of Hewitt and Batchelor (1975) was developed for bridge decks with lateral restraint, it is primarily applicable to reinforced concrete slabs in which the reinforcement is a boundary condition.

Also, the restraint factor proposed by Hewitt and Batchelor (1975) was empirical and can only be found through experimentation. Based on investigations of other models, as well as observations from experimental work, this author also believes that the Kinnunen and Nylander (1960) rational model is the most reasonable approach to modelling the punching behaviour of bridge decks. This process allows for the inclusion of the four characteristics of punching stated above. The use of this model was first proposed by Wegner and Mufti (1994); however, significant changes have been made by the author, Section 1.4.1.

The basic model assumptions will be presented first, followed by the mathematical development of the equations of equilibrium and an explanation of the failure criteria. Discussion of two key concepts will be deferred until after the solution algorithm has been defined. These two items are the concrete confinement relationship and the value of the restraint stiffness parameter.

2.3.1 Basic Assumptions

1. The crack pattern described in Section 2.2.1 is idealized as shown in Figure 2.2. The three types of cracks are the radial cracks, the circumferential cracks

and the inclined shear crack. The sections of the concrete outside the shear crack can be divided into "wedges" bound by the three types of cracks (Figure 2.3). Under loading, these wedges act as rigid bodies in the radial direction rotating about a centre of rotation as shown in Figure 2.4.

2. At the intersection of the wedges and the loaded area is the region which Kinnunen and Nylander (1960) described as a conical shell of very high compressive stress (Figure 2.5). This region is in a state of three dimensional compressive stress. The load is transferred into compressive membrane forces through this conical shell.

3. Kinnunen and Nylander (1960) demonstrated that, immediately after the appearance of the shear crack, the centre of rotation of the wedges is located at the root of the shear crack. As the load increases, the centre of rotation moves towards the centre of the load point. For this model, the centre of rotation will be assumed to always be at the centre of the load. The centre of rotation will be located at a distance **y** from the top surface of the slab (Figure 2.4).

4. The model developed by Kinnunen and Nylander (1960) assumed axisymmetric geometry and loading. Hewitt and Batchelor (1975) proposed a method of idealizing bridge deck loading and geometry into an equivalent axisymmetric condition. This same method is followed here. The loaded area of a bridge deck from a vehicle tire is approximately a rectangular patch. For purposes of the theoretical model, the non-circular load area is converted into a circular load area of equivalent perimeter, with a diameter B. An equivalent circular slab is defined by the largest circle of diameter C which can be inscribed between the centre lines of adjacent girders (Figure 2.2).

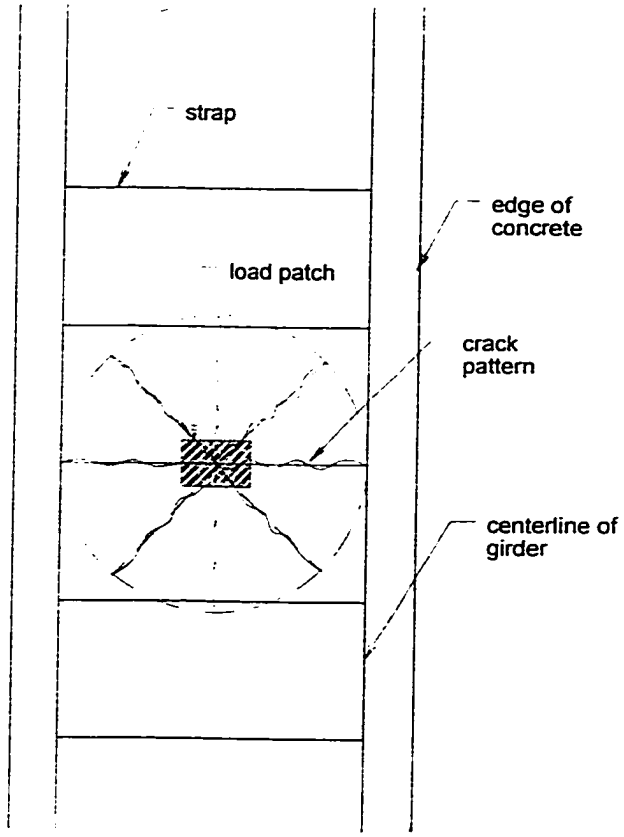

Figure 2.2 Idealized slab crack pattern

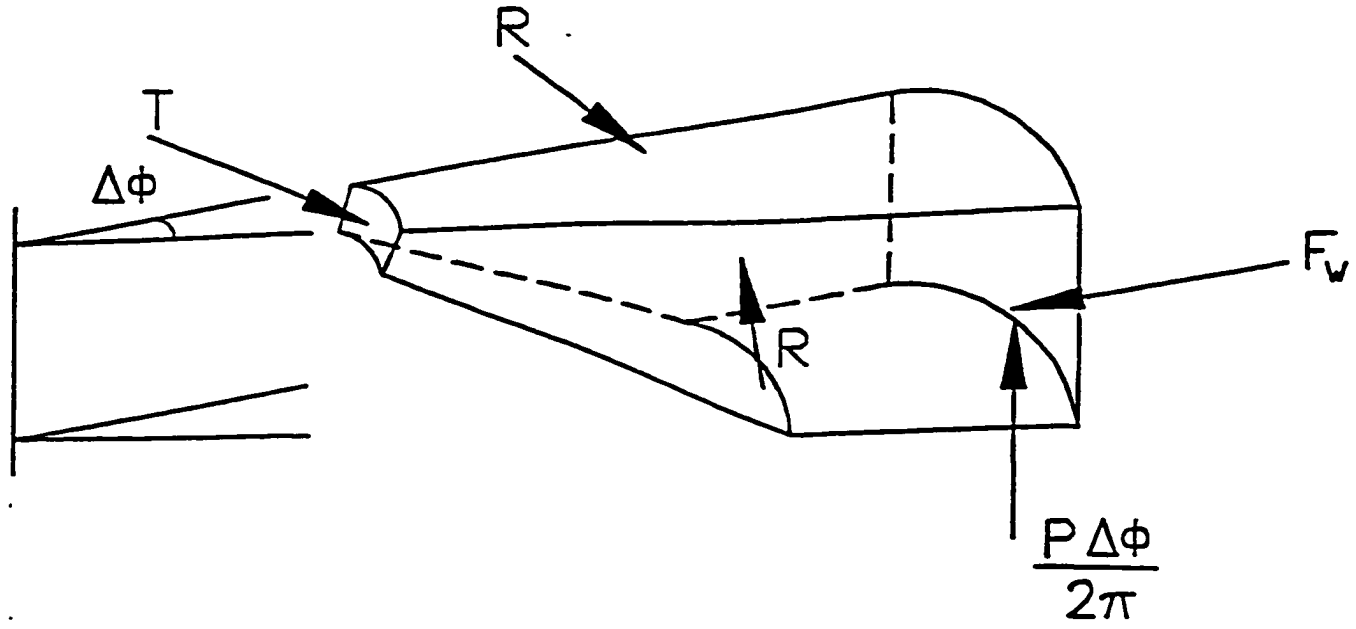

Figure 2.3 Wedge component

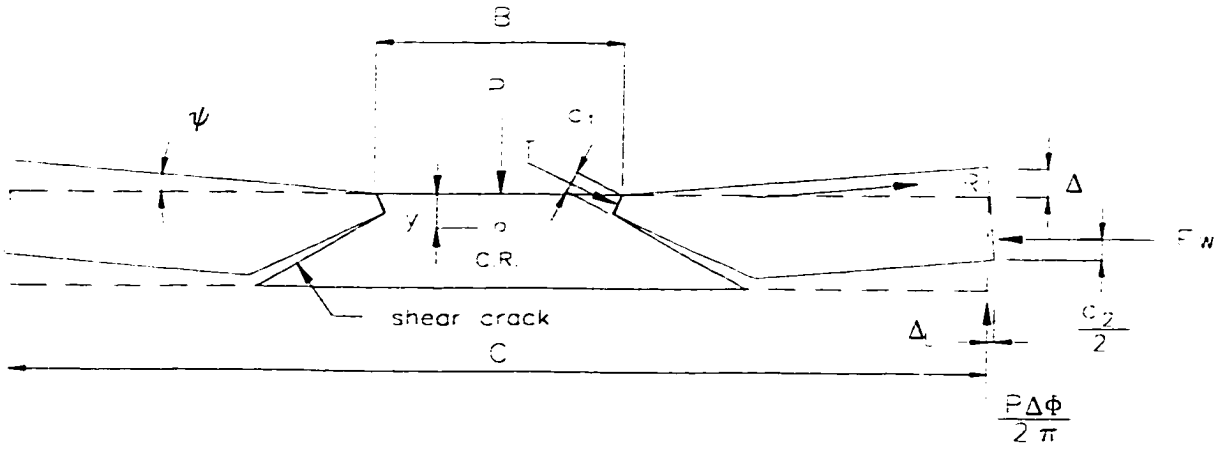

Figure 2.4 Rotation of a wedge under loading

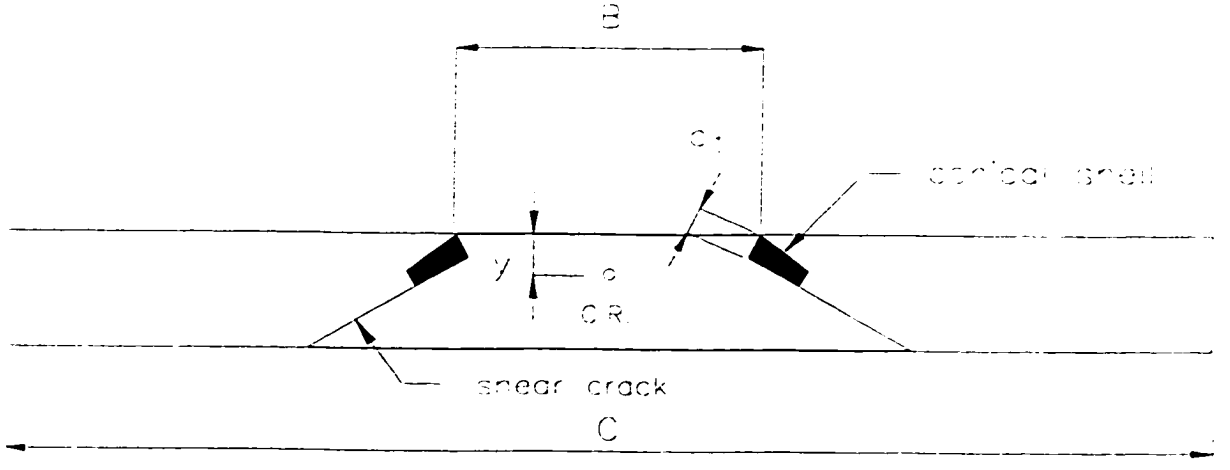

Figure 2.5 Cross-section showing conical shell region

2.3.2 Expression of Forces and Deformations Of the Rigid Body Wedge

2.3.2.1 Geometry of Wedge

The outer radius of the wedge is **C/2**. The inner radius is **B/2**. The depth of the wedge is the full depth of the slab, **d**. The shear crack of angle α forms the inclined surface of the wedge. The base of the conical shell at the root of the shear crack is designated $\mathbf{c_1}$. The depth of the compressive stress block due to restraining forces is $\mathbf{c_2}$. The angle inscribed by the two radial cracks forming the sides of the wedge is $\Delta\phi$.

2.3.2.2 Deformations

The angle of rotation of the wedge is ψ and the accompanying deflection under load is

$$\Delta = \frac{C}{2}\psi \tag{5}$$

The lateral deflection of the point of support is

$$\Delta_L = \psi(d - y) \tag{6}$$

2.3.2.3 Vertical Load at Support

The vertical load at the support for the sector of the circle equivalent to the wedge is given by the expression

$$V = \frac{P\Delta\phi}{2\pi} \tag{7}$$

2.3.2.4 Oblique Compressive Force

The compressive stress in the conical shell is assumed to act in a direction parallel to the shear crack. If **T** is the resultant force, acting on the wedge, then as the wedge rotates, **T** acts at an angle to the horizontal of $(\alpha\text{-}\psi)$ such that the vertical component of the force is

$$T_v = T \cdot \sin(\alpha - \psi) \tag{8a}$$

The horizontal component of this force is

$$T_h = T \cdot \cos(\alpha - \psi) \tag{8b}$$

2.3.2.5 Lateral Restraining Force

If we designate **K** as the stiffness of the elements providing lateral restraint, principally the straps, and remember that the rotation of the wedge leads to a lateral deflection, Δ_L, at the support point, then the restraining force **F** can be expressed as

$$F = K\Delta_L \tag{9}$$

or substituting from (6)

$$F = K\ \psi(d-y) \tag{10}$$

The derivation of the value of restraint stiffness, **K**, will be given in Section 2.5. The variable **K** has units of force/displacement per unit length of circumference and can be thought of as the restraint stiffness per unit length of circumference. For simplicity **K** will be referred to only as restraint stiffness. This being understood, the restraining force acting on the wedge, $\mathbf{F_w}$, is derived as

$$F_w = F \cdot \frac{C}{2}\ \Delta\phi \tag{11}$$

$$F_w = K\psi\ (d-y)\ \frac{C}{2}\ \Delta\phi \tag{12}$$

The restraining force is developed in the wedge through compression in the bottom outside edge of the wedge and acts only in the radial direction. The compressive stress is idealized by a rectangular compression block of depth $\mathbf{c_2}$ and magnitude of $\mathbf{0.85\ f'_c}$. The force $\mathbf{F_w}$ acts at a height of $\mathbf{c_2/2}$ above the bottom of the slab. Resolving the resultant $\mathbf{F_w}$ from the stress block

$$F_w = 0.85 f_c' \frac{C}{2} \Delta\phi \cdot c_2 \qquad (13)$$

Equating equations (12) and (13), we find that

$$c_2 = \frac{K \psi(d-y)}{0.85 f_c'} \qquad (14)$$

It is important to note two assumptions regarding this formulation. Firstly, the restraining force is related directly to the lateral deflection Δ_L by the stiffness **K**. The calculation of Δ_L neglects any elastic shortening of the concrete wedge due to the restraining force. This is approximately true when one considers that the area of the steel strap is typically only 0.6% of the area of the concrete deck. Even with a modular ratio of 7, $\mathbf{E_cA_c}$ is still over 20 times $\mathbf{E_sA_s}$, consequently the elastic shortening of the concrete is small compared to the elongation of the straps. This factor is reduced somewhat by the fact that there is very localized bearing stresses in the tip of the conical shell and at the support points; however, it is acceptable to neglect any shortening of the slab. Secondly, the model assumes that the system is axisymmetric, such that a uniform restraint is provided around the entire circumference of the idealized circular slab. While it is easy to visualize restraint in the transverse direction being provided by the steel straps, the restraint in the longitudinal direction is less apparent. It is postulated that the in-plane stiffness of the concrete deck coupled with the girders acting as very stiff straps in the longitudinal direction provides a sufficiently high degree of restraint such that a uniform restraint, equivalent to the restraint in the transverse direction, can be assumed around the entire circumference. This seems reasonable when one considers the results of testing of early half-scale models (Mufti et al., 1993). Although a high punching load was achieved in the central portion of the slab, lower failure loads resulted as the load location approached a transverse free edge. In some cases the failure mode degenerated into a hybrid mode of flexure and punch. It is easily understood that, as we approach the free edge, the in-plane longitudinal restraint diminishes such that the assumption of uniform radial restraint around the circumference is no longer valid. In subsequent tests (Newhook

et al., 1995), edge beams were added to increase the in-plane stiffness of the deck at the free edge.

Punching shear failure was achieved for loads close to the edge, although at a lower load value than for a centrally located load. It is therefore reasonable to assume that the deck and girders provide lateral restraint to the system.

2.3.2.6 Circumferential Compressive Force

If we consider the rotation of the wedge about a centre of rotation located a distance y below the horizontal top surface of the wedge, then all points above the plane defined by the y-normal can be seen to be moving closer to the central axis of the circular slab by a dimension δ (Figure 2.6).

As the location of the point above the y-normal plane increases, so does the displacement δ. The consequence is that the radial distance from the central axis is now **r-δ** and the change in circumference is **2π(r-δ)**. Equating the circumferential strain to the change in circumference

$$\epsilon_{ct} = \frac{\delta}{r}. \qquad (15)$$

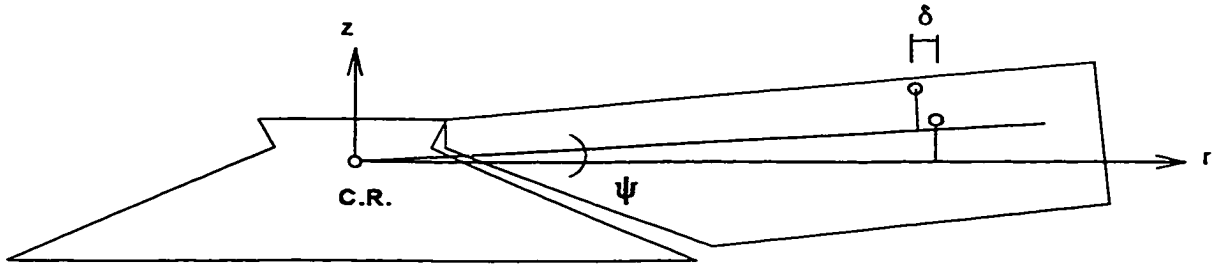

Figure 2.6 Rigid body rotation of a wedge

The displacement δ is readily approximated by $\Psi \cdot z$ where **z** is the distance above the y-normal plane. Therefore

$$\epsilon_{ct} = \psi \frac{z}{r} \tag{16}$$

with

$$\begin{aligned} \epsilon_{ct_{MIN}} &= 0 \qquad @\ z=0 \\ \epsilon_{ct_{MAX}} &= \frac{\psi y}{r} \qquad @\ z=y \end{aligned} \tag{17}$$

The corresponding circumferential stress can be expressed as

$$\sigma_{ct} = E_c\ \psi \frac{z}{r} \tag{18}$$

It is noted that at **z=y** and **r = B/2,** σ_{ct} is maximum and confirms that a state of three dimensional compressive stress exists in this region. If we integrate this circumferential stress in the vertical direction from **0** to **y** and in the radial direction from **r = B/2 + y** to **r = C/2**, we obtain an approximation of the total circumferential compressive force **R** acting on the wedge.

$$\begin{aligned} R &= \int_{r=\frac{B}{2}+y}^{r=\frac{C}{2}} \int_{z=0}^{z=y} E_c\ \psi \frac{z}{r}\, dz dr \\ R &= E_c\ \psi \int_{r=\frac{B}{2}+y}^{r=\frac{C}{2}} \frac{1}{r}\left[\frac{y^2}{2}\right] dr \\ &= E_c\ \psi \frac{y^2}{2}\left[ln \frac{C/2}{B/2+y}\right] \end{aligned} \tag{19}$$

This integration neglects the triangular portion of the wedge above the y-normal between **r = B/2** and **r = B/2+y**. However, this portion is small compared to the total force and has been omitted. Furthermore, Kinnunen and Nylander (1960) found that the radial concrete strain in this region, near the load area, often decreased or became positive prior to failure such that a mechanical model based on plane deformation is not valid for this region. It is worth noting that the compressive conical shell is contained within this region.

While $\mathbf{E_c}$ is shown as a constant, it is actually a non-linear function of the concrete strain, approximately similar to the uniaxial stress strain relationship for concrete in compression. While several idealizations have been developed, concrete researchers have yet to reach a consensus on a rigorous mathematical description of this function. Nevertheless it is important to account for the decreasing value of $\mathbf{E_c}$ as ϵ_c increases, otherwise the value of **R** will be overestimated. To address this we follow the approach of Kinnunen and Nylander who related **R** to the compressive stress in the top of the slab σ_{cty} at **r = B/2 + y**. This is achieved by substituting

$$\sigma_{cty_{r=\frac{B}{2}+y}} = \frac{E_c \, \psi \, y}{\frac{B}{2}+y} \tag{20}$$

into (19) such that

$$R = \left(\frac{B}{2}+y\right) \cdot \frac{y}{2} \left[ln \frac{\frac{C}{2}}{\frac{B}{2}+y} \right] \cdot \sigma_{cty_{r=\frac{B}{2}+y}} \tag{21a}$$

or

$$R = \left(\frac{B}{2y}+1\right) \frac{y^2}{2} \left[ln \frac{\frac{C}{2}}{\frac{B}{2}+y} \right] \cdot \sigma_{cty_{r=\frac{B}{2}+y}} \tag{21b}$$

This eliminates E_c and ψ from the equation and relates the force to stress at a point at which the stress can be measured.

Kinnunen and Nylander (1960) empirically established that for **B/d** $\geq$ **2** using

$$\sigma_{ct_{r=\frac{B}{2}-y}} = 1007 + 0.392\ \sigma_{cube} \qquad \textbf{(22)}$$

in psi, yields accurate values of **R**.

The relationship for σ_{cube} in terms of cylinder strength, f_c' as given by Batchelor and Hewitt (1975) is

$$\sigma_{cube} = \frac{f_c'}{0.75 + 0.000025 f_c'} . \qquad \textbf{(23)}$$

Accepting this formulation, a value of **R** can be found for a given value of **y**.

If we now consider the wedge with a sector angle of $\Delta\phi$, then the component of **R** in the radial direction through the centre of the wedge is given by

$$R_r = R \cdot 2 \sin\left(\frac{\Delta\phi}{2}\right) \qquad \textbf{(24a)}$$

such that R_r is approximately

$$R_r = R\Delta\phi . \qquad \textbf{(24b)}$$

2.3.3 Equilibrium Conditions

2.3.3.1 Vertical Equilibrium

Equating the vertical components acting on a wedge we find that

$$T = P \frac{\Delta\phi}{2\pi \sin(\alpha-\psi)} \tag{25}$$

2.3.3.2 Horizontal Equilibrium - Radial Direction

The horizontal component of the oblique compressive force T from equation (8b) is $T_H = T \cos(\alpha-\psi)$.

Substituting from above, we find

$$T_H = P\frac{\Delta\phi}{2\pi} \cdot \frac{\cos(\alpha-\psi)}{\sin(\alpha-\psi)} \tag{26a}$$

or

$$T_H = P \frac{\Delta\phi}{2\pi} \cot(\alpha-\psi) \tag{26b}$$

Equating the three horizontal forces acting on the wedge, we have

$$P \frac{\Delta\phi}{2\pi} \cot(\alpha-\psi) + R\Delta\phi = K \frac{C}{2} \psi(d-y)\Delta\phi \tag{27a}$$

or

$$\frac{P}{2\pi} \cot(\alpha-\psi) + R = K \frac{C}{2} \psi(d-y) \tag{27b}$$

This can be re-written as

$$P = 2\pi \tan(\alpha-\psi)W \tag{28}$$

where

$$W = K \frac{C}{2} \psi(d-y) - R \tag{29}$$

2.3.3.4 Moment Equilibrium

A third equation of equilibrium may be obtained by summing moments in the vertical plane about the point defined by the intersection of the horizontal restraining force, $\mathbf{F_w}$, and the vertical support force $\mathbf{P\Delta\phi/2\pi}$.

$$R(d - \frac{y}{3} - \frac{c_2}{2}) + \frac{P}{2\pi}\cot(\alpha-\psi)\left[d - \frac{\beta_1 y}{2} - \frac{c_2}{2} - \psi(\frac{C}{2} - \frac{B}{2})\right] = \frac{P}{2\pi}\left[\frac{C}{2} - \frac{B}{2} + \psi(d - \frac{\beta_1 y}{2} - \frac{c_2}{2})\right] \quad (30)$$

Substituting for **P** and solving for α

$$\alpha = \tan^{-1}\left\{\frac{\frac{R}{W}(d - \frac{y}{3} - \frac{c_2}{2}) + [d - \frac{\beta_1 y}{2} - \frac{c_2}{2} - \psi(\frac{C}{2} - \frac{B}{2})]}{\frac{C}{2} - \frac{B}{2} + \psi(d - \frac{\beta_1 y}{2} - \frac{c_2}{2})}\right\} + \psi \quad (31)$$

2.3.4 Triaxial Compressive Stress

To find an expression for **y** we consider the region surrounding the conical shell. Following the procedures of CSA-A23.3-M84, we can idealize the stress distribution at the intersection of the conical shell and the edge of the loaded area as a rectangular stress block of depth $\beta_1 y$ and magnitude of $\mathbf{0.85\sigma_r}$ where

$$\begin{aligned} \beta_1 &= 0.85 && f_c' \le 30MPa \\ \beta_1 &= 0.85 - 0.08\frac{(f_c'-30)}{10} && 30MPa < f_c' < 55MPa \\ \beta_1 &= 0.65 && f_c' \ge 55MPa \end{aligned} \quad (32)$$

Relating $\beta_1 y$ to the stress block $\mathbf{c_t}$ associated with the force **T**, we have

$$y = \frac{c_1 \cos(\alpha-\psi)}{\beta_1} . \tag{33}$$

The sum of all oblique forces around the perimeter of the loaded area is **P/sin (α-Ψ)** acting on a stress block of area $\mathbf{c_1 \pi B}$ such that the stress σ_r

$$0.85\sigma_r = \frac{\frac{P}{\sin(\alpha-\psi)}}{c_1 \pi B} \tag{34a}$$

or

$$c_1 = \frac{P}{0.85\ \pi B\ \sin(\alpha-\psi)\sigma_r} . \tag{34b}$$

Considering the triaxial condition with $\sigma_1 \le \sigma_2 \le \sigma_3$ then $\sigma_3 = \sigma_r$, $\sigma_2 = \sigma_\theta$ and $\sigma_1 = \sigma_z$

$$\sigma_1 = \frac{P}{A_p} \tag{35}$$

where A_p is the actual area of the tire print.

Richart (Demers and Neale, 1994) proposed the following model for the behaviour of concrete under confinement

$$\sigma_{3c} = f_c' \left(1 + k \frac{\sigma_1}{f_c'} \right) \tag{36a}$$

$$\frac{\sigma_{3c}}{f_c'} = 1 + k \frac{\sigma_1}{f_c'} \tag{36b}$$

where k = 4.1.

Adopting equation (36a) with k = 10 for this application, see Section 2.4 on concrete confinement relationship, yields an expression for $\mathbf{c_1}$ based on **P**

$$c_1 = \frac{P}{0.85\ \pi B\ \sin(\alpha - \psi) f_c' \left(1 + k \frac{\sigma_1}{f_c'}\right)} \tag{37}$$

and thereby gives a relationship for **y** in terms of applied load **P** through equations (33) and (34).

2.3.5 Solution Algorithm

Based on the formulation given, the following parameters are necessary to define the system: **C, B, d,** $\mathbf{f_c'}$ and **K**. If these parameters are known, then an iterative procedure can be used to predict the equilibrium load for a given deflection, **Δ**. Using equation (5), the angle of rotation. **Ψ**, is determined. An initial estimate on **y** is made; a convenient estimate would be y = d/10. Values for $\mathbf{R_r}$, **W**, **α** and **P** are calculated in that order using equations (21) with (22), (29), (31), and (28) respectively. A calculated value for **y** is determined by equations (32) through (34). If the assumed **y** is equal to the calculated **y**, within a predetermined tolerance (say 0.0001), then the equilibrium load **P** is correct for the chosen value of deflection. If not, a new value of **y** is assumed and the process is repeated until convergence is achieved.

This procedure can be repeated for incremental values of **Δ** between zero and a cut-off point of **Δ= d**. A curve of equilibrium load versus deflection is plotted as shown in Figure 2.7 and can be considered to represent the load-deflection history of the system. The failure load of the steel free bridge deck system is then determined by applying one of three possible failure criteria.

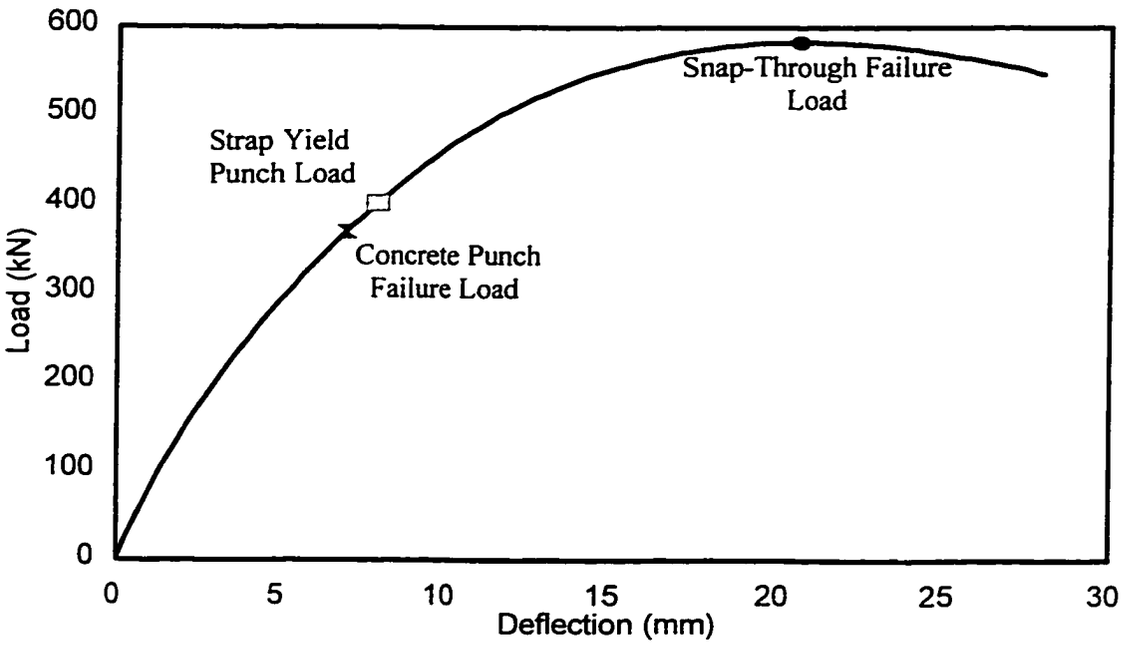

Figure 2.7 Equilibrium load versus deflection

2.3.6 Failure Conditions

The mechanism postulated in this rational model can have three modes of failure or collapse: instability, crushing of the concrete, or yielding of the restraint straps.

Instability collapse is best understood by examining the load-deflection history shown in Figure 2.7. Each point on the curve represents the system equilibrium load, **P**, for a given value of deflection, Δ. The wedge rotation mechanism can reach a state of geometric instability such that any additional deflection leads to a reduction in the value of the load required to maintain the equilibrium of the system. This condition occurs when the deflection reaches the value corresponding to the maxima of the load-deflection curve or

$$\frac{dP}{d\Delta} = 0 \tag{38}$$

In this situation the outer wedges, unable to reach a condition of static equilibrium, continue to rotate and the deck collapses. This mode of collapse is referred to as snap-through failure.

The second failure mode, crushing of the concrete, leads directly to punching failure of the deck. To understand this mode of failure, we must recall two important characteristics. Firstly, the section of concrete inside the shear crack is supported by a compressive conical shell developed in the wedge sections. Secondly, this conical shell is in a state of three-dimensional compressive stress and these stresses increase proportionally as the wedges rotate under increasing load. Under this triaxial compressive state of stress, the strength and modulus of elasticity are substantially increased such that the maximum principle stress reaches a value much greater than $\mathbf{f_c'}$. Provided that the mechanism remains geometrically stable, stresses in the supporting shell will reach an ultimate state where compressive failure occurs. The conical shell can no longer support the inner core and it punches through the deck.

Kinnunen and Nylander (1960) established an empirical criterion for this mode of failure. When the circumferential strain at the top surface of the slab near the loaded area ($\mathbf{r = B/2 + y}$) reaches a critical value, the concrete softens in the circumferential direction and the triaxial state is compromised. The strength of the conical shell is reduced and failure occurs. Kinnunen and Nylander (1960) found that the strain behaviour of the concrete near the loaded area was very complicated, particularly near the failure loads and could not be related to the linear elastic theory of the model. However, at a distance equal to y from the edge of the load area, correlation was established between the circumferential strain ϵ_{ct} and punching failure. Kinnunen and Nylander (1960) give the critical value of strain as $\epsilon_{ct} = 0.0019$.

In similar work on steel-reinforced high strength concrete slabs, Marzouk and Hussien (1991) report that the average tangential strain next to the load patch was 0.00215 at punching failure. These values correspond very closely to the value of strain at the maximum uniaxial compressive stress, $\mathbf{f_c'}$ and the commonly used value of $\epsilon_{ct} = \mathbf{.002}$ is adopted. The value for the tangential compressive strain ϵ_{ct} can be calculated using the following equation:

$$\epsilon_{ct} = \frac{\psi y}{\frac{B}{2} + y} \tag{36}$$

The third failure mode, yielding of the restraint straps, is also considered to be a punching failure criterion. The lateral restraint is provided to the system by means of the transverse steel straps, generally made of steel. As given in equation (9), the magnitude of the restraining force is controlled by the lateral restraint stiffness, **K**, and the amount of lateral deformation, Δ_L. In simple terms, the value of **K** is determined by both the geometry of the strap system and the modulus of elasticity of the strap matertial. For steel straps the value of **K** is constant while the stresses are in the linear elastic range. Therefore, as the load and consequently Δ_L increases, the magnitude of the restraining force **F** increases. However, if the stress in the strap reaches the yield stress of steel then no further increase in **F** is possible for that strap. The influence of the lateral restraint of that strap on the system behaviour is reduced and the level of confining forces in the concrete are also reduced. Due to this reduction in confinement, punching of the slab will occur with only a slight increase in applied load. Thus, the yielding of the straps is set as a failure criterion and punching is assumed to occur when yield strain is obtained. The actual failure load may be slightly higher than the load corresponding to $\epsilon_s = \epsilon_y$ however this load is conservative. The increased complexity of the solution algorithm does not warrant its development for a small increase in predicted failure load value.

The actual failure load of the system is the lowest equilibrium load corresponding to the three failure criteria. The instability mode dominates only at very low values of restraining stiffness and is generally not of interest. The punching failure load is determined by monitoring ϵ_{ct} and ϵ_s throughout the load history.The punching failure load is reported as punching failure due to either yielding of the straps, $\epsilon_s = \epsilon_y$, or punching due to yielding of the concrete, $\epsilon_{ct} = \mathbf{0.002}$.

A FORTRAN program developed to automate the solution algorithm and check for punching failure is presented in Appendix I.

2.4 Concrete Confinement Relationship

The concrete within the region of the conical shell, and most particularly adjacent to the load patch, is in a state of triaxial compressive stress. The vertical compressive stress arising from the applied load and given in equation (35) is designated as the maximum principal stress, σ_1. The circumferential stress which leads to the development the force, **R**, is the intermediate principal stress, σ_2. The horizontal component of the compressive membrane force, **T**, is the minimum principal stress, σ_3. The triaxial condition is defined by $\sigma_1 \geq \sigma_2 \geq \sigma_3$; however, because the stresses are compressive, the magnitude of σ_3 is greater than the magnitude of σ_1. To be consistent with the nomenclature of this thesis $\sigma_1 = \sigma_z$, $\sigma_2 = \sigma_\theta$ and $\sigma_3 = \sigma_r$.

Because of the triaxial compressive stresses, the concrete in this region is confined and the values of σ_3 can far exceed the uniaxial compressive stress of the concrete. Therefore we need to define a relationship for the behaviour of concrete under confinement such that we can relate σ_3 to σ_1 , the value of σ_1 being readily available from equation (35).

Richart (Demers and Neale, 1994) proposed the following model for the behaviour of concrete cylinders under confinement. This equation was given previously as equation (36a) and is repeated here for clarity.

$$\sigma_{3c} = f_c' \left(1 + k \frac{\sigma_1}{f_c'} \right) \qquad \textbf{(36a)}$$

Richart gives a value of **k=4.1** for concrete cylinder tests.

In other literature, Hobbs and Pomeroy (Hannant, 1974) propose a similar relationship based on a number of available triaxial compression testing results

$$\frac{\sigma_{3c}}{f_c'} = 1 + k \frac{\sigma_1}{f_c'} \qquad \textbf{(36b)}$$

For the data used by these authors, the value of **k = 4.8 ±0.6**. Similarly, Hannant (1974) proposes that the value of **k** could range from **4.8 to 5.0**. Both groups indicate that the value of **k** is not significantly affected by the value of the intermediate principle stress, σ_2.

The confinement relationship given in equation (36) is of the right form to be used in the rational model; however, it remains to select the appropriate value of **k**. An empirical assessment of the punching strength results from a number of slab tests indicate that the theoretical model correlates very well when a value of **k=10** is used. This is much larger than the values proposed by others, which ranges from **4.1 to 5.0**.

Investigating this difference in **k** values we consider several important points. Firstly, the constant is empirical and is derived directly from a number of test results. All researchers acknowledge that their proposed value of **k** is only valid for the concrete matrices and test setups covered by their research. Most of these results relate to a variety of test setups on concrete cylinders and cubes. Testing on a bridge deck structural system had not been performed by other researchers. By definition an empirical constant is specific to the testing performed and it is quite possible that a different empirical constant is applicable to testing which results in the punching failure of a slab rather than a constant which relates to the crushing of concrete cylinders.

Secondly, one must consider the nature of the principal stresses. Richart's constant of 4.1 was developed for cylinders wrapped with a material which provides confinement against radial and circumferential expansion. The expansion occurs in a plane orthogonal to the applied load. In this case, the confining stress can be described as a passive stress which

develops in response to the poisson's ratio type expansion of the cylinder. This is the lower bound of the confinement condition. On the upper bound, all three stresses are directly applied to the element by external conditions. This case can be described as active confinement. It is proposed that active confinement has a much more beneficial effect on the maximum principal stress which can be attained. The triaxial stress condition in the steel-free deck more closely resembles the active stress condition. It is therefore reasonable to expect that the confinement constant will have a higher value than the passive condition.

Finally, we examine the test results reported by Hannant (1974). Three figures showing σ_3/f'_c versus σ_1/f'_c are given by Hannant which summarize the test results of many researchers. The constants given by Hannant represent the lower bound estimate such that all test results fall above the line. This approach is conservative but is certainly valid for the purpose of developing general design guidelines. However. for the steel-free bridge deck, we examine a line which characterizes the upper bound of these test results. This gives an equation of the form

$$\frac{\sigma_3}{f'_c} = a + b \cdot \frac{\sigma_1}{f'_c} \qquad \textbf{(40)}$$

This equation can also be used to describe Equation (36b) where **a=1.0** and **b=k**. The values of **a** and **b** for the upper bound of three figures given in Hannant (1974) are shown in Table 2.1 along with the corresponding values for Richart, Hobbs and Pomeroy and the one proposed for the steel-free deck.

Table 2.1 Coefficients of Equation (40)

Equation	Description	a	b
40a	Hannant, Fig. 7, upper bound	2.25	3.46
40b	Hannant, Fig. 8, upper bound	1.50	5.00
40c	Hannant, Fig. 14, upper bound	2.35	3.75
40d	Hobbs and Pomeroy	1.00	4.86
40e	Richart	1.00	4.10
40f	Steel-Free Deck	1.00	10.0

For the steel-free deck test, σ_1/f'_c at failure ranges between 0.15 and 0.30. It is interesting to note that the intermediate stress ratio σ_2/f'_c is approximately equal to 1.0. Table 2.2 can be constructed of σ_3/f'_c values at failure for the range of σ_1/f'_c. This information is also represented graphically in Figure 2.8.

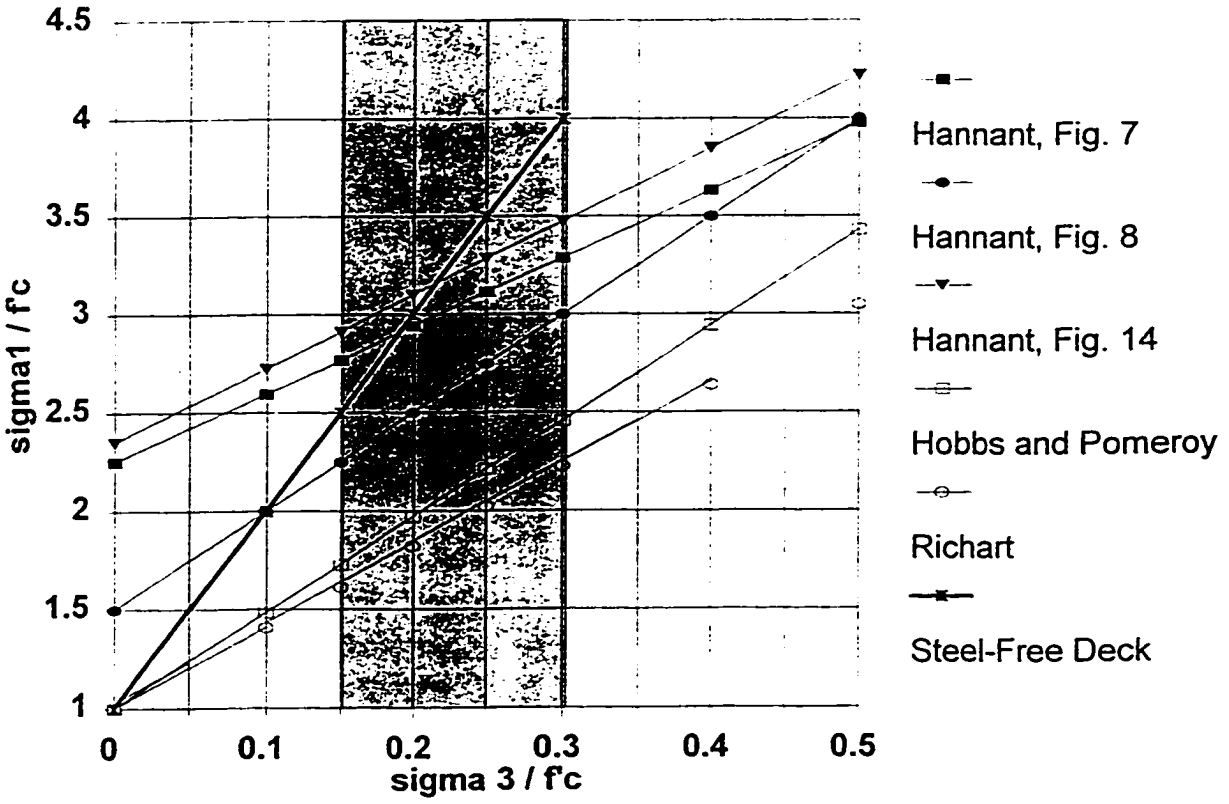

Figure 2.8 σ_3/f'_c versus σ_1/f'_c

Table 2.2 σ_3/f'_c Values for the Range of σ_1/f'_c

	σ_1/f'_c			
Equation	**0.15**	**0.20**	**0.25**	**0.30**
40a	2.77	3.94	3.12	2.29
40b	2.25	2.50	3.75	3.00
40c	2.91	3.10	3.28	3.48
40d	1.73	1.97	2.22	2.46
40e	1.62	1.82	2.03	2.23
40f	2.50	3.00	3.50	4.00

It can be seen that the results of the proposed equation are consistent with the upper bound results of other researchers. Considering all of the above, the use of an empirical confinement constant of **k=10.0** is justifiable for the particular application of the punching failure of the steel-free decks.

It is interesting to compare the values of σ_3/f'_c for equations 40e and 40f. The former represents Richart's equation with **k = 4.1** and the latter represents the proposed equation with **k = 10.0**. For the lower bound, Richart's constant yields σ_3/f'_c = 1.62 where as the proposed constant yields σ_3/f'_c = 2.50. Correspondingly, for the upper bound, the values are σ_3/f'_c = 2.23 and σ_3/f'_c = 4.00 respectively. Although the ratio of the proposed constant to Richart's constant is almost 2.5, the corresponding ratio of σ_3/f'_c is only 1.78.

2.4.1 Sensitivity to Concrete Confinement Constant

To further demonstrate the importance of the correct selection of a confinement constant let us examine several typical steel-free bridge deck configurations. Each configuration will be analysed using the rational model with all input parameters, except the confinement constant held constant. The value of the confinement constant will be varied from Richart's value of 4.1 to the proposed value of 10. The effect of the varying **k** value on the predicted failure load and deflection will be examined.

Three bridge deck configurations will be examined. The important input parameters are the spacing of the girders, Sg, the thickness of the deck, **d**, the compressive strength of the concrete, $\mathbf{f'_c}$, the area of the tire print, **A**, the equivalent loaded area diameter, **B**, the restraint stiffness, **K**, the distance between the centerline of the load patch and the centerline of the closest strap, **Ss**, and the yield strain of the strap, ϵ_y. The values for each case study is given in Table 2.3.

Table 2.3. Input Parameters for Sensitivity Case Studies

Case	S_g (mm)	d (mm)	f'_c (MPa)	A (mm^2)	B (mm)	K (N/mm/mm)	S_s (mm)	ϵ_y
1	2700	300	39	125000	477.5	246	0	0.0015
2a	2000	200	30	125000	477.5	300	0	0.002
2b	2000	200	30	125000	477.5	300	500	0.002
3	1067	100	46	32258	244.5	630	0	0.002

The theoretical results from the rational model are given in Table 2.4. A ratio is calculated for the deflection or load at the given value of **k** over the value corresponding at $\mathbf{k = 10}$. The predicted mode of failure is also noted as *concrete* for crushing of the concrete and *strap* for yielding of the strap.

It can be seen from Case 1 in Table 2.4 that the value of the confinement constant does not have a significant effect on the predicted results when the punching failure is initiated by yielding of the straps. However, Cases 2 and 3 illustrate that the choice of the proper confinement constant is essential when crushing of the concrete initiates the punching failure.

Table 2.4 Concrete Confinement Constant Sensitivity Results

Case	k	δ (mm)	δ/δ_0	P (kN)	P/P_0	mode
1	10.0	10.29		1073		strap
	8.0	10.29	1.00	1058	0.99	strap
	6.0	11.14	1.08	1029	0.96	strap
	4.1	11.14	1.08	1088	1.01	strap
2a	10.0	12.00	-	851	-	strap
	4.1	12.74	1.06	801	0.94	concrete
2b	10.0	15.98	-	1047	-	concrete
	4.1	12.75	0.80	800	0.76	concrete
3	10.0	7.00	-	415	-	concrete
	4.1	5.65	0.81	313	0.75	concrete

2.5 Lateral Restraint Constant

In equation (9) of the rational model the lateral restraint stiffness provided by the straps was designated as **K**. It has been noted in Section 2.2, that the level of lateral restraint has a significant effect on the punching failure load. Many researchers have acknowledged this fact and some attempted to include the lateral restraint stiffness as a model parameter, most notably Hewitt and Batchelor (1975). However, a value of **K** for a given bridge deck configuration is not given but rather back calculated from experimentation once the failure load is known. The relative simplicity of the steel-free bridge deck system allows us to examine this term more carefully and arrive at a reliable method of calculating a value for restraint stiffness directly.

To facilitate a better understanding of the contribution of the straps, let us examine in detail the situation shown in Figure 2.9. The straps have an overall length equivalent to the centre to centre spacing of the girders, S_g, and each strap has a cross-sectional area, A_s. The spacing of the straps is given as S_s. If we consider the strap directly beneath the load, then we know from our rational model that the elongation at either end of the strap from the rotation of the

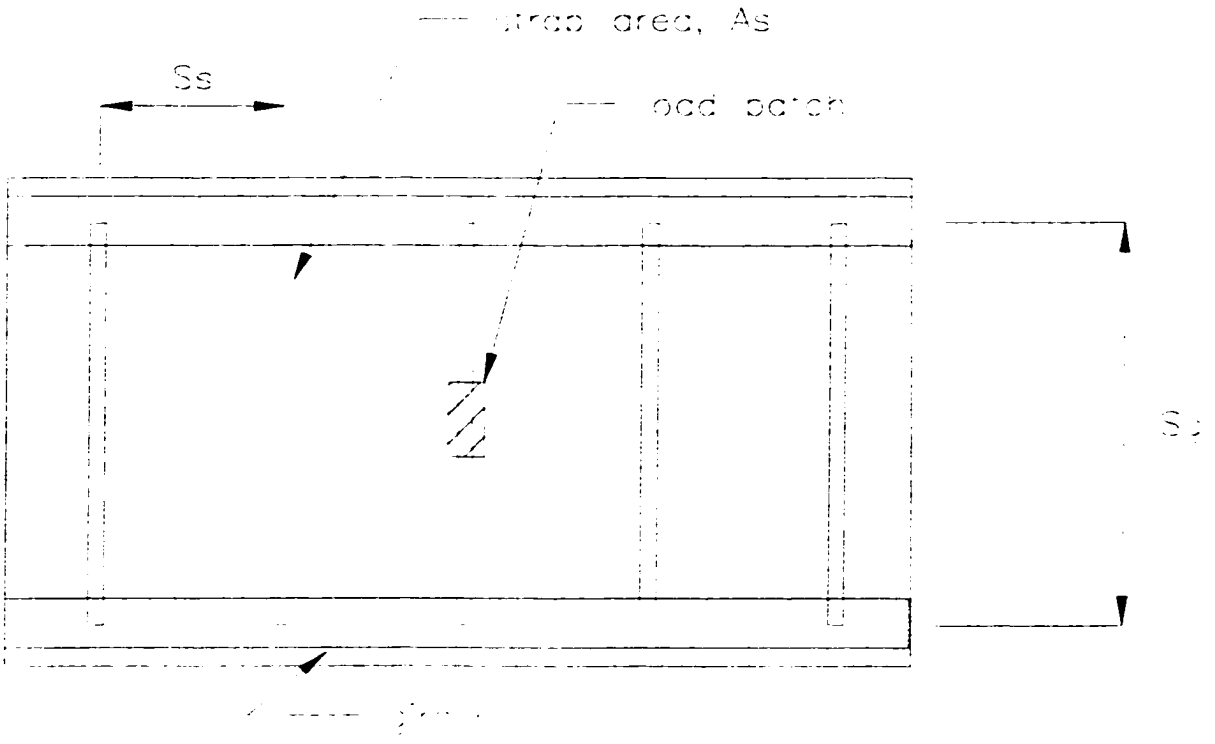

Figure 2.9 Plan view of steel-free bridge deck

wedge is Δ_t. The strap can be seen to have a total elongation of $2\Delta_t$. We know from strength of materials that the force in the strap is given by equation (41a).

$$F = \frac{EA_s}{L} \cdot 2\Delta_t \qquad \textbf{(41a)}$$

where **E** is the modulus of elasticity of the strap and **L** is the overall length of the strap. Equation (9) is of the form

$$F = K \cdot \Delta \qquad \textbf{(41b)}$$

It would appear therefore that the restraint stiffness term can be expressed as

$$K = \frac{EA_s}{\frac{S_g}{2}} \qquad \textbf{(42a)}$$

where S_g is substituted for **L** in equation (41a). However, in equation (9), **K** has units of force per displacement per unit length of circumference of a wedge. In equation (41), **K** has units of force per displacement. The zone of influence of an individual strap is considered to be half the distance to its adjacent straps. This is equivalent to $S_s/2$ on either side of the strap. The total zone of influence for one strap is therefore S_s. If we now considered the stiffness value as calculated in equation (42a) to be evenly distributed over this zone of influence then we arrive at the following equation for restraint stiffness in units of force per displacement per unit length

$$K = \frac{EA_s}{\frac{S_g}{2} \cdot S_s} \qquad \textbf{(42b)}$$

A further refinement can be made if we consider the situation of a welded connection between the strap and the girder flange. If the strap is welded all around to the girder flange then the effective length of the strap free to elongate with a prismatic cross-section of A_s is actual S_g minus the width of the girder flanges or simply the clear spacing between the top flanges of the adjacent girders. For connection details other than welding (Bakht and Mufti, 1996) the length of the strap may be greater or smaller than S_g. Therefore, equation (42b) should be re-written using the term S_l to designate the effective length of the strap.

$$K = \frac{EA_s}{\frac{S_l}{2} \cdot S_s} \qquad \textbf{(43)}$$

Equation (43) is a conservative estimate of the lateral restraint stiffness of the system and is seen to give good results when used to predict the failure of the half-scale and one third scale experimental models tested by others (Newhook et al., 1995).

The conservative nature of Equation (43) arises from two considerations. Firstly, the equation neglects any contribution of the girders themselves in resisting the lateral deflection

from the rotating wedges. Azad et al. (1994), Ebeido and Kennedy (1996) and Kuang and Morley (1992) all acknowledge the fact that the girder size will affect the amount of lateral restraint provided to the deck. Intuitively, for the strap directly below the load to elongate and displace laterally, one of two situations must occur. Either the girder itself must displace laterally as a rigid body or the girder must bend to the appropriate lateral deflected shape. The former situation is obviously improbable; therefore, the girder must have a deflected shape. This requires that it contribute to the restraint stiffness of the system. Secondly, equation (43) neglects the effect of the proximity of the strap to the point of load application. In Figure 2.9, the strap directly beneath the load is contributing to the lateral restraint in the manner predicted by equation (43). The adjacent straps are not contributing as greatly to the lateral restraint; however, their contribution is not negligible. The influence of individual straps lessens farther away from the load point. This is seen in the small strap levels in straps far away from the point of load reported by Thorburn and Mufti (1995). The interaction of the straps, the deflected shape of the girders and the effect of load proximity is very complicated to describe exactly and may only be possible using full finite element models of the system. A reasonable approximation of this behaviour is to consider the system to be a beam on elastic supports in the lateral direction as shown in Figure 2.10. The beam properties are determined from the flexural rigidity of the girder in the lateral direction and the elastic support properties are determined from the straps by equation (44).

$$K' = \frac{EA_s}{\frac{S_l}{2}} \tag{44}$$

Each spring represents a strap and is spaced equivalent to actual strap spacing, S_s.

As before in deriving equation (43), we need to calculate a value of restraint stiffness in force per displacement per unit length. For a particular tire load location, as shown in Figure 2.11, the response of the system along a unit length centred on the tire print has the most influence on the punching behaviour. The resultant force, **P**, for a 1000 mm width of slab is applied

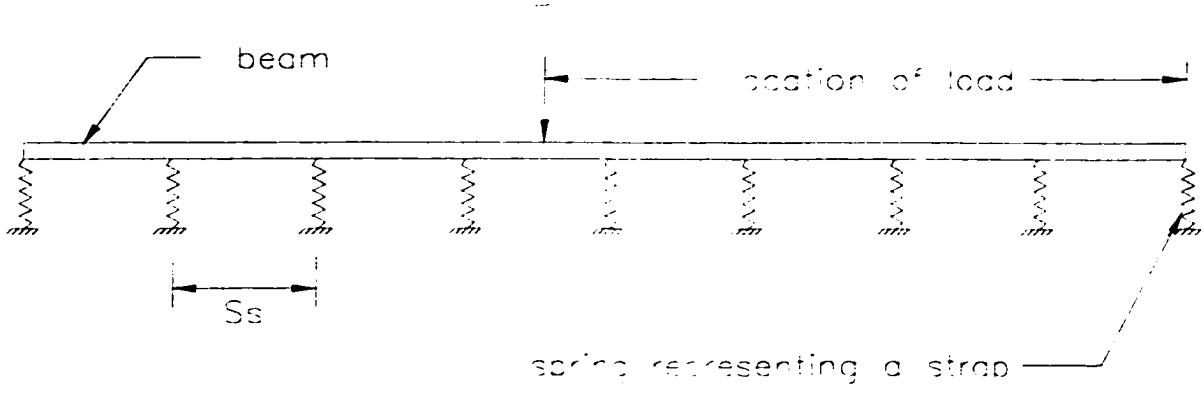

Figure 2.10 Beam on elastic supports model

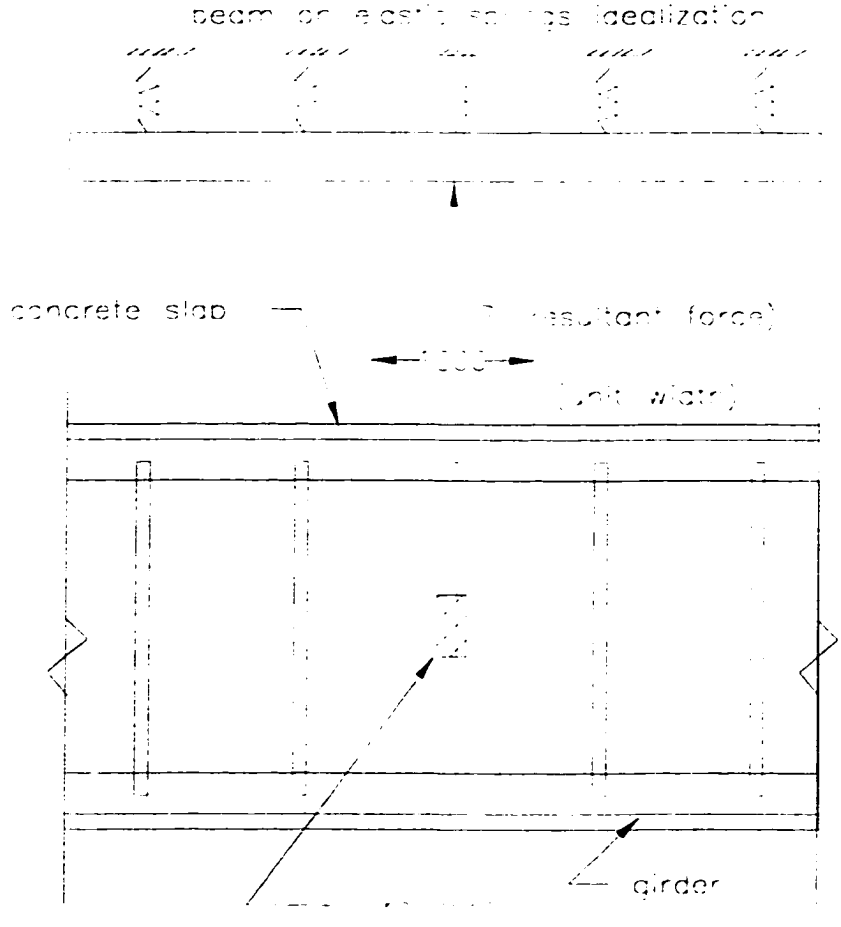

Figure 2.11 Unit width of slab for determination of restraint stiffness

at the centerline of the tire print. A deflection is calculated from beam on elastic springs analysis for a unit load at **P**. The restraint stiffness is calculated as the unit load divided by the deflection. Remembering that **P** is the resultant force for a unit width, the calculated stiffness is assumed to be uniformly distributed over that width. This yields a value for the restraint stiffness term **K** in units of force per displacement per unit length. The actual response of the system is obviously more complex; however, the advantage of this method is that it reduces the behaviour to one characteristic value, **K**, which can be easily calculated. In addition, the level of approximation is consistent with other idealizations made in the rational model development.

This approximate method of calculating restraint stiffness is very simple and versatile. It allows for calculation of restraint stiffness at any location along the beam and the inclusions of parameters not covered by equation (43) such as changing the girder size, having variable strap spacing and having variable strap sizes.

2.5.1 Experimental Testing for Restraint Stiffness

An experimental program was designed to test the validity of the beam on elastic springs method of calculating lateral restraint stiffness. The testing helped to determine the appropriate beam properties to input into the model and the contributions of intermediate diaphragms to lateral restraint stiffness. A steel frame for a steel-free bridge deck system was constructed as shown in Figure 2.12. Two W 610 x 241 steel girders were spaced 2700 mm apart and simply supported at the ends. Nine steel straps of 100 x 12.5 mm dimensions were welded to the top flanges of the girders at a spacing of 1200 mm centre to centre. At each end a C 380 x 50 channel was bolted to the girder flanges and a K - type diaphragm was constructed from L 100 x 100 x 10 sections as shown in Figure 2.13a. At mid-span a full X-type diaphragm was constructed, again using L 100 x 100 x 10 sections as shown in Figure 2.13b. A lateral load was applied to the top flanges of the girders using the setup shown in Figure 2.14 and the lateral deflections recorded. This procedure was repeated at the five locations indicated in Figure 2.12. Once the five tests had been completed, the transverse

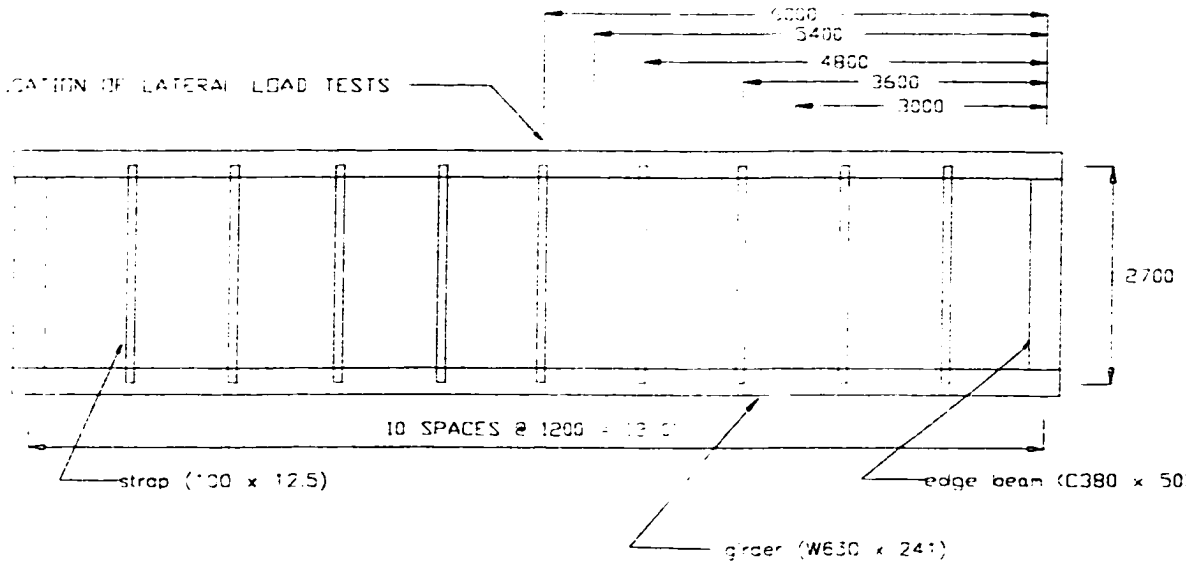

Figure 2.12 Location of lateral load tests

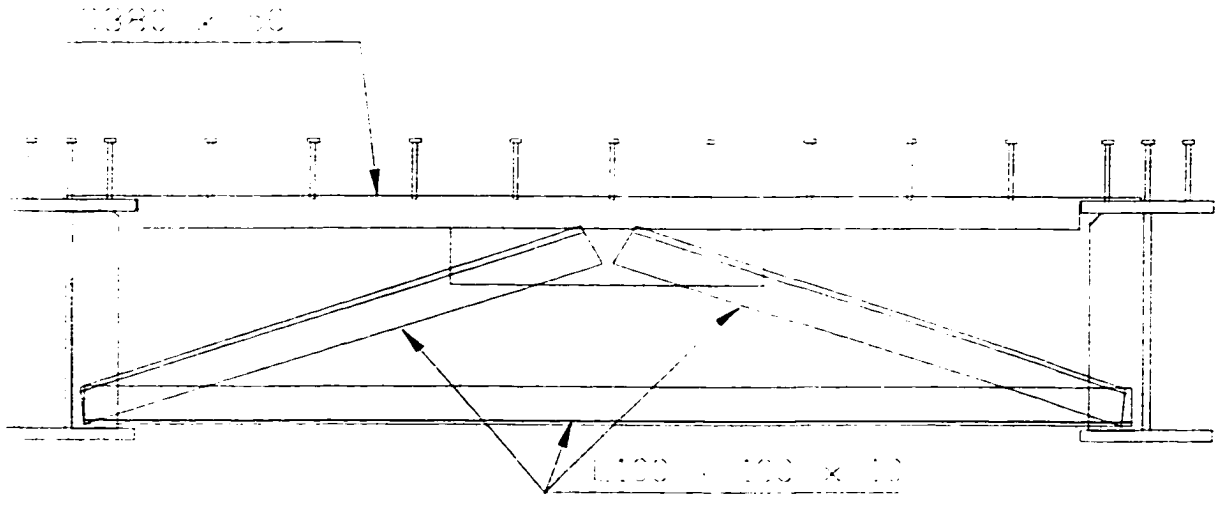

Figure 2.13a K-type diaphragm

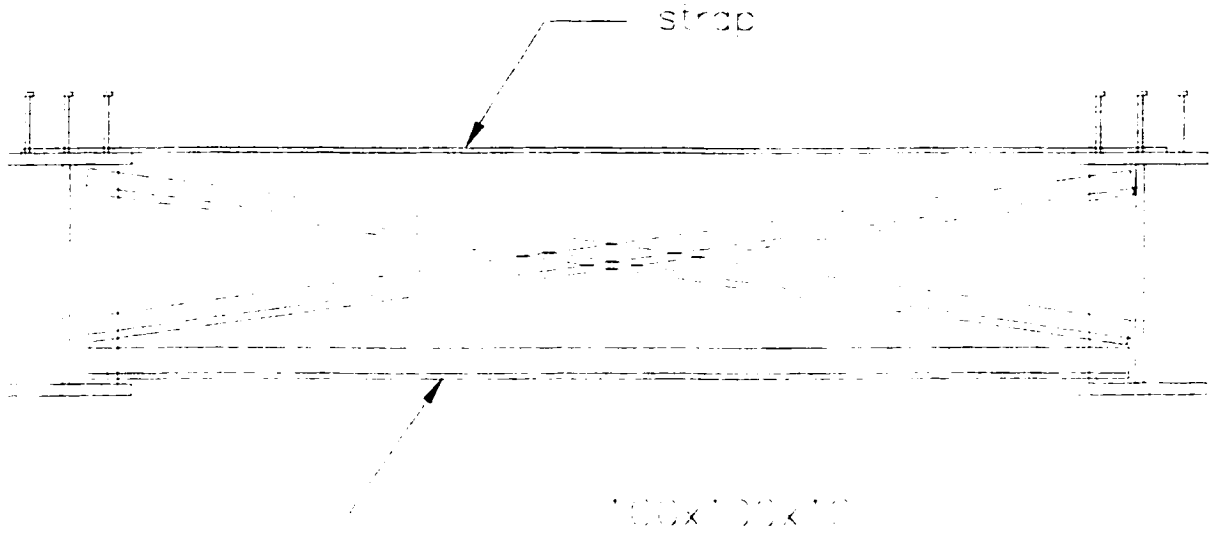

Figure 2.13b X-type diaphragm

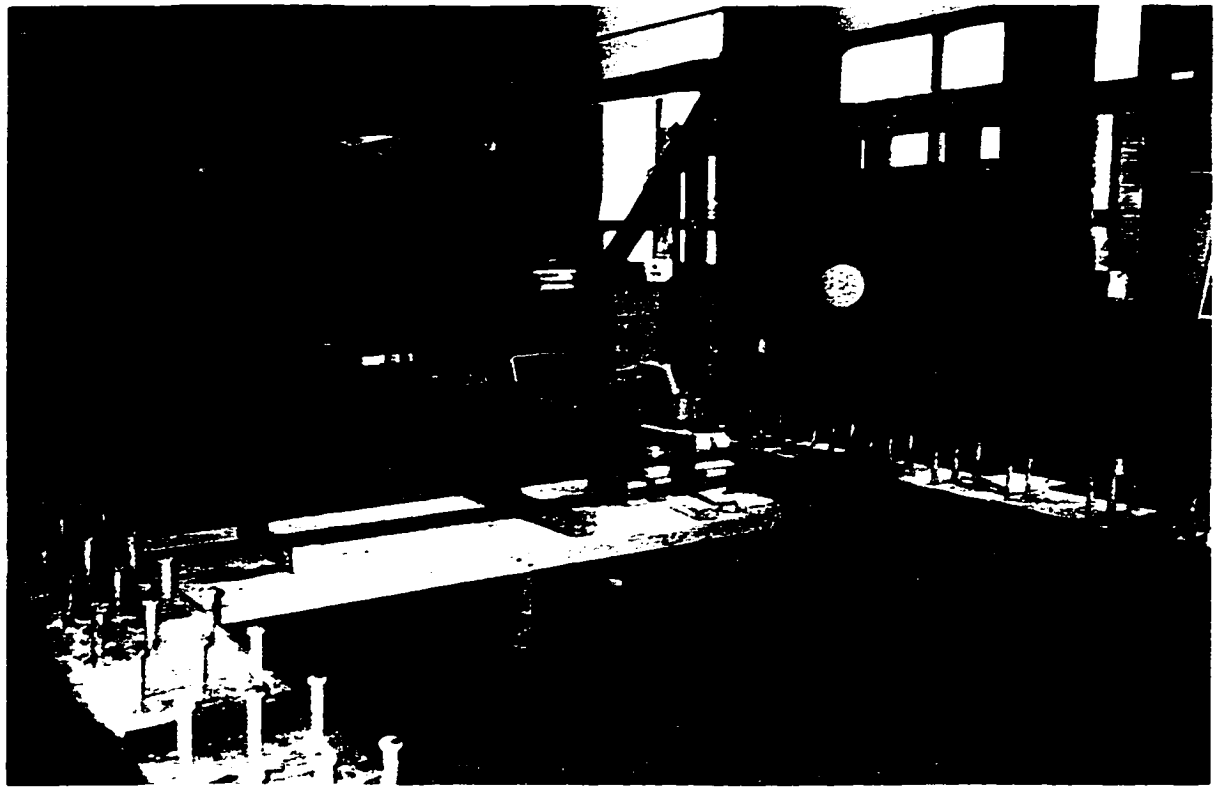

Figure 2.14 Experimental lateral load setup

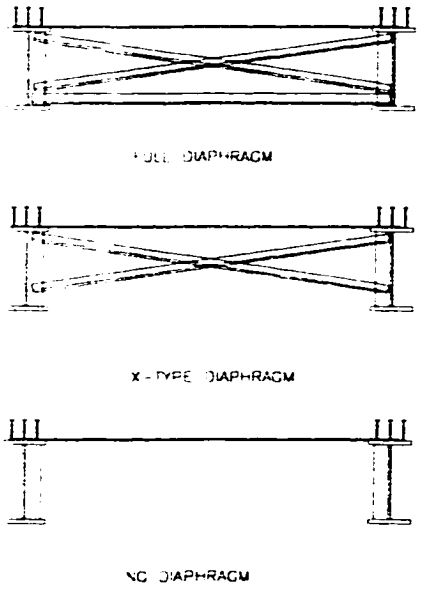

Figure 2.15 Removal of diaphragm at mid-span

chord of the full X-type diaphragm was removed leaving only the two diagonal members to form an X-type diaphragm at mid-span as opposed to a full diaphragm. The five lateral load tests were repeated. Finally, both diagonals were removed, Figure 2.15, leaving no intermediate diaphragm in the system. The five lateral load tests were repeated. For each set of load-deflection data linear regression analysis was performed and the lateral restraint stiffness determined. This is the equivalent of dividing the applied load by the measured deflection to determine a restraint stiffness value for the point of load application.

2.5.1.1 Diaphragm Contribution

It is important to assess the effect of intermediate cross-bracing on lateral restraint stiffness. Intermediate cross-bracing of bridge girders is typically constructed using L sections in one of the two configurations shown in Figure 2.13. These diaphragms are spaced no more than 7 500 mm apart along the length of the girders. If their effect on lateral restraint is significant, then they must be included in the calculations and can perhaps be used to optimize strap design. The experimental restraint stiffness value for each of the three tests sets are given in Table 2.5.

Table 2.5. Restraint Stiffness Values (N/mm/mm) for Lateral Load Experiment

Test Set		1	2	3
Mid-Span Diaphragm Type		Full	X-Type	None
Test Number	Location			
1	3 000	262	264	256
2	3 600	270	330	336
3	4 800	286	290	302
4	5 400	262	242	232
5	6 000	318	296	282

Note: Test 2,3,5 are at strap locations; Test 1,4 are midway between straps.

It can be seen from Table 2.5 that, at the diaphragm location, the effect of the diaphragm on lateral restraint stiffness is less than 12% of the total stiffness and quickly diminishes as the load moves away from the diaphragm location. It is also seen that the X-type bracing has a lesser effect than the full X-type bracing. Ignoring the diaphragms in the lateral restraint calculations is a reasonable and marginally conservative simplification for design purposes. Their inclusion would not lead to any significant reduction in strap size or spacing.

This finding is consistent with the findings of other researchers who have investigated the effects of diaphragms on bridge behaviour. Stallings et al (1996) reported that under field loadings the strains in the channel type diaphragms of a simple span steel girder bridge were small and that their removal had little effect on load distribution in the bridge superstructure. Azizinamini et al. (1995) performed laboratory testing on steel girder bridge models with both K-type and X-type diaphragms. They report that the diaphragms have little effect on the behaviour of bridges after construction.

2.5.1.2 Beam on Elastic Supports Model

For the test configuration given in Figure 2.12, a beam on elastic springs model was developed and analysed. The input parameters for this model are given in Table 2.6. The end springs were modelled from the properties of the C 380 x 50 channels and the nine

intermediate springs were modelled from the properties of the straps. In both cases equation (44) was used to calculate the spring constants. The theoretical analysis was carried out with two different values of moment of inertia for the girders. Initially the moment of inertia for both the top and bottom flange was used and then the analysis was repeated using the moment of inertia of just the top flange. A unit load of 1000 kN was applied at the location of the test load and the deflection calculated using finite element analysis. The restraint stiffness was calculated by dividing 1000 kN by the calculated deflection and distributing the stiffness over a unit width of 1000 mm. The results are given in Table 2.7. The restraint stiffness value as calculated using equation (43) is also shown.

Table 2.6. Beam on Springs Input Parameters

Elastic Spring Parameters			
	Area	Length	K' (Equ. 44)
Channels (C 380 x 50)	6430 mm^2	2700/2 = 1350 mm	476 296
Straps (12.5 x 100)	1250 mm^2	2370/2 = 1185 mm	210 970
Beam Parameters (W 610 x 241)			
		Moment of Inertia	
Case 1 (top and bottom flanges)		184 x 10^6 mm^4	
Case 2 (top flange only)		92 x 10^6 mm^4	

Table 2.7 Restraint Stiffness Comparisons (N/mm/mm)

Experimental		$I_{top\ and\ bottom\ flange}$			$I_{top\ flange}$			**Equ. (43)**	
Location	K_{exp}	δ (mm)	K_{theor}	K_{theor}/K_{exp}	δ (mm)	K	K_{theor}/K_{exp}	K	K_{theor}/K_{exp}
3000	256	3.12	321	1.25	3.93	254	0.99	176	0.69
3600	336	2.89	346	1.03	3.34	299	0.89	176	0.52
4800	302	2.89	346	1.16	3.34	299	0.99	176	0.58
5400	232	3.13	319	1.38	3.93	254	1.09	176	0.76
6000	282	2.89	346	1.23	3.34	299	1.06	176	0.62
average				1.21			1.00		0.63

In a beam on elastic support analogy the critical beam properties are the modulus of elasticity and the moment of inertia for bending in the lateral direction. For the moment of inertia it would seem appropriate to use the moment of inertia corresponding to that of the top and bottom flanges. However, as can be seen from Table 2.7, using the moment of inertia of the top flange only yields a much better correlation with experimental results. It can also be seen that the **K** value from equation (43) is conservative and, on average, only 63% of the experimental restraint stiffness.

Several conclusions can be drawn from this experiment. Firstly, it verifies that the girders do play a significant role in providing lateral restraint to the system; in this case it was an average of 37% of the total value. It should be clarified that the girders have two inter-related mechanisms for providing this additional stiffness. One mechanism is the lateral bending stiffness of the girder itself. The other mechanism is to transfer load through this bending action to straps that are some distance away from the load point such that every strap participates in the lateral restraint based on its proximity to the load point. Secondly, the beam on elastic springs model appears to be a reliable method of predicting the lateral restraint stiffness at any given location along the length of the girder. Finally, the restraining stiffness appears to be provided mostly by the top flange and not the entire depth of the section. This is reasonable when one considers that the load is applied directly to the top flange and that the restraint straps are also connected directly to this flange. The web itself is weak in lateral bending and the connection between the web and the flanges is weak in rotation about the longitudinal axis. Therefore, force transfer to and engagement of the bottom flange in the restraint system is minimal, particularly in the region local to the load point. This situation is true for any steel W-type section or plate girder section and will be more prevalent as the depth of such sections increase. Similar testing has not been performed for concrete girder sections; however, extrapolation of these results would suggest that considering only the top flange of an I-shaped precast prestressed concrete girder would be conservative.

2.5.2 Restraint Stiffness verses Load Location

The experimental and theoretical work presented in Table 2.5 and Table 2.7 reveal that there is a relationship between the location of the load and the magnitude of the lateral restraint stiffness. Most noticeably, when the load is directly between two straps, the restraint stiffness is lower than when the load is directly at a strap. This is evident in all experimental results and in the beam on elastic supports theoretical results. The relative difference between the two locations is obviously affected by the spacing of the springs and the relative stiffnesses of the straps and girder. Equation (43) can not predict this phenomenon as it predicts the same value of restraint stiffness along the entire length of the girder. The beam on elastic springs model can provide a reliable estimate of this behaviour.

The experimental results in Table 2.7 also suggest that there is a trend towards slightly lower stiffness values as the load moves closer to the mid-point of the girder span. The theoretical results do not reflect this same trend. The beam-on-springs model is however, a simple idealization of the system and it is not unreasonable that in actual behaviour the restraint is marginally softer towards the mid-span of the girders. It would also be expected that as the load point moved closer to the support points or the ends of the girders, the lateral restraint stiffness would decrease. Experimental results are not available; however, the beam on springs model can provide a useful tool in assessing this effect. A parameter that will affect these results is the stiffness of the last spring. In the models used in Table 2.7 the end springs were modelled on the end channels (see Table 2.6). As the point of load application moves closer to this stiffer spring its influence will be greater. While the other springs may be considered to be system parameters, the end springs can be considered as boundary conditions. In general, one of three boundary conditions may be chosen: the end may be pinned such that no displacement is possible, the end of the girder may have a spring with the same stiffness as the rest of the straps in the system, or the end spring may be modelled on the properties of the edge beam which is the C 380 x 50 channel for the experimental setup given.

To test both the effect of the boundary condition and the effect of the load location on the lateral restraint stiffness, the same beam-on-springs model was analysed for three different cases. In the first case, the end spring was given very large stiffness to simulate a pinned end condition. In the second case, the end spring was given the stiffness corresponding to the end channel. In the third case, the end spring was given the same stiffness as the other straps in the system. In each case the analysis was performed with the load moving from the end of the girder, location 0, to the mid-span of the girder, location 6000. The load was moved in increments of 600 mm thereby alternating between a strap location and directly between two straps. The results are given in Table 2.8.

Table 2.8 Assessment of the Effects of Load Location and Boundary Conditions

	Case 1		**Case 2**		**Case 3**	
	$K'_{end} = 10^{10}$		K'_{end}=952592		K'_{end}=210970	
Load Location	δ (mm)	K (N/mm/mm)	δ (mm)	K (N/mm/mm)	δ (mm)	K (N/mm/mm)
0	0	∞	2.05	488	4.49	223
600	3.06	327	3.55	282	4.12	243
1200	3.48	287	3.51	285	3.54	282
1800	3.98	251	3.98	251	3.99	251
2400	3.33	300	3.34	299	3.34	299
3000	3.93	254	3.93	254	3.99	254
3600	3.34	299	3.34	299	3.34	299
4200	3.93	254	3.93	254	3.93	254
4800	3.34	299	3.34	299	3.34	299
5400	3.93	254	3.93	254	3.93	254
6000	3.34	299	3.34	299	3.34	299

It can be seen from Table 2.8 that up to 1800 mm from the end of the girder the boundary conditions and the proximity of the load to the end of the span both have an effect on the lateral restraint stiffness values. After this point the restraint stiffness remains constant for

each case, varying only based on whether it is directly over a strap or between two straps. These results are valid only for the configuration and system parameters given. However, they do indicate that modelling of end conditions is important only when the load is near the ends of the girders.

It can be seen that the beam on elastic supports model is a very effective and simple method of estimating the lateral restraint stiffness of the system. As shown in this section it is also versatile and able to account for different parameters with relative ease and accuracy. The models investigated in this section involved systems where all the straps had the same stiffness, except at the boundary, and the straps were all evenly spaced. In the Chapter 3, the model will be used to account for the effects of both varying strap sizes within the same model and in Chapter 4, the model will be used to account for the effect of varying strap sizes within the same model. The simple model of equation (43) cannot fully account for these parameters.

3 VERIFICATION OF RATIONAL MODEL FROM EXISTING EXPERIMENTAL DATA

Previous experimental work by others on steel-free concrete bridge decks was outlined in Chapter 1. This work consisted mostly of a steel free concrete deck slab on a series of two or three equally spaced girders. The girders were connected by transverse steel straps welded to the top flanges of the girders. Each deck was tested to failure to determine the experimental punching load. Each of these experimental tests has now been analysed using the rational model of Chapter 2 and the theoretical punching load and deflection at failure determined. This comparison verifies the validity of the rational model in predicting steel-free bridge deck behaviour. In addition, two reinforced concrete decks, for which detailed experimental data was available, were analysed using the rational model. This comparison verifies that the rational model can predict the behaviour of bridge decks in general and leads to a better understanding of the mechanism of failure of reinforced concrete bridge decks. All these comparisons are presented below.

3.1 Half-Scale Models at TUNS

A complete description of all half-scale model testing performed at TUNS can be found in Mufti et al. (1993) and Newhook et al. (1995). The relevant geometric and material properties for each of these models is given in Table 3.1.

Table 3.1 Geometric and Material Properties of Half-Scale Test Decks

Test Deck	1	2	3	4	5a	5b
Girder size	W460x82	W460x82	W460x82	W460x82	W460x82	W460x82
Girder Spacing (mm)	1067	1067	1067	1067	1067	1067
# of Girders	2	2	2	3	3	3
Strap Size (mmxmm)			64 x 10	64 x 10	64 x 10	64 x 10
Strap Spacing (mm)			457	457	457	610
Deck Thickness (mm)	100	100	100	100	95	95
Concrete f'_c (MPa)	30	30	46	42	43	51
Load Area (mmxmm)	127 x 254	127 x 254	127 x 254	127 x 254	127 x 254	127 x 254
Edge Beam Size	C200x17	C200x17	C200x17	C200x17	C200x17	C200x17

It should be noted that Test Deck 5a and 5b are the same deck but the tests were performed at different locations. This was done because two different strap spacings were used on either side of the mid-span of the girders (Newhook et al., 1995). As well, Test Decks 1 and 2 did not have steel straps, similar to those shown in Figures 1.2 and 1.3. Instead, these decks had a number channel sections (C 200 x 17) that were connected to the web of the W 460 x 82 as shown in Figure 3.1 and 3.2. While these channels were not connected directly to the top flanges of the girders, they were connected very close to the top of the web and did have some influence on lateral restraint stiffness. The amount of influence is not easily calculated without the use of a three dimensional finite element analysis or experimentation. However, as will be demonstrated later, the restraint stiffness can be back calculated using the rational model and the known experimental failure load. It is also important to note that this system of channels remained in place for Test Decks 3, 4 and 5. Again, this makes it difficult to account for the effect of these channels, even using a beam on springs model as outlined in Section 2.5. Therefore, equation (43) will be used as a first approximation of the lateral restraint stiffness of the system. Obviously the stiffness for Test Decks 1 and 2 can not be calculated in this manner. The calculated stiffness values are given in Table 3.2.

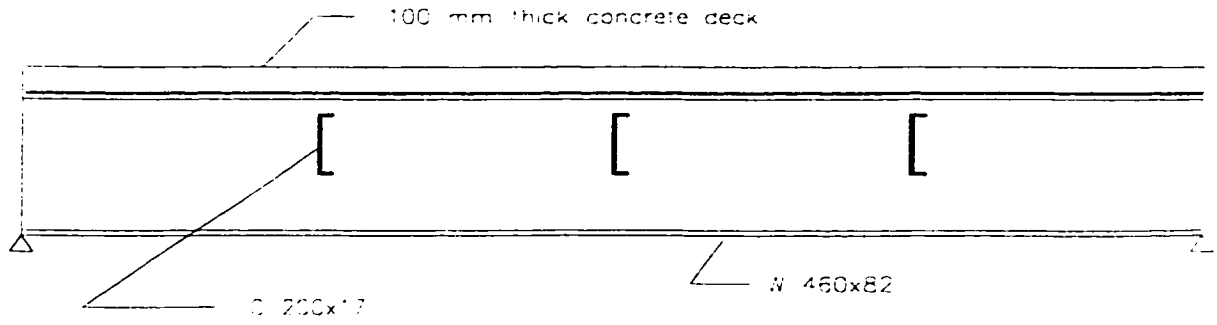

Figure 3.1 Elevation of half-scale model 1

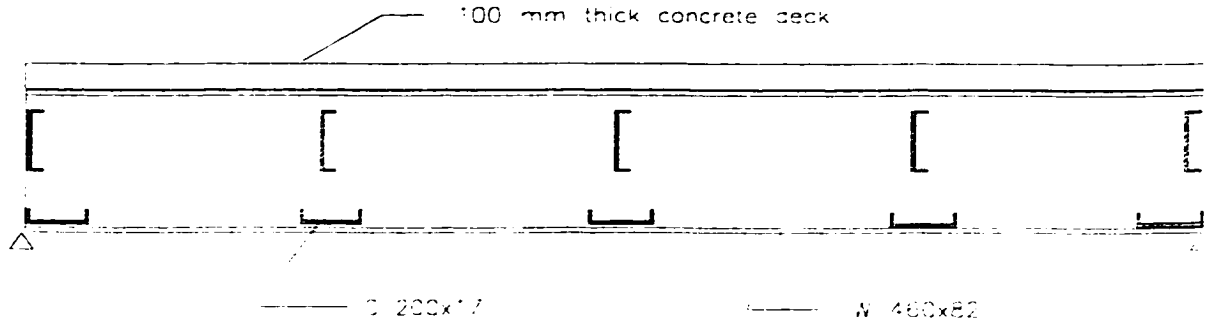

Figure 3.2 Elevation of half-scale model 2

Table 3.2 Lateral Restraint Calculations for Half-Scale Tests Using Equation (43)

Test Deck	E_s (MPa)	L_s (mm)	A_s (mm^2)	S_s (mm)	K (N/mm/mm)
1	200 000	438	640	-	-
2	200 000	438	640	-	-
3	200 000	438	640	457	640
4	200 000	438	640	457	640
5a	200 000	438	640	457	640
5b	200 000	438	640	610	480

First, let us consider Test Decks 3 through 5b. Table 3.3 contains the input parameters for the rational model.

Table 3.3 Input Parameters for Rational Model

Model Parameter	Test 3	Test 4	Test 5a	Test 5b
C (mm)	1067	1067	1067	1067
B (mm)	244.5	244.5	244.5	244.5
K (N/mm/mm)	640	640	640	480
Strap to Load (mm)	0	0	228	305
d (mm)	100	100	95	95
f'_c (MPa)	46	42	43	51
β	0.72	0.75	0.75	0.68
k (confinement)	10	10	10	10
load patch area (mm^2)	32258	32258	32258	32258
ϵ_y (strap)	0.002	0.002	0.002	0.002

For each case, the theoretical punching load and ultimate deflection are compared with the available test results. As can be seen in Table 3.4, the rational model predicts very closely the behaviour of the deck.

Table 3.4 Comparison of Rational Model Results for Half-scale Test Decks

Test Deck	P_{exp} (kN)	P_{theor} (kN)	δ_{exp} (mm)	δ_{theor} (mm)
3	418	415	5.9	7.0
4	418	409	7.1	7.0
5a	370-388	362	5.5	5.6
5b	313	315	6.5	6.0

Note: Test 5a was performed twice and therefore has two failure loads

The comparison in Table 3.4 shows very close agreement between the theoretical results from the rational model and the experimental test decks. The deflection data for Test Decks 5a and 5b are plotted in Figure 3.3 and Figure 3.4 It can be seen that for Test Deck 5a the theoretical

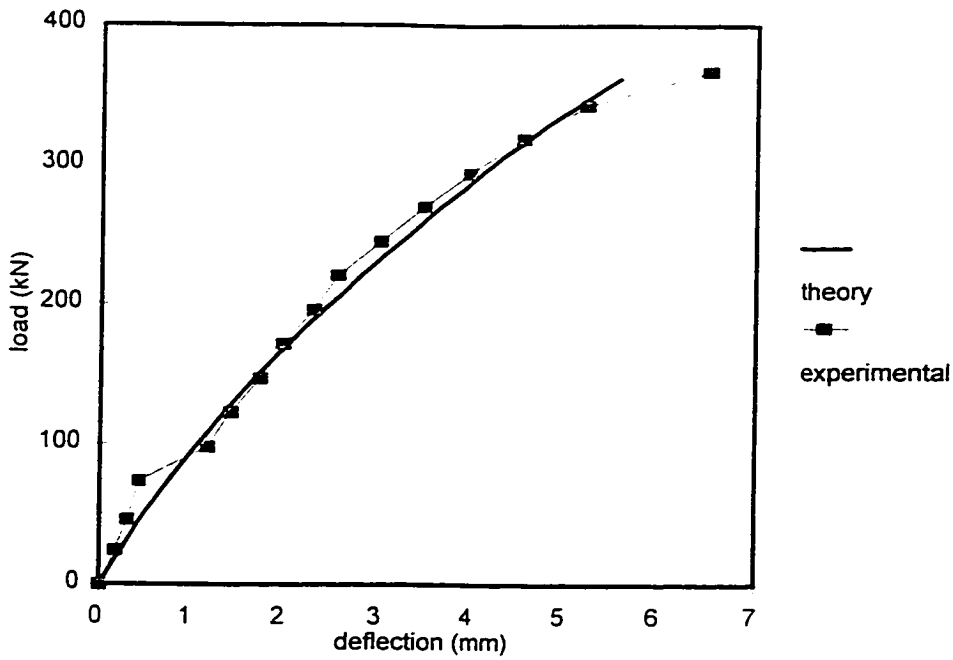

Figure 3.3 Load-deflection curve for Test 5a

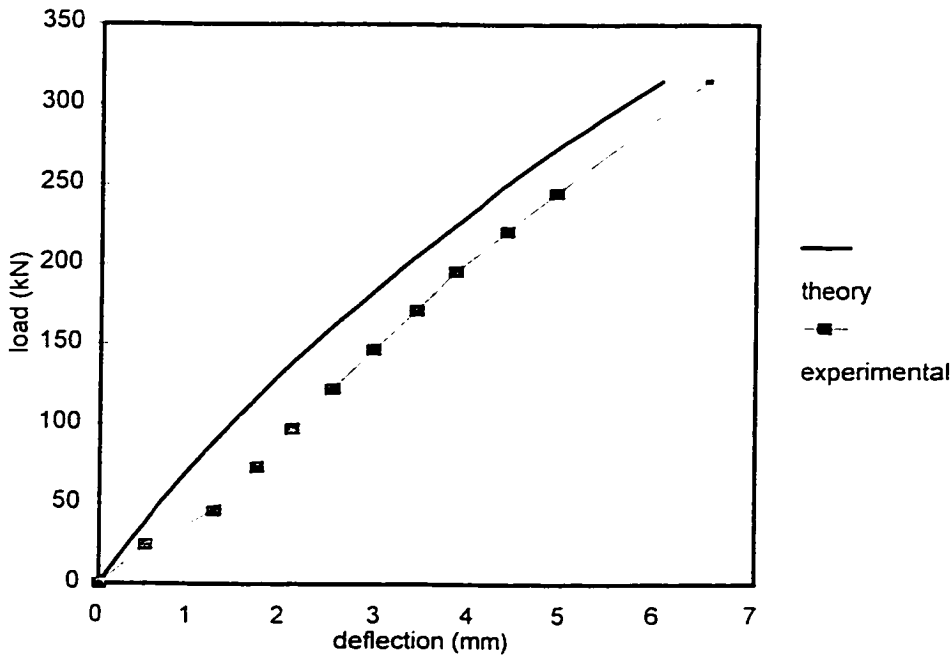

Figure 3.4 Load-deflection curve for Test 5b

load-deflection curve is in very good agreement with the experimental data. For Test Deck 5b the experimental curve is of the same general form as the theoretical; however, it is offset by approximately 0.5 mm. It is noted that the experimental curve exhibits a "jump" at approximately 50 kN. This shift is presumably due to cracking of the deck and redistribution of forces. The results therefore validate that the rational model can predict the load capacity and deflection behaviour of these decks.

Although the restraint stiffness was calculated using equation (43), which as discussed in Chapter 2 is believed to be conservative, the restraint stiffness values of Table 3.2 would appear to be correct. This is reasonable if we consider that two other effects discussed in Chapter 2 are influencing this value. Equation (43) is believed to be conservative because the influence of the girder stiffness and the proximity of all the straps to the point of load application is not included in the calculations. This effect increases the value of K. However, the close proximity of the load to the end of the girder span was also pointed out to have the effect of lowering the value of K. It is not unreasonable that the effects of these two parameters balance each other and the value from equation (43) is very close to the actual value.

Considering Test Decks 1 and 2, it was stated that the restraint stiffness could not be directly calculated because no straps were used. The situation is further complicated by the fact that neither Test Deck 1 or 2 failed in a pure punching mode but rather in a manner more consistent with the instability snap-through mode. However, we can use a method of back-calculation to demonstrate that the rational model can predict this behaviour as well. Figure 3.5 plots failure load versus restraint stiffness for the geometric and material properties of Test Decks 1 and 2 as given in Table 3.1. Both the curve for instability (snap-through) failure and the curve for punching failure are shown. Knowing that the deck failed by instability we can plot the failure loads on the instability curve and extend the points downward to the restraint stiffness axis. Doing so we get restraint stiffness values of approximately 60 N/mm/mm for Test Deck 1 and 85 N/mm/mm for Test Deck 2. The punching failure curve

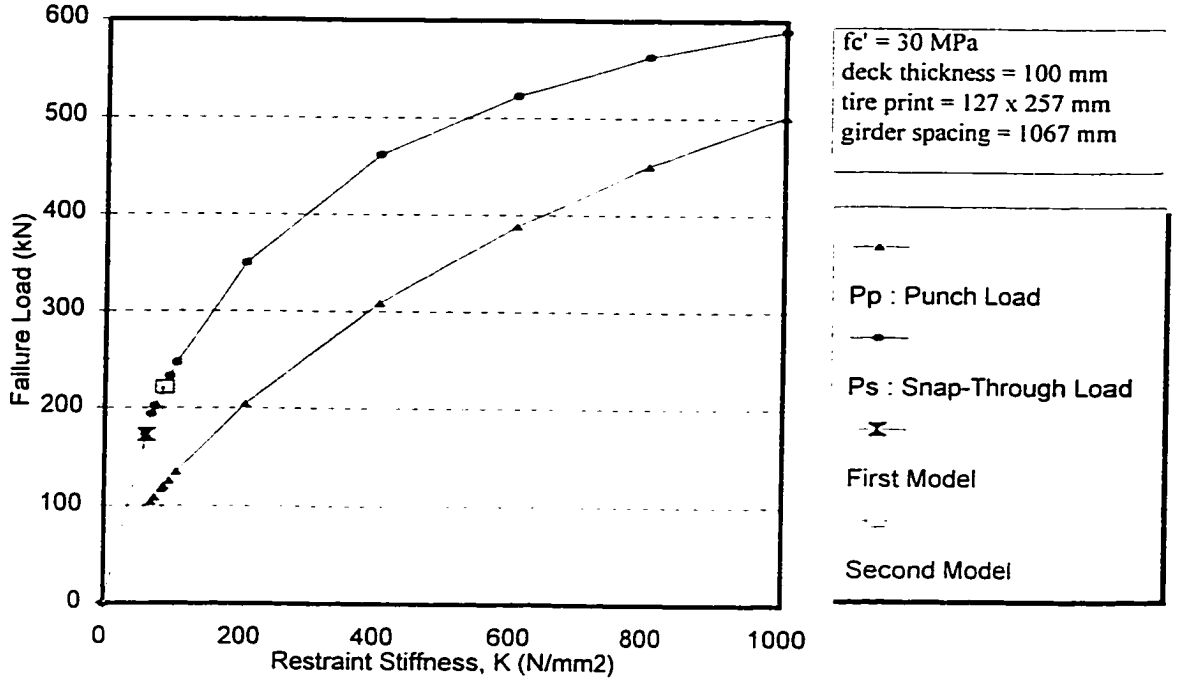

Figure 3.5 Failure load versus restraint stiffness for half-scale tests 1 and 2

begins at a K value of approximately 75 N/mm/mm which means that punching failure will not occur at restraint stiffness below this value. Test Deck 1 clearly falls into this category. Test Deck 2 appears to be on the limit of instability versus punching failure. As with most stability problems, the mechanism can be easily influenced by small deviations from ideal conditions such that bridge decks with restraint stiffness values close to the limit may initial indicate punching but ultimately fail in instability. Mufti et al. (1993) describe this very situation when discussing the failure of Test Deck 2. Therefore, it can be concluded that even in situations of very low restraint stiffness where punching does not occur, the rational model can indirectly predict the behaviour of the bridge deck system. A further conclusion regarding Test Deck 2 is that decks should not be designed with restraint stiffness very close to the lower limit to avoid the undesirable instability failure mode.

3.2 Skewed Bridge Deck Model

Bakht and Agarwal (1993) tested a one-third scale model of a laterally restrained, steel-free bridge deck with a skew angle of 45° and demonstrated that punching failure was possible even with large skew angles. The relevant model parameters for input into the theoretical model are given in Table 3.5. The rational model is used to predict the failure load and ultimate deflection of punching tests that were performed near the centre of this test model. The results of this comparison are given in Table 3.6. Once again the model gives results consistent with the reported experimental work.

Table 3.5 Input Parameters for Skewed Bridge Deck Model

Model Parameter	Value
Girder spacing (mm)	800
Strap Size (mmxmm)	64x9.5
strap spacing (mm)	400
deck thickness	80
f'_c (MPA)	56
β	0.65
Load area (mm^2)	23358
E_s (MPa)	200 000
A_s (mm2)	608
L_s(mm)	660
S_s(mm)	400
K (N/mm/mm)	921
k (confinement constant)	10
ϵ_y	0.002

Table 3.6 Comparison of Theoretical and Experimental Results for Skewed Deck

	P_{exp} (kN)	P_{theor} (kN)	δ_{exp} (mm)	δ_{theor} (mm)
Skewed Deck	323-352	388	5.5-8.0	5.2

3.3 Full-Scale Bridge Deck at TUNS

Thorburn and Mufti (1995) tested a full-scale two-girder steel-free bridge deck. The bridge girders spanned 12 000 mm with straps spaced every 1000 mm and edge beams at either end. In total, 11 straps and 2 edge beams were used. The testing program was designed to evaluate the effect of varying the strap size, and consequently the restraint stiffness, to experimentally optimize of the strap system. Because several tests could be performed along the length of the deck, several different sizes of straps were initially used and changed as the optimization testing continued. In all, eight separate punching tests were performed. The general geometry of the test setup which remained constant for all tests is given in Table 3.7. The strap configuration for each test is given in Table 3.8. The location of the load in reference to the end of the girder span is also given.

Compared to the half-scale model tests, the system for the full-scale test was clean. The support system contained girders, straps and three diaphragms. No channels or other sections were connected to the web. Therefore a beam on elastic springs model could be easily constructed to calculate the lateral restraint stiffness values. The model contains a spring for each edge beam and one for each of the eleven straps. In this manner, the model accounted for the effect of the varying strap sizes along the length of the beam. The bending properties of the beam were taken from the characteristics of the top flange only, giving a moment of inertia of 92×10^6 mm^4. A summary of the spring and beam properties are given in Table 3.9. The spring stiffness are calculated using equation (44) and the properties given in Tables 3.7 and 3.8.

Table 3.7. Geometry of TUNS Full-Scale Deck

Model Parameter	Value
Girder Size	W 610x241
Girder spacing (mm)	2000
# of girders	2
strap spacing (mm)	1000
deck thickness	175
f'_c (MPa)	27
β	0.85
Load area (mm^2)	250x500
E_s (MPa)	200 000
A_s (mm^2)	varies
L_s(mm)	1670
S_s(mm)	1000
edge beam size	2 L150x150x20
k (confinement constant)	10
ϵ_y	0.0015

Table 3.8. Strap Size (mm^2) for Each Load Test

		Strap Number										
Test	Location	1	2	3	4	5	6	7	8	9	10	11
1	1 500	2500	2500	2500	1875	1875	1875	1250	1250	1250	950	950
2	7 500	2500	2500	2500	1875	1875	1875	1250	1250	1250	950	950
3	10 500	2500	2500	2500	1875	1875	1875	1250	1250	1250	950	950
4	4 500	2500	2500	2500	650	650	650	1250	1250	1250	950	950
5	9 000	2500	2500	2500	650	650	650	650	650	650	650	950
6	6 000	2500	2500	2500	650	650	650	650	650	650	650	950
7	1 500	2500	2500	2500	650	650	650	650	650	650	650	950
8	4 500	2500	2500	2500	650	650	650	650	650	650	650	950

Table 3.9 Spring Properties for Beam-on-Springs Model for Full-Scale Deck

Area (mm^2)	K' (N/mm)
edge beam	
11 200	2 715 000
straps	
2500	598 800
1875	449 100
1250	299 400
950	227 550
650	155 700

For each load case the restraint stiffness value was determined and the ultimate failure load was calculated from the rational model. For purposes of comparison, the restraint stiffness value as calculated by equation (43) was also used to predict the failure load. The results of each are compared in Table 3.10 along with the experimental failure loads reported by Thorburn and Mufti (1995). Unfortunately, the ultimate deflection values from the experimental results were not available for comparison.

Table 3.10 Comparison of Punching Failure Loads for Full-Scale Deck

		Beam-on-Springs			Equation (43)		
Test	P_{exp} (kN)	K (N/mm^2)	P_{theor} (kN)	P_{theor}/P_{exp}	K (N/mm^2)	P_{theor} (kN)	P_{theor}/P_{exp}
1	1127	592	1087	0.96	599	1094	0.97
2	923	387	860	0.93	300	693	0.75
3	911	315	745	0.82	228	565	0.62
4	844	250	608	0.72	156	403	0.48
5	576	265	491	0.85	156	317	0.55
6	715	265	491	0.69	156	317	0.44
7	785	592	1040	1.32	599	1094	1.39
8	687	250	608	0.89	156	403	0.59

Based on the ratio of theoretical load to experimental load for the two methods of calculating restraint stiffness as shown in Table 3.10, it can be concluded that the beam-on-spring model produces better results than the Equation (43) model. From Table 3.10 the theoretical predictions are much better for Tests 1 and 2 than for the other tests. The test numbers indicate the order in which the testing occurred. Therefore crack patterns formed from Test 1 and 2 may have had some influence on the experimental results of Test 3. This situation would continue to occur through to Test 6. For Tests 7 and 8 the punch cones from Tests 1 and 4 were removed and the void filled with new concrete. Tests 7 and 8 were then performed in the exact same location. For these tests, the radial and circumferential cracks outside the shear cone existing from initial loading. Failure at Test 7 is believed to have occurred prematurely due to some slippage at the conical shell interface with the shear cone. However, it is important to note that the failure load was significantly large and that the deck was behaving as predicted up to this failure point. The results of Test 8 were more favourable and demonstrate that the mechanisms related to the formation of wedges and subsequent rigid body rotation assumed in the rational are indeed correct. The presence of the existing cracks means that the deck had no flexural capacity as the "yield lines" were already formed at zero load. The load carrying mechanism had to be due solely to the assumptions of arching, wedge rotation and lateral restraint which are the foundations for the rational model. Test 7 and Test 8 are therefore very important validations of the rational model.

It should be noted that Newhook and Mufti (1995) reported different K values and theoretical failure loads for this same set of experimental tests. Although the beam-on-springs analogy was used to calculate the restraint stiffness, the moment of inertia of both the top and bottom flange of the girder was used. Because of the higher moment of inertia for the beam elements, the overall restraint stiffness values were higher, consequently the predicted failure loads reported by Newhook and Mufti (1995) were higher. This theoretical work was performed without the benefit of the results of the lateral load testing described in Chapter 2. The lateral load testing indicated that only the top flange should be included in lateral stiffness calculations and this procedure was followed for the results presented in Table 3.10.

It is worth noting that even though there is a 15% difference in restraint stiffness values reported by Newhook and Mufti (1995) and Table 3.10, there is less than a 10% difference in predicted failure loads for Tests 1,2 and 3. It is also worth noting that the numbers reported in Table 3.10, with the exception of Test 7, do not over estimate the capacity of the steel-free bridge deck structural system.

3.4 Isotropically Reinforced Concrete Bridge Decks

The behavior described by the theoretical model for steel-free bridge deck is believed to be equally applicable to steel-reinforced concrete slab on girder bridge decks. Isotropically reinforced decks designed by the OHBDC empirical method fail in a punching shear mode. The theoretical PUNCH model developed here is tested on two reinforced concrete bridge deck models.

Fang et al. (1986) designed and tested a full scale bridge deck with the reinforcement as shown in Figure 3.6. The level of reinforcement provided was consistent with the OHBDC empirical design criteria. Based on the work with steel-free decks, it is believed that the reinforcement in conventional concrete deck slabs behaves as a lateral restraint mechanism and not as flexural reinforcement. In the lateral direction, the bottom layer of # 4 bars @ 220 mm provides lateral restraint to the system, in a similar manner as steel straps. Analyzing the system with # 4 bars @ 220 mm as straps in a beam on spring model gives K =113 N/mm/mm. The ultimate load reported by Fang et al. (1986) is 631 kN. The ultimate load predicted by the rational model is 627 kN. For comparison, a load deflection curve is given in Figure 3.7. A summary of the comparison is presented in Table 3.11.

Bakht (1996) constructed and tested a one-third scale model of a bridge that had one section steel-free and one section reinforced. In the bottom transverse layer of reinforcement several of the bars were replaced by an instrumented Dywidag bar. A longitudinal section and a cross-section from Bakht (1996) is reproduced directly in Figure 3.8. From the strain results

of this bar, Bakht (1996) demonstrated experimentally that the reinforcement was behaving as a tie and not as flexural reinforcement. The theoretical model was used to predict the punching

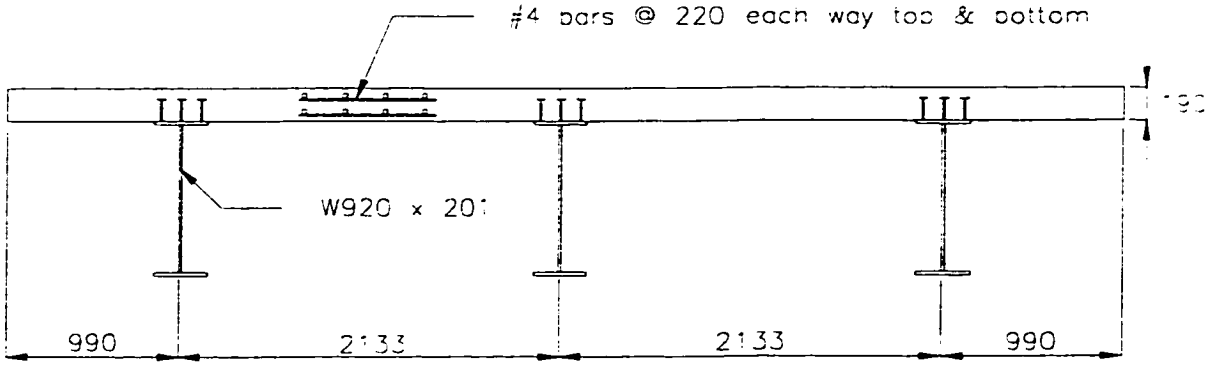

Figure 3.6 Isotropically reinforced bridge deck tested by Fang et al. (1986)

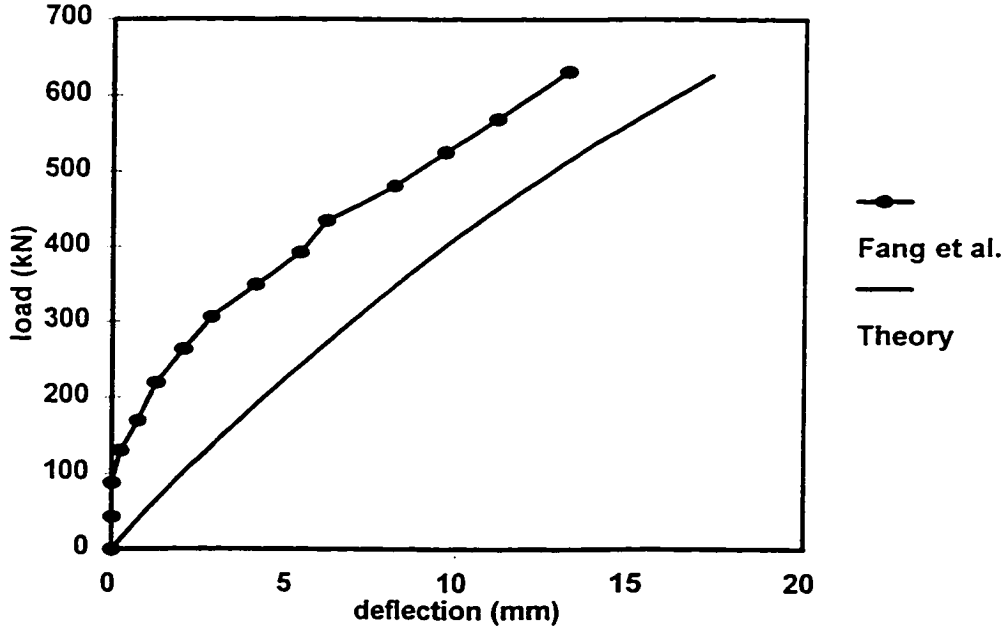

Figure 3.7 Load-deflection curves for test by Fang et al. (1986)

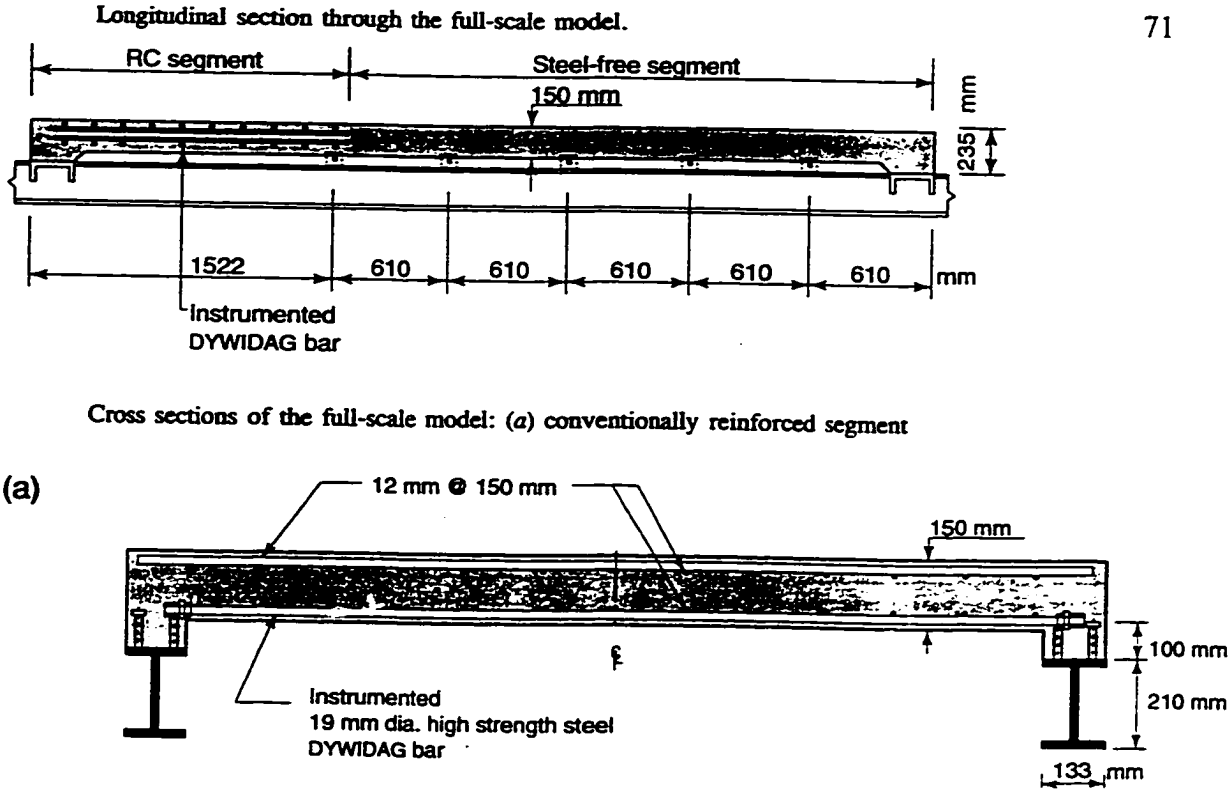

Figure 3.8 Reinforced deck tested by Bakht (1996)

failure of this system. Again the bottom layer of transverse reinforcement is assumed to serve the same function as the steel straps and the appropriate lateral restraint stiffness is calculated. The comparison is presented in Table 3.11.

From these two comparisons, it can be concluded that the same arching behaviour assumed for the steel-free deck occurs in reinforced concrete decks. Hence, the theoretical model presented here can also be used to aid in the design and analysis of these decks.

Table 3.11 Comparison of Theoretical and Experimental Results for Isotropically Reinforced Concrete Decks

Test	S_g (mm)	Straps	Depth (mm)	K (N/mm^2)	Ptheor (kN)	Pexp (kN)	Ptheor/ Pexp
Fang et al.	2133	Rebar	190	200	627	631	0.99
Bakht	2000	Rebar	150	428	629	622	1.01

Hewitt and Batchelor (1975) estimated the lateral restraint empirically. The above discussion indicates that the empirical estimation of lateral restraint stiffness is not necessary. The lateral restraint stiffness can be calculated directly as illustrated.

4 EXPERIMENTAL INVESTIGATION OF BRIDGE DECK BEHAVIOUR

4.1 Experimental Program

4.1.1 Description of Experimental Model

An experimental program was undertaken to examine the behaviour of the steel-free bridge deck structural system. A full scale two girder bridge model was constructed in the lab. The 12 000 mm long girders (W 610 x 241) were spaced 2700 mm apart and were connected at either end by diaphragms. Nine steel straps (12.5 x 100) were welded to the top flanges of the girders and spaced at 1200 mm intervals. The C 380 x 50 channels served as the straps at either end of the span. The fibre reinforced concrete deck was 200 mm thick with 100 mm haunches over each girder. Typical cross-sections and plan views are shown in Figures 4.1 and 4.2.

The mix design and mechanical properties of the fibre reinforced concrete are given in Table 4.1. The mechanical properties of the concrete were tested both before and after the addition of the fibres and are reported accordingly in the Table.

Table 4.1. Fibre Reinforced Concrete Mix Design and Properties

Component	Value
Type 10 Cement	415 kg/m3
Water	160 kg/m3
Coarse Aggregate	980 kg/m3
Fine Aggregate	754 kg/m3
Fibres	7.28 kg/m3
Low Range Water Reducer	1 L/m3
High Range Water Reducer	3 L/m3
Air Content	6.0%
Before Fibres:	
Compressive Strength	41.4 MPa
Modulus of Rupture	6.0 MPa
After Fibres:	
Compressive Strength	39.0 MPa
Modulus of Rupture	5.9 MPa

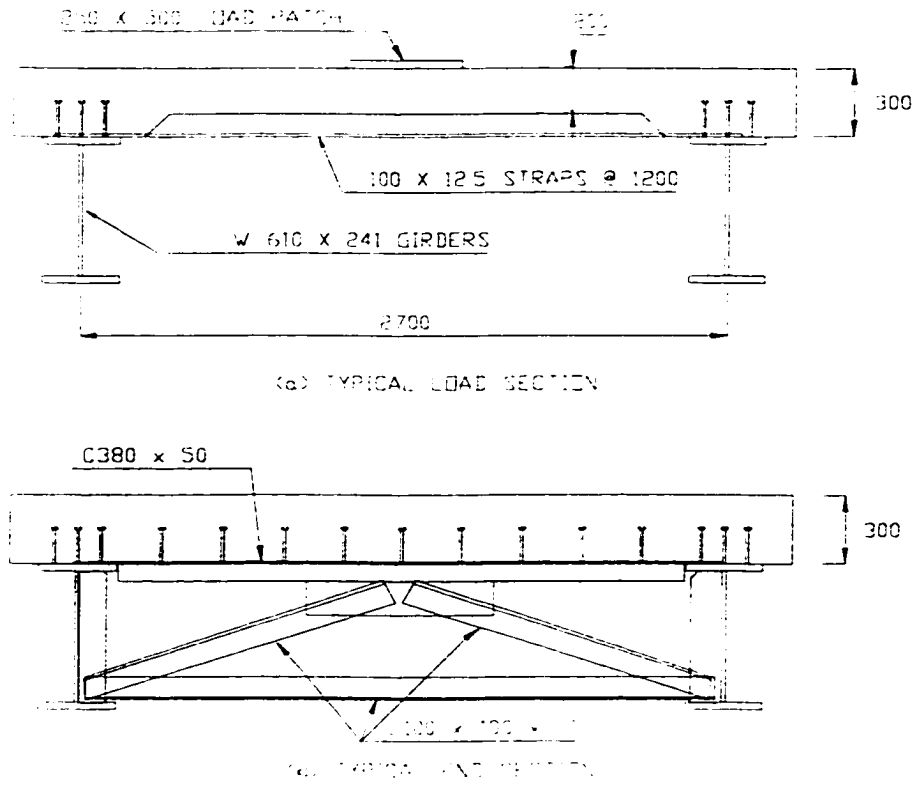

Figure 4.1 Cross-section of test model

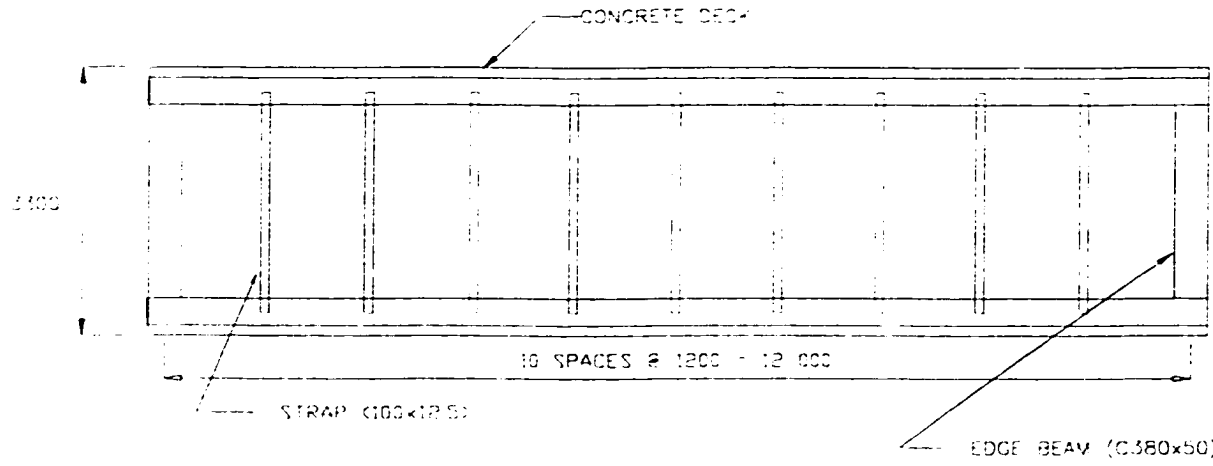

Figure 4.2 Plan view of test model

4.1.2 Description of Instrumentation

In all tests the load was applied using hydraulic cylinders ranging from 50 tonnes to 100 tonnes in capacity. The value of applied load was determined by calibrating the in-line hydraulic pressure with load using a universal testing machine. An electronic foil gauge with a 6 mm gauge length was bonded to each of the nine straps to record the strain during loading. The gauges were located at the midpoint of the underside of each strap and oriented along the length of the strap to measure axial strain. Three electronic strain gauges were also mounted on the web of each girder at the mid-span location. The height of each of these gauges is given in Figure 4.3. The gauges were oriented along the longitudinal axis of the girders to measure flexural strains.

At each load location a series of dial gauges were used to measure deflections. A typical dial gauge setup is shown in Figure 4.4. Six dial gauges were located along a line perpendicular to the girders to obtain the transverse deflection profile of the deck at the point of load application. In addition, two gauges were placed at the top flanges of the girders to measure the horizontal deflection of the girders at the point of load application.

4.1.3 Description of Testing

Initially, a load of 17.5 tonnes was applied to 25 different load points as shown in Figure 4.5. For each load test, all deflection and strain readings were recorded. The 17.5 tonne load range was chosen to be comfortably less than the load which would cause cracking of the slab. The results of this set of testing reflects the linear elastic serviceability behaviour of the deck. The location of each of these tests can be established by referring to grid lines as shown on Figure 4.5. By way of example, load point 1 is load test 4c.

Three ultimate load tests were also performed on the full-scale model and the location of each is shown in Figure 4.6. At the location of load Test 1, the load was cycled between 0 tonnes and 40 tonnes. This was done to investigate any 'shakedown' effect which may occur.

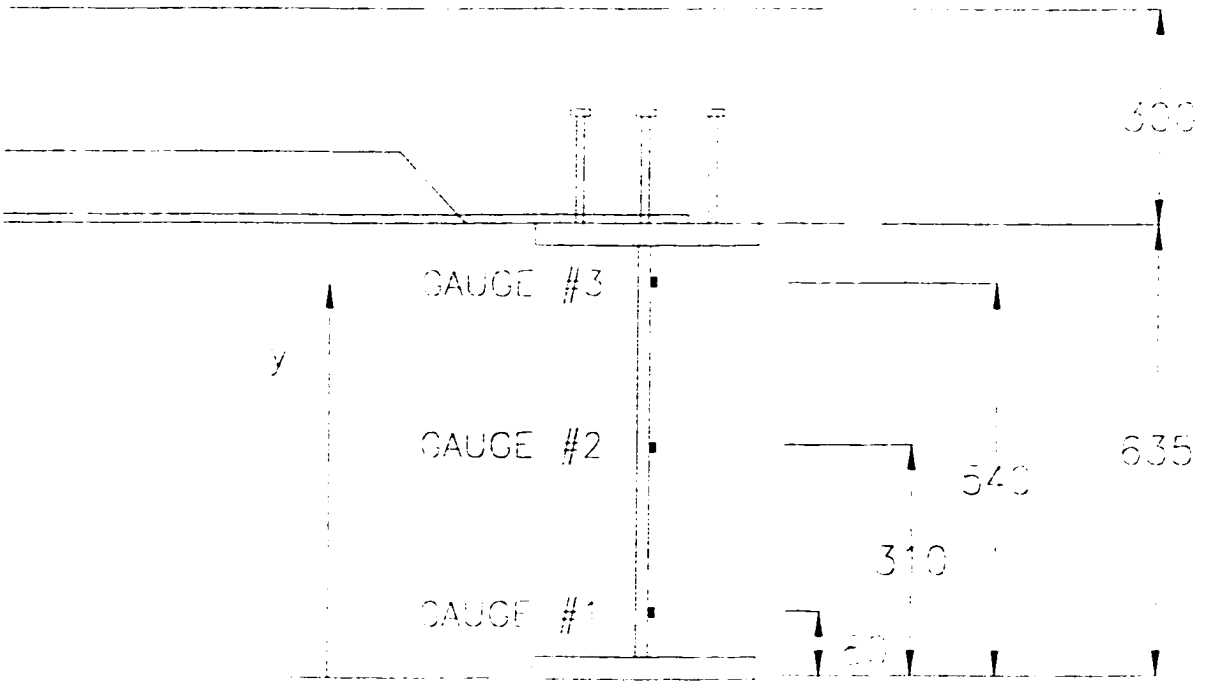

Figure 4.3 Location of gauges on girder web

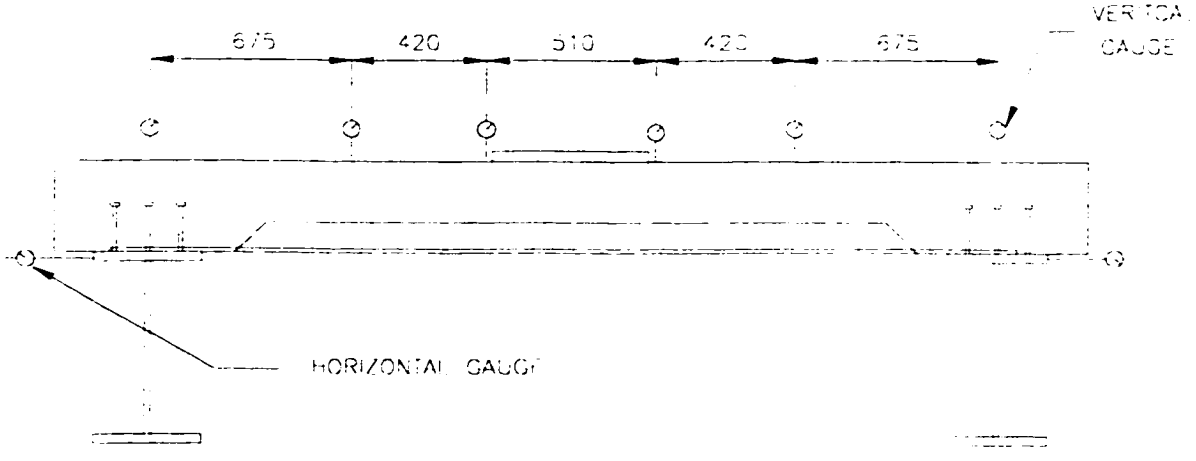

Figure 4.4 Location of deflection gauges

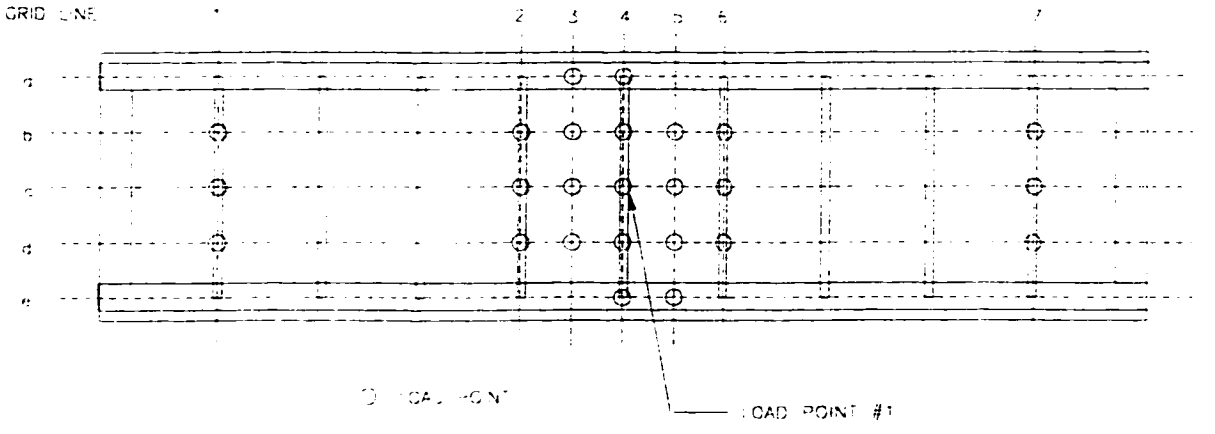

Figure 4.5 Location of 25 service load tests

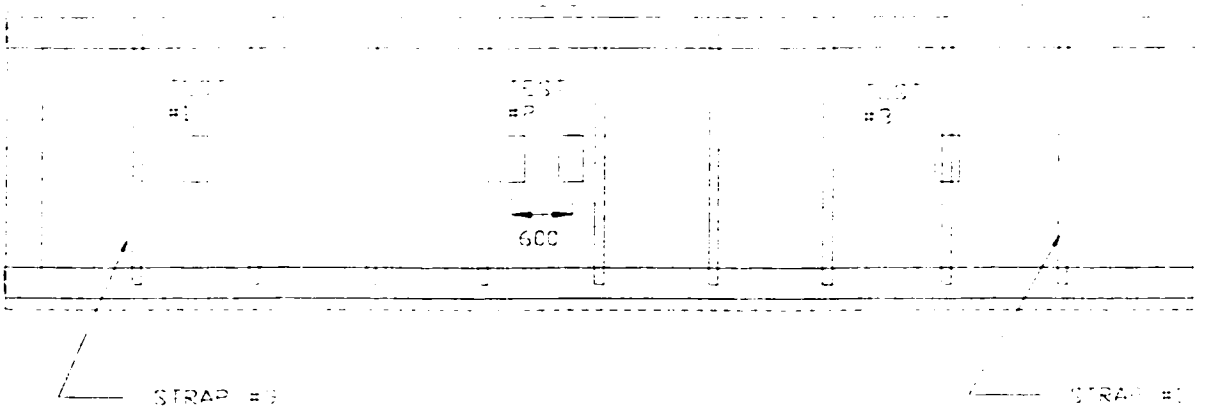

Figure 4.6 Location of ultimate load tests

The shakedown phenomenon was reported by Bakht (1996) and will be discussed later in the context of the test results. After the five cycles of load a single point monotonically increasing static load was applied to determine the behaviour the system up to and at failure.

For load test 2, two loads were applied to simulate the effect of multiple wheel loads which result from the axles of a truck. The was done to investigate how the load effects from one axle may influence the ultimate failure load of another adjacent axle. It is obvious that the proximity of the two loads will have some effect on the degree of influence and it is intuitive that the closer the two loads, the greater the effect. OHBDC gives a design truck where the closest spacing of two axles is 1200 mm. For test 2 an axle spacing of 600 mm was chosen and is believed to be more severe than any situation which may occur on an actual bridge. The load on each point was increased simultaneously such that, at each of the load points, the load was exactly half the total applied load. Due to the capacity of the loading frame and concerns about safety, the testing was stopped at a total load value of 145 tonnes. Although the deck was severely cracked, it still had capacity in excess of this load value. The double axle load was removed and replaced by a single wheel load in the centre of the previous two points. This single wheel load was increased until failure to determine the reserve capacity of the system in a deteriorated state.

For load test 3, the strap directly beneath the load point was removed. This test assessed three key parameters: the reserve capacity of the system in the event of a strap failure, the ability of the structural system to sustain loads by alternate load paths, and the effect of a strap spacing of 2400 mm, which is approximately the clear spacing between the adjacent girders. The deck was initially loaded to 830 kN, causing severe cracking of the deck. The load was removed and then reapplied up to punching failure. This sequence of load is very important in establishing a level of comfort with the structure strength and safety of the steel-free bridge deck structural system. In addition to the strap being removed, the remaining straps had yielded from previous testing and exhibited visible signs of plastic deformation. The concrete deck in general was cracked from load Test 1 and 2 and the concrete surrounding the load point was severely cracked from the initial loading up to 830 kN. The ability of the system to still sustain significant loads in this highly deteriorated condition clearly demonstrates the validity of this design approach.

4.2 Experimental Behaviour of the Structural System

The behaviour of the bridge deck system can be divided into two categories: the behaviour before cracking of the concrete deck slab and the behaviour after the cracking of the slab. Data on the former comes from the 25 service load testing points and the initial stages of the first ultimate load tests. Data for the latter comes from the three ultimate load tests. The observed behaviour of the system in both the uncracked and cracked condition is reported.

4.2.1 Deformations

The general deflected shape of the deck before cracking is similar to that of most rectangular bridge deck slabs on steel girders. The girders deflect longitudinally in proportion to their load acceptance and stiffness. The deck deflects transversely as a structural slab spanning two supporting girders. A typical transverse deflection profile, taken from test 4c, is shown in Figure 4.7. In addition, Figure 4.7 shows the deflection profile for test 4b and 4d in which the load is not applied at the mid-span of the deck. Similar deflected shapes can be seen in all load tests b, c and d gridlines. The noteworthy aspect of the transverse deflection profile is that it is not a smooth sagging shape similar to that of a simply supported beam. Although there are only five deflection points, it is clear that the deflected shape has some reverse curvature at the ends. This indicates that some moment is being taken at the ends of the span due to the rotational stiffness of the girders. This is typical of composite bridge deck construction. The importance of this fact is it demonstrates that in the uncracked condition the steel-free deck has positive and negative bending stresses. To examine the deflection profile after cracking we compare three deflected shapes from ultimate load test 1 shown in Figure 4.8. The first curve represents the deflected shape in the uncracked stage and shows the reverse curvature near the girders. The second curve represents the deflected shape after cracking has occured on the underside of the slab. Again the reverse curvature can be seen near the girders indicating that they are still carrying some moment. The final curve represents the deflected shape just prior to failure. At this point the deck is cracked on the topside near the girders.

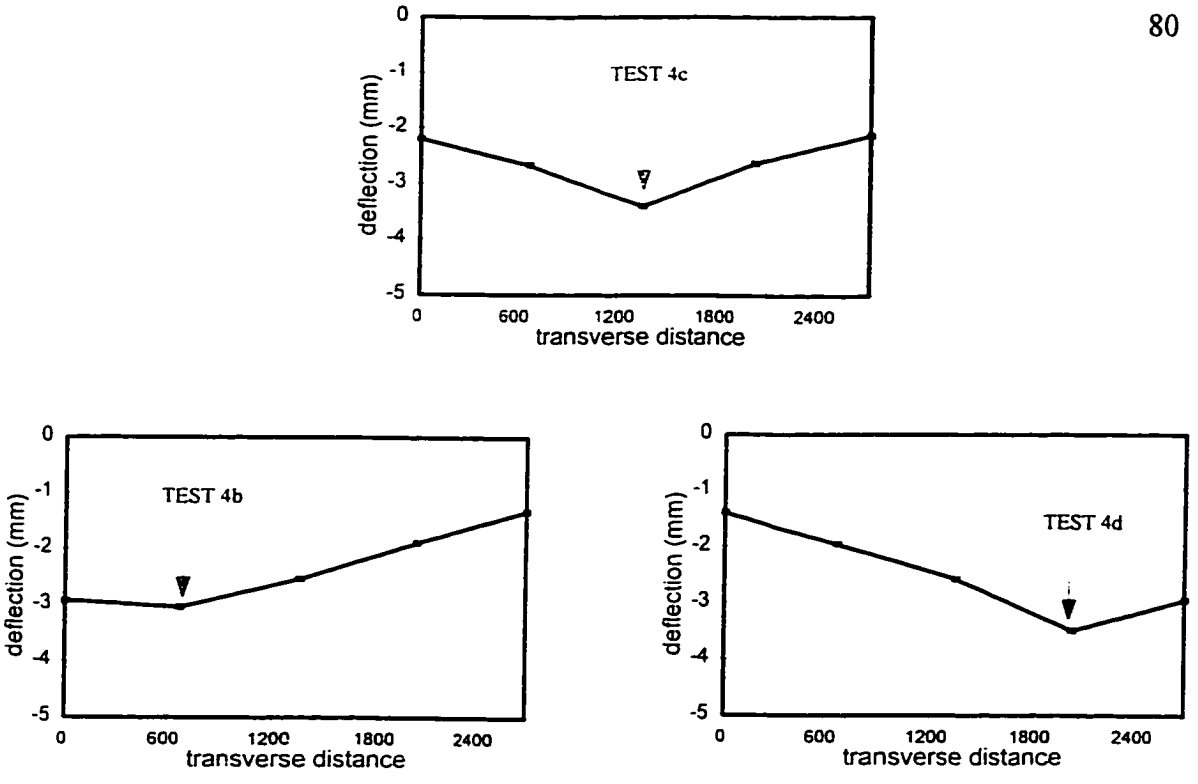

Figure 4.7 Transverse deflection profiles for tests 4b, 4c and 4d

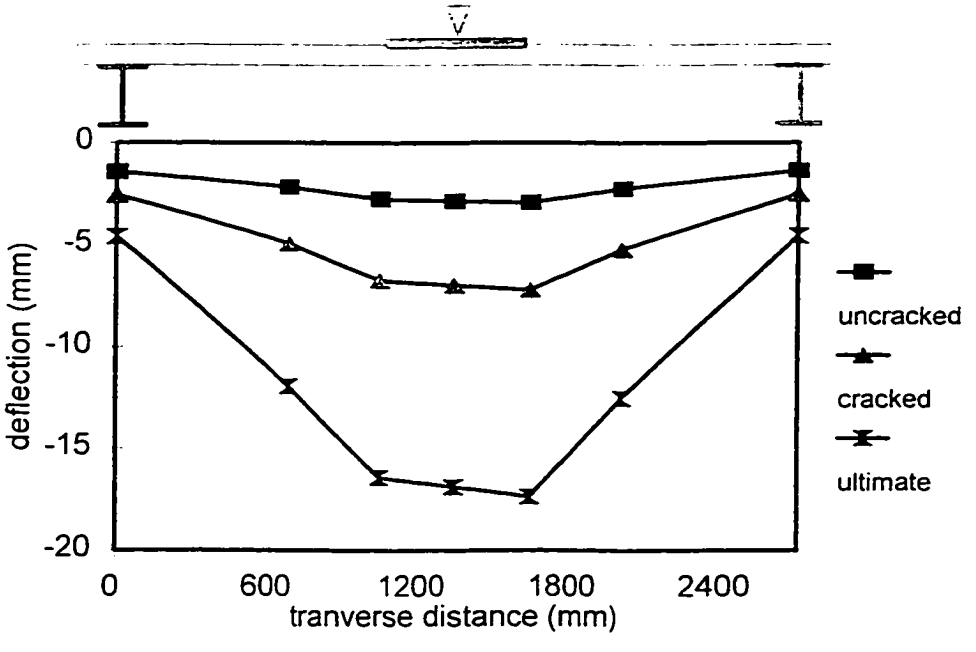

Figure 4.8 Transverse deflection profile from ultimate load test 1

This curve can be seen to be flattened out near the girders indicating that the girders are no longer carrying any negative moment and the deflection of the deck is now governed purely by the rotation of the wedges.The deflected shape of the deck with a load applied directly over one of the two girders is shown in Figure 4.9 for tests 4a and 4e as well as load test 5e and 3a. Common to all these curves is the fact that the deflected shape resembles a hogging moment deflected shape. This indicates that with a load directly over a girder, the deck was almost entirely in negative bending moment stresses. Because cracking had not occurred, it is safe to assume that the bending stresses in this situation at a wheel load of 17.5 tonnes does not exceed the tensile capacity of the concrete.

A further important deformation in the system is the lateral deflection of the girders, and in particular the top flanges of the girders. The rational model assumes that the top flanges displace away from the point of load application due to the rotation of the wedges. Using test 2c as a typical example, it can be seen in Figure 4.10 that the flanges do move laterally away from the load point even before cracking of the deck occurs. Using the data from ultimate load test 1, it is again demonstrated that the girders rotate away from the load, Figure 4.11. During ultimate load test 1, cracking of the deck occurred at a load of approximately 48 tonnes. This can be seen in the change in slope of the lateral deflection curve. The lateral deformation occurs at a greater rate after cracking as the deflection is governed by the rotation of the wedges rather than the bending of the deck. To further verify this outward displacement of the girders, the deflection values for a load of 17.5 tonnes for all load tests on grid line c are shown in Figure 4.12.

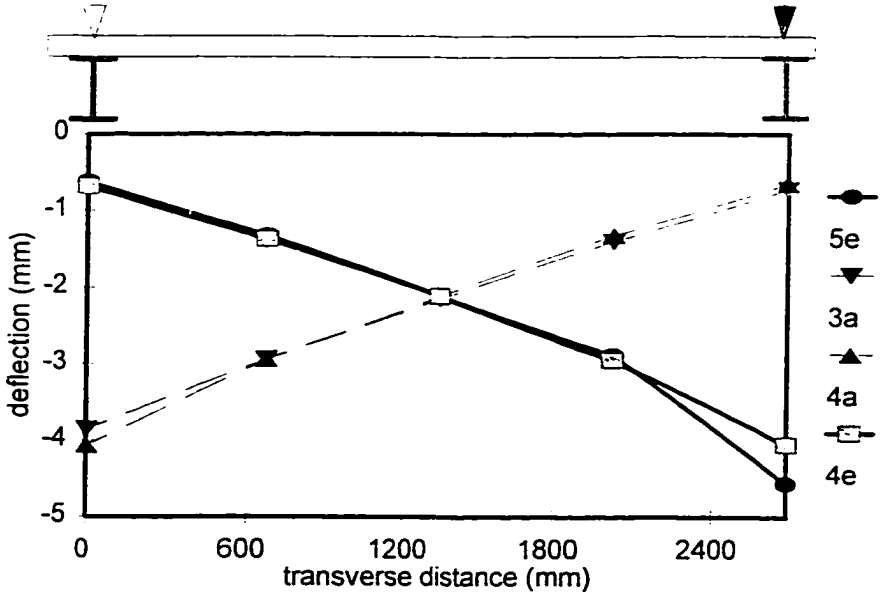

Figure 4.9 Transverse deflection profile for loads applied over girders

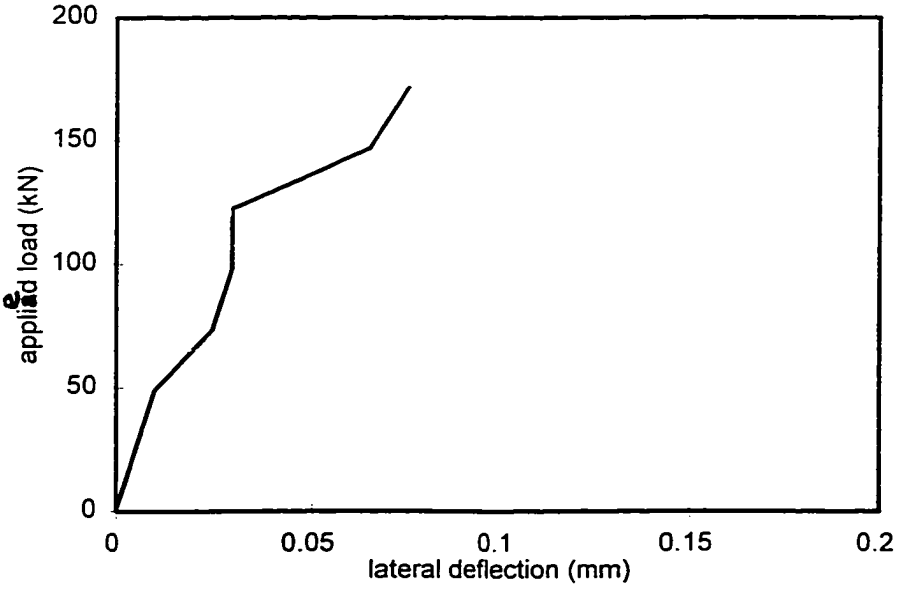

Figure 4.10 Lateral deflection from test 2c

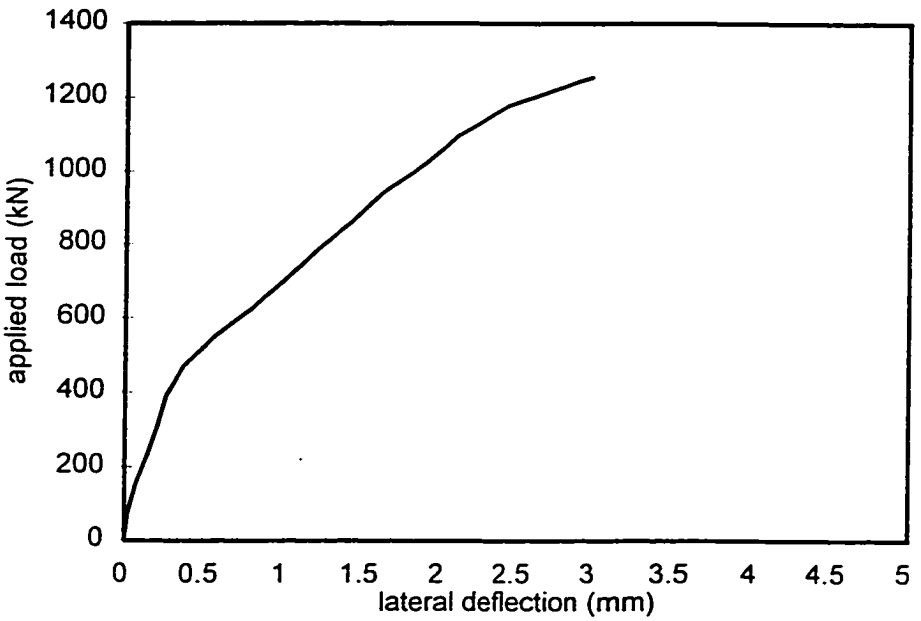

Figure 4.11 Lateral deflection from ultimate load test 1

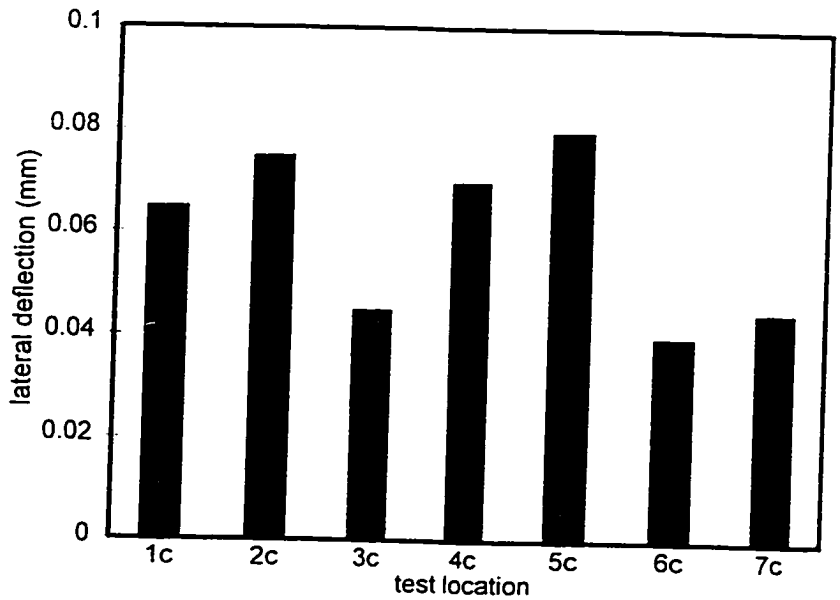

Figure 4.12 Lateral deflections at 17.5 tonnes for tests on gridline c

4.2.2 Unsymmetrical Loading

In tests by other researchers, behaviour was evaluated based on the load being applied directly between two girders at the mid-span of the deck. This creates a symmetry in which the arching action is well accepted. Because vehicle loads are live loads and can be located anywhere on the surface of a deck, it is important to know if the same tendency for arching behaviour occurs if the load is applied unsymmetrically. Indicators of arching behaviour will be an outward displacement of the girder top flanges and a tensile strain in the strap adjacent to the load. Figures 4.13 and 4.14 show the lateral deflection of the top flanges and the strain in strap 5 for load test 4a through 4e, respectively. It is noted that outward displacement is positive. These results are typical of all other service load tests performed. The values are maximum at 4c; however, the same behaviour is exhibited to a smaller degree at 4b and 4d. This indicates that some arching is still occurring with loads applied at the quarter points of the span. When the load is directly over the centerline of a girder as in 4a and 4e, the lateral deflection behaviour is not predictable and the strain in the straps is negative. These values are however consistent with the deflected shape which suggested that the deck was almost entirely in negative bending for this load situation. Therefore, some arching action does take place when the load is placed between the two girders, however, no arching is present when the load is directly over a girder. This statement applies only to a two girder system in which the concrete is not cracked. The behaviour of a cracked decked with an unsymmetrical load could not be determined from this experimentation.

4.2.3 Composite Action

The Ontario Highway Bridge Design Code, typical other bridge and building codes, specifies the width of the slab overhang that may be considered to be the effective width of the compression flange when the concrete deck acts compositely with the steel girders. The design of the steel-free deck assumes that the same level of composite action is present in the steel-free system as would be present in reinforced concrete slab systems. During the service load testing, the strain in the steel girders was measured at the mid-span of the girders using the gauges shown in Figure 4.3.

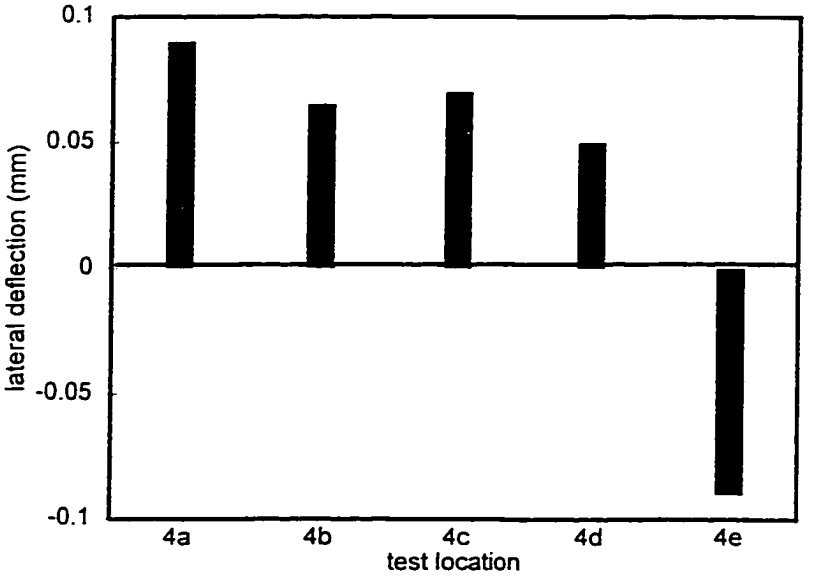

Figure 4.13 Lateral deflection for tests on gridline 4

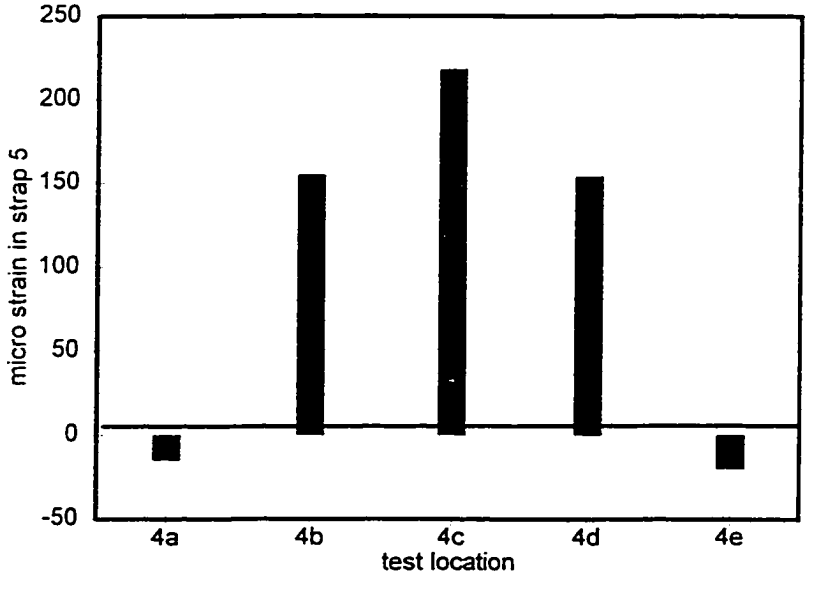

Figure 4.14 Strap strain for tests on gridline 4

Using the OHBDC Clause 3-10, the total effective width of the compression flange should be 1650 mm. Calculating the location of the neutral axis using the first moment of area of the transformed section, y is found to be 635 mm up from the bottom of the steel girder. Coincidentally, this corresponds to the full depth of the girder. A typical strain profile for the theoretical composite section is shown in Figure 4.15.

Eleven of the twenty five service load tests were chosen to be representative of the behaviour of the system. A typical strain profile is shown for various load increments of test 1c in Figure 4.16. From the strain profile the location of zero strain and consequently, the location of the neutral axis of the composite section, can be calculated. For each test, a strain profile similar to those shown in Figure 4.16 was used to locate the neutral axis in each girder. The strain profile at an applied load of 17.5 tonnes was chosen as characteristic of the behaviour of the beams and free from any initial settling-in effects. The values of strain and the corresponding values of y from the bottom of the girders are shown in Tables 4.2 a, b, and c.

Table 4.2a Strain Values and Neutral Axis Locations for Tests on Gridline c

Gauge Location (mm)	**Test 1c**		**Test 4c**		**Test 6c**	
	Girder 1	Girder 2	Girder 1	Girder 2	Girder 1	Girder 2
540	4	4	-16	-13	7	10
310	12	11	29	33	44	48
80	20	20	84	73	81	83
y (mm)	655	643	458	475	585	606

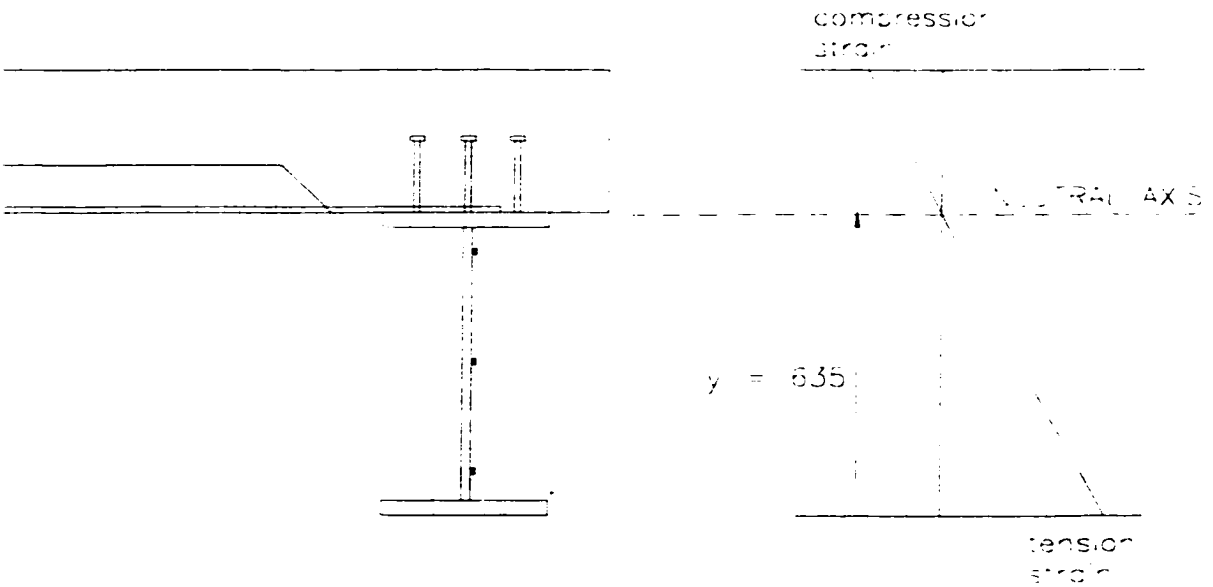

Figure 4.15 Typical girder strain profile for theoretical composite section

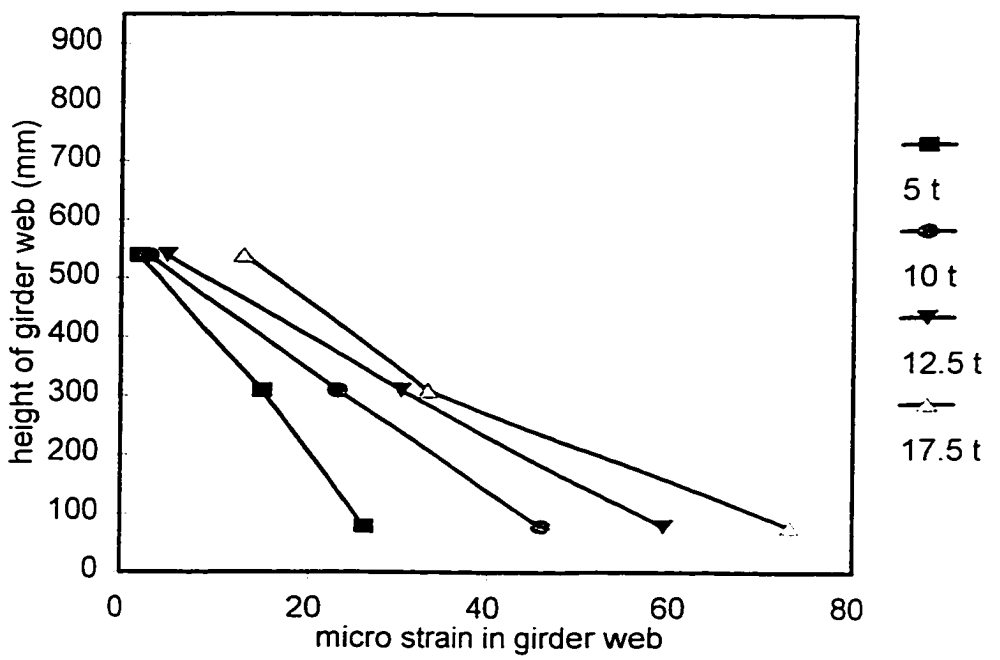

Figure 4.16 Typical girder strain profiles for test 4c

Table 4.2b Strain Values and Neutral Axis Locations for Tests on Gridline b

Gauge Location (mm)	Test 1b		Test 4b		Test 6b	
	Girder 1	Girder 2	Girder 1	Girder 2	Girder 1	Girder 2
540	3	3	85	80	6	10
310	10	13	118	137	31	59
80	15	24	137	193	56	588
y (mm)	664	601	1288	866	595	588

Table 4.2c Strain Values and Neutral Axis Locations for Tests on Gridline a & e

Gauge Location (mm)	Test 4a		Test 4e		Test 5a	
	Girder 1	Girder 2	Girder 1	Girder 2	Girder 1	Girder 2
540	66	83	97	23	16	6
310	65	139	138	40	79	21
80	82	197	192	57	152	29
y (mm)	1745	873	995	851	588	672

In the tests along grid line c, Table 4.2a, the loading of the deck is symmetrical. At load test 4c the longitudinal location of the load corresponds to the longitudinal location of the gauges. In this case, the strain readings indicate that full composite action does not occur. As the point of load application moves farther away from the strain gauge location, test 6c and 1c respectively, the location of the neutral axis moves closer to the theoretical location of y=635 mm such that full composite action is recorded at mid-span for a load at test 1c. Therefore, the girders develop full composite behaviour in the global sense; however, girder section very close to the applied load are not able to develop the full effective concrete compressive flange width. This effect is local to the applied load region and does not appear to significantly effect the assumption of overall full composite behaviour.

The loads in tests along grid line b, Table 4.2b, are offset such that the loading is no longer symmetrical. This causes additional stresses due to the warping of the deck and the twisting of the girders. This effect dominates in load test 4b in which the location of the neutral axis does not have any physical meaning. These strain values are obviously affected by the unsymmetrical loading. However, as the load moves farther away from the gauge location, the location of the neutral axis moves closer to the theoretical location.

The loads in tests along grid lines a or e, Table 4.2c, are directly over one of the girders. This is the most severe form of unsymmetrical loading. The strain values at test 4a and 4e are affected by the unsymmetrical effects. However, the values at test 5a give a neutral axis close to the theoretical value.

It is concluded that composite-action criterion of OHBDC is valid globally for the steel-free system with the exception that at sections very close to the load points, local effects may prevail. This is the case for the deck in an uncracked condition.

The girder strains were monitored during the ultimate load test 1. The load was applied at 1800 mm from the end of the span while the strains gauges were located 6000 mm from the end of the span. Based on the response of the system from the service load tests, full composite action should be occurring at the strain gauges. During the ultimate load test local cracking occurred on both the underside and the top side of the deck at failure. A longitudinal crack on the underside extended past the gauge locations.. In a field structure, it is this longitudinal crack which is most likely to occur and it is the one of concern with regard to its effect on the composite behaviour. The strain profiles from load test 1 were interpreted in the same manner as above. The strain values are given below in Table 4.3 along with the calculation of the neutral axis location, y.

Table 4.3 Girder Strains for Load Test 1

Load (KN)	Girder 1 strains			N.A.	Girder 2 strains			N.A.
	Gauge 1	Gauge 2	Gauge 3	y (mm)	Gauge 1	Gauge 2	Gauge 3	y(mm)
0	0	0	0		0	0	0	
78	2	7	14	601	2	7	12	632
157	4	14	26	616	5	13	24	646
235	7	20	38	629	7	20	35	648
314	9	27	50	630	10	27	47	657
392	11	33	58	642	12	33	57	657
471	14	40	70	649	14	39	68	653
549	18	46	80	665	18	47	80	668
628	22	54	94	670	23	55	92	687
706	27	61	104	690	29	63	105	706
785	32	68	117	698	34	69	116	716
863	37	76	129	710	39	79	130	726
942	42	84	142	717	44	84	140	734
1020	49	92	155	733	49	94	156	734
1099	53	100	168	733	53	101	166	741
1177	62	108	181	754	60	110	182	747

Four typical strain profiles are shown for Girder 1 in Figure 4.17. The profiles represent the strain in the girder when the concrete is in an uncracked condition, after cracking of the underside, after cracking of the topside and just prior to failure. Although the profile for the uncracked condition is approximately linear, the other profiles become increasingly non-linear. In addition, the location of the neutral axis calculated from the strain values, Table 4.3, is initially close to the theoretical value of 635 mm but becomes increasingly larger as the load increases. In the higher load range the calculated value of the neutral axis is too large for the physical limitations of the deck. To understand this phenomenon we examine a plot of load versus strain for each of the gauge readings. The plots for both girders are shown in Figure 4.18. Initially all the curves are linear; however, at approximately 470 kN the curves for gauges 1 and 2 become non-linear with gauge 1 increasing at a faster rate. For ease of interpretation, dashed lines are drawn to represent the initial slope of each gauge. This non-linearity is not consistent with a beam

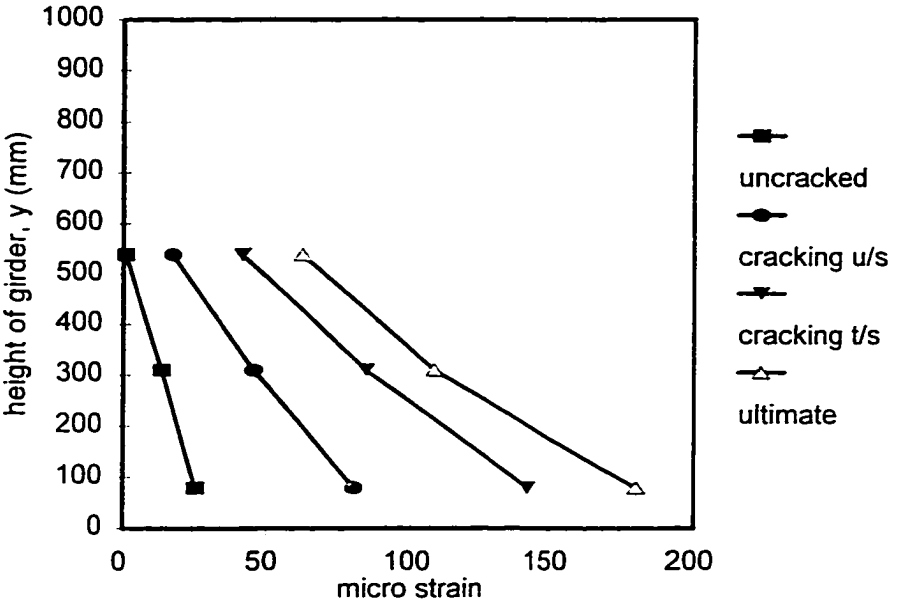

Figure 4.17 Girder 1 strain profiles for ultimate load test 1

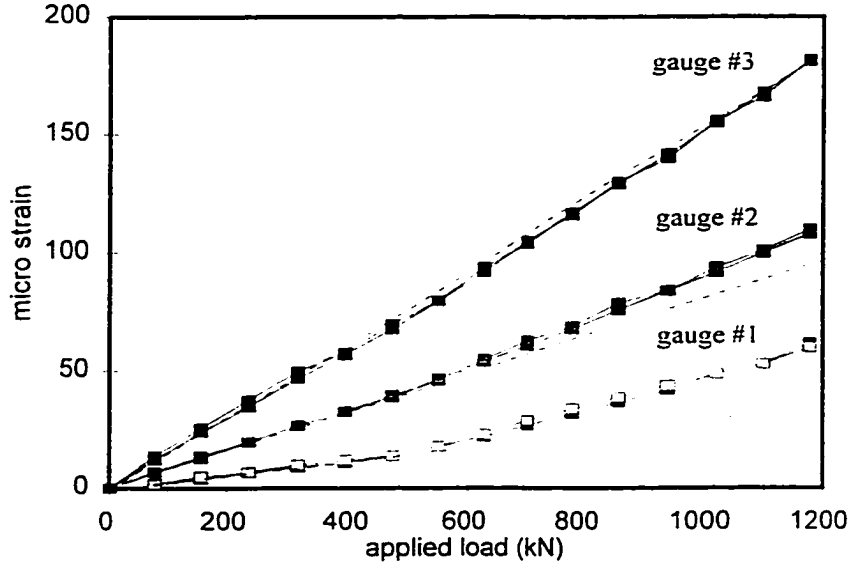

Figure 4.18 Load versus girder strains for ultimate load test 1

in pure bending about one axis. The non-linearity does explain however the increasing value of y calculated shown in Table 4.3. It also means that the calculation of y using the simple bending theory is not appropriate at load values greater than 470 kN and must also be considered carefully at load values lower than 470 kN. Therefore the calculated values of y which seem to indicate that the neutral axis is well above 635 mm are incorrect and meaningless as shown. The non-linear behaviour of the strain readings though is not insignificant and can be explained by the behaviour of the steel-free bridge deck system. Cracking of the deck occurred at the 470 kN load increment. After this point, the arching behaviour becomes effective and the system deforms accordingly. As outlined Section 4.2.1, the top flanges of the girders will rotate outward at a much faster rate than before the deck cracks. If the top flange is deflecting outward, then the web of the girder must bend to maintain compatibility at the web flange connection. The bending of the plate will cause a component of strain to occur in the longitudinal axis of the girder web. This is the additional strain being recorded by gauges 1 and 2 and causing the apparent non-linear behaviour. The lateral load testing indicated that only the top flange, and not the top and bottom flange, acted to resist the lateral bending. This means that the bending of the web and the accompanying longitudinal strains are larger near the top flange of the girder. This appears to be the case as the non-linear behaviour is greatest for gauge 1 which is closest to the top flange. Gauge 2 exhibits non-linear behaviour but to a lesser degree and gauge 3 appears to be unaffected by this web bending.

Re-examining Figure 4.18 we see that gauge 3 increases at a constant slope which indicates that the bending behaviour recorded by this gauge is the same throughout the loading. The initial readings before 470 kN show that the neutral axis for experimentation is close to the theoretical neutral axis location. The constant slope of gauge 3 would therefore indicate that the bending strain rate remains constant and hence the composite section behaviour in pure bending remains constant.

Figure 4.19 shows the experimental gauge readings plotted alongside the theoretical strains determined from the applied moment and the composite section size given by the OHBDC. The theoretical values are slightly higher than the experimental values because the modulus of elasticity, E, value for concrete, which is used to calculate the moment of inertia, I, of the transformed section, is conservative and hence the theoretical I value is slightly conservative. However, the plot does illustrate that the readings of gauge 3 are consistent with the same theoretical composite section strains. The readings of gauge 1 are initially consistent with the theory but deviate from the theory at higher loads.

Using gauge 3 as an indicator, it is concluded that the composite section behaviour for longitudinal bending did not change after cracking of the deck. There is however, some lateral bending of the web which causes additional bending stresses in the web near the top flange. Fortunately, the longitudinal strains are low in this region such that the combination of the two strains will still be within acceptable limits.

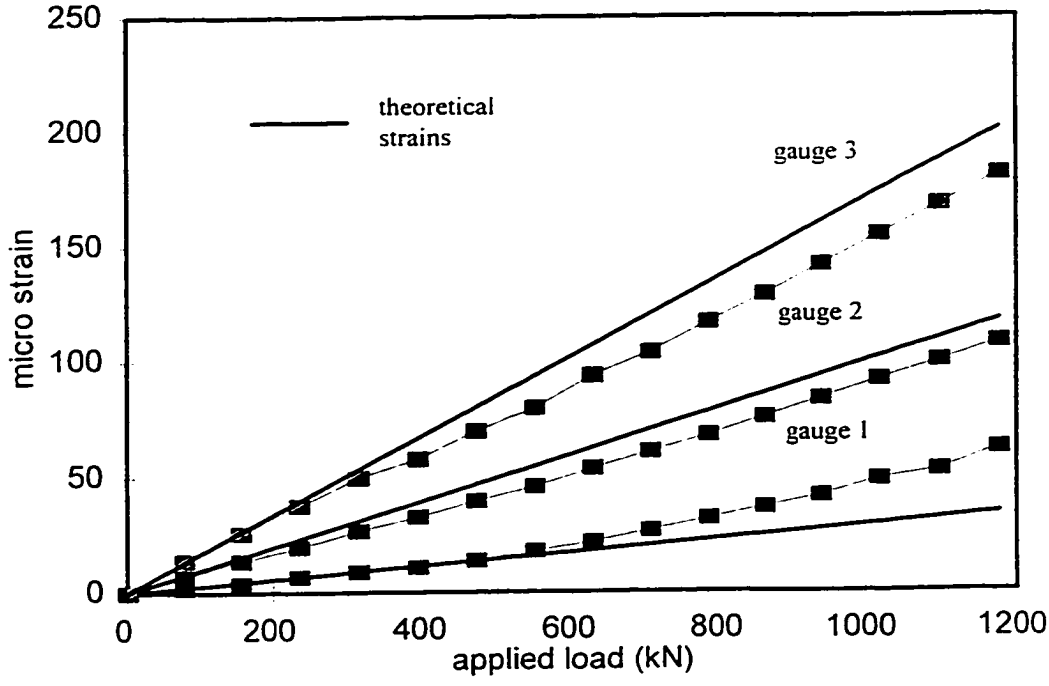

Figure 4.19 Gauge readings versus girder strains for ultimate load test 1

4.2.4 Load Sharing Between Girders

In reinforced concrete bridge deck design, the load sharing between the girders in the system can be calculated using a number of methods from the coefficient method of either OHBDC or CSA S6 Design of Highway Bridges to the semi-continuum method (Jaeger and Bakht, 1989). In these systems it is clear that the deck transfers the load to adjacent girders through flexure and shear. In the steel-free deck system, arching action is being relied upon as the principle load carrying mechanism. For design purposes two important questions need to be answered: firstly, does load transfer occur in this system and secondly, does the same level of load sharing occur ? While the two girder model tested will not provide a complete answer to these questions, it will provide a useful indicator of the behaviour. Unfortunately, the results of this testing program apply only to the behaviour of the deck in a uncracked state. While it remains uncracked, the deck can transfer loads in flexural action and not just purely by arching action. The results must be regarded with due consideration to this fact.

The first question is easily answered by examining the deflection of the girders under a variety of loadings. Table 4.4 presents the deflection of each girder for an applied load of 17.5 tonnes. A variety of load cases are selected from the twenty five service load tests to represent the range of possible load positions.

Table 4.4 Girder Deflections

Location	Deflections (mm)	
Test	Girder 1	Girder 2
1b	0.68	0.21
1c	0.45	0.41
4a	4.06	0.65
4b	2.92	1.32
4c	2.20	2.13
5e	0.62	4.56
6b	2.76	1.32
6c	2.04	1.98

It is clear that load sharing does take place even when the load is applied directly over one of the girders. To examine the second question related to the amount of load sharing we will consider the deflection values to be indicators of the amount of moment carried by each beam. The girder strain readings would be a better indicator of load sharing, except that the secondary strain effects discussed in the previous section make simple interpretation of the moment strains impossible. The theoretical load sharing is determined by analysing the system with the SECAN program (Mufti et al., 1992). The theoretical moments for an applied load of 17.5 tonnes are given in Table 4.5

Table 4.5 Theoretical Girder Moments from SECAN

Location	Moments (kN-m)	
Test	Girder 1	Girder 2
1b	134.2	51.6
1c	92.8	92.8
4a	454.8	61.2
4b	358.0	158.0
4c	258.0	258.0
5e	60.2	404.0
6b	317.0	178.0
6c	247.7	247.7

Using Tables 4.4 and 4.5 the amount of load sharing is calculated for the experimental model and the theoretical analysis. The load sharing is reported as a percentage of load taken by each girder. The comparison is presented in Table 4.6.

Table 4.6 Comparison of Experimental and Theoretical Load Sharing

Location	Theoretical		Experimental	
Test	Girder 1	Girder 2	Girder 1	Girder 2
1b	76%	24%	72%	28%
1c	52%	48%	50%	50%
4a	86%	14%	88%	12%
4b	69%	31%	69%	31%
4c	51%	49%	50%	50%
5e	12%	88%	13%	87%
6b	68%	32%	64%	36%
6c	51%	49%	50%	50%

This simple comparison indicates that the same amount of load sharing which is assumed to occur on a reinforced concrete slab on girder system can safely be assumed to occur in the steel-free bridge deck system. This conclusion only applies to the deck in the uncracked condition and has only been verified for a two girder system. Load sharing of a cracked deck and of a multi-girder system were beyond the scope of this work.

4.2.5 Strap Force Distribution

A typical distribution of strain in the straps for a specified load is shown in Figure 4.20. The distribution is for a 17.5 tonne load applied directly in the centre of the model, test 4c. As expected the straps closest to the load take the larger portion of the lateral force and the straps farther away from the load take a smaller portion. Because all the straps are of the same material, size and length, the distribution of restraint forces is similar to the distribution of strap strains.

By way of comparison the strain distribution for the same 17.5 tonne load applied directly over the strap closest to the end of the span, test 7c, is shown in Figure 4.21. It can be

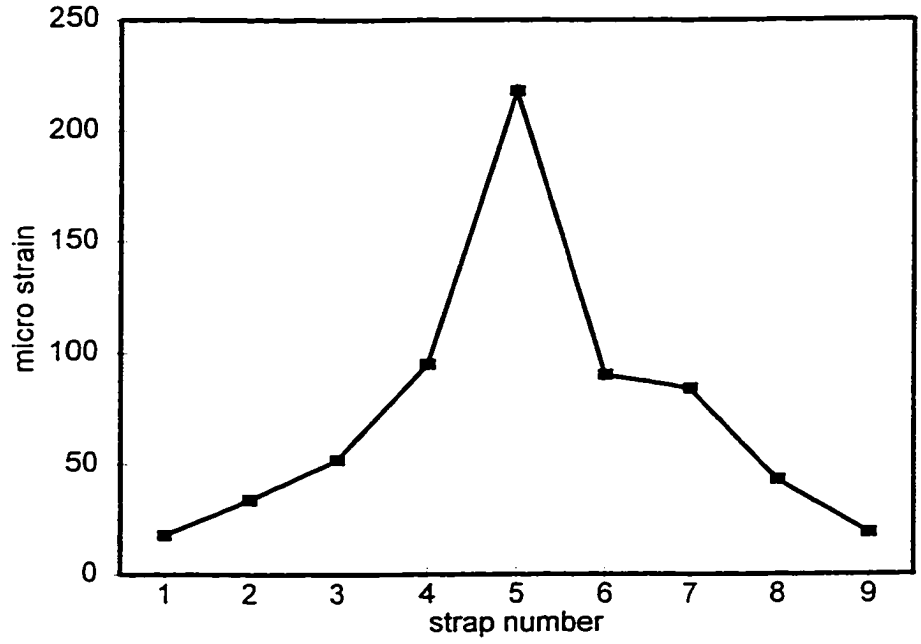

Figure 4.20 Distribution of strap strains for test 4c

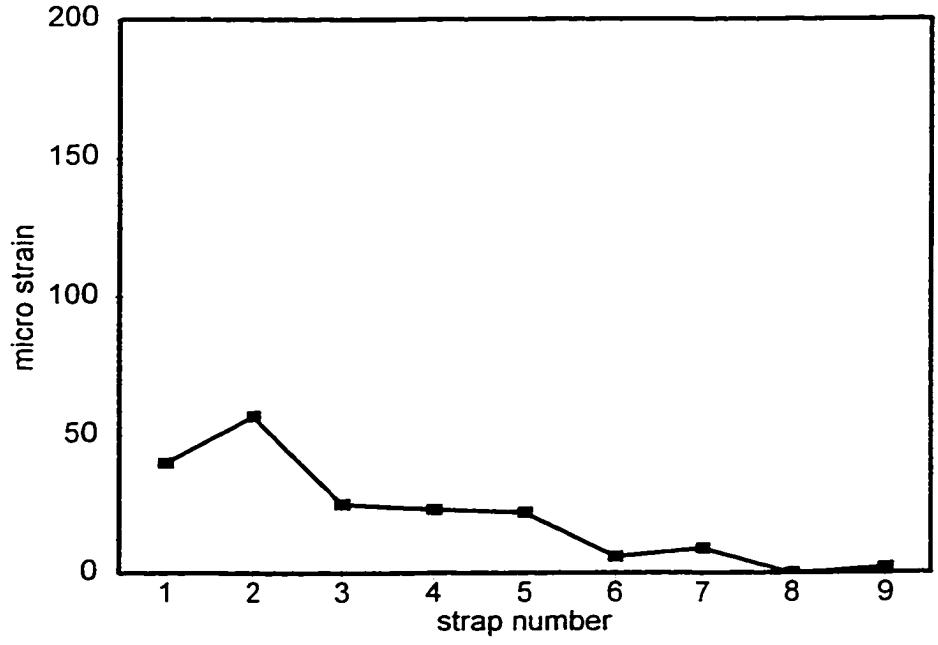

Figure 4.21 Distribution of strap strains for test 7c

seen for both these plots that the force in the straps dies away very quickly. After four strap spacings the force in the straps becomes very small. This is important for assessing the field of influence of a load on the straps, particularly when considering the effect of adjacent wheel loads on the overall strap forces.

It is noted from Figures 4.20 and 4.21 that the magnitude of the strap forces is not the same. In other words, the strap strain for strap 5 for Test 1c is not the same as the strap strain for strap 1 for Test 7c even though both straps are directly beneath the respective loads. This is undoubtedly due to boundary conditions playing a more dominant role in load tests near the edge of the deck. As a further aid in examining the distribution of strap forces, a series of influence lines is constructed for the strain in a given strap as the load moves along the span, Figure 4.22. The strains are given as micro strain per kN of applied load. In this manner the influence lines will be consistent with the standard form of response due to an applied unit load. Only the influence lines for straps 5 through 9 are shown as those for straps 1 to 4 are symmetrical with straps 6 to 9 due to the reciprocity in the system. The influence line for strap 6 does not seem to be consistent with the others. It is believed that this strap had some sag in the unloaded condition such that, at low loadings, it does not participate fully in the load sharing. Once the initial sag has been overcome the strap will participate more fully. This same behaviour is observed for strap 4. It should be noted that the diaphragm at mid-span was present during the welding of the straps. The removal of the diaphragm may have caused some change in the unstressed position of the girder such that some straps relaxed, mainly 4 and 6, causing this sagging to occur.

It is clear that the relative magnitude of the strap force increases for straps which are farther away from the end of the span. For the model tested, this appeared to be maximum at the centre strap. However, it is not clear that this trend would continue for longer spans. It seems more reasonable that at a certain distance from the end of the span, all straps would have the same influence line shifted by their location along the span.

The strain distributions shown in Figures 4.20 to 4.22 are for the deck in the uncracked condition. While the magnitude of strain per kN of load will change for the cracked condition, the overall shape of the distribution curves remain unchanged. For verification, the strain distribution curves for the three ultimate load tests are shown in Figures 4.23. The strains are given in micro strain per kN of applied load and are taken from readings after the deck has cracked. For load test 1 the strain distribution was also available for the deck in the uncracked condition. The distributions for both conditions is compared in Figure 4.24.

As a final comparison, the strain distribution for a load at the mid-span of the deck is compared to that of a load at the quarter span of the deck. As expected, the strain distribution is of the same general shape but the magnitude is smaller for the quarter point loading. The distributions for test 4c and 4b only are shown in Figure 4.25; however, the trend is similar for other load combinations.

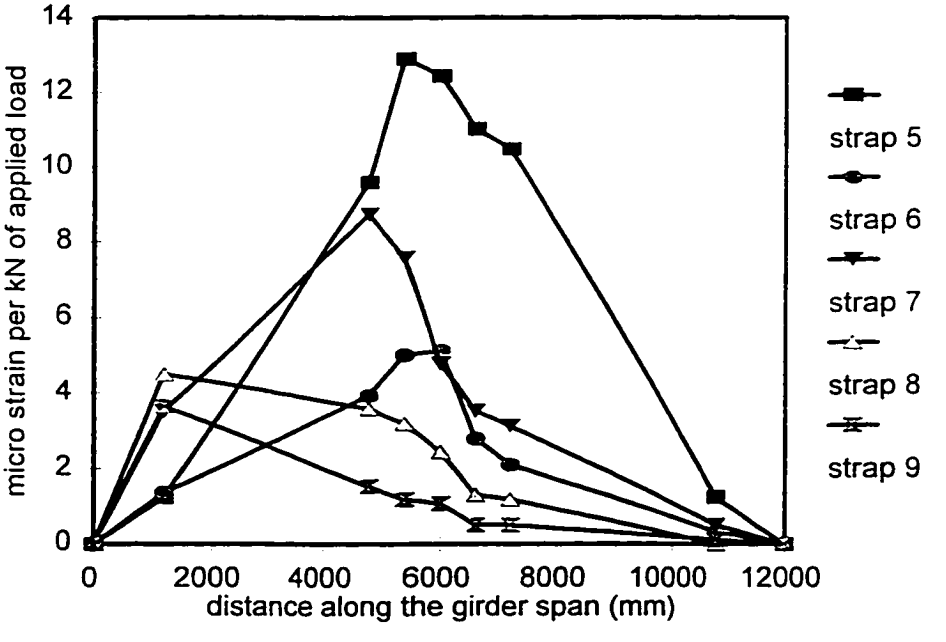

Figure 4.22 Influence lines for strap strains

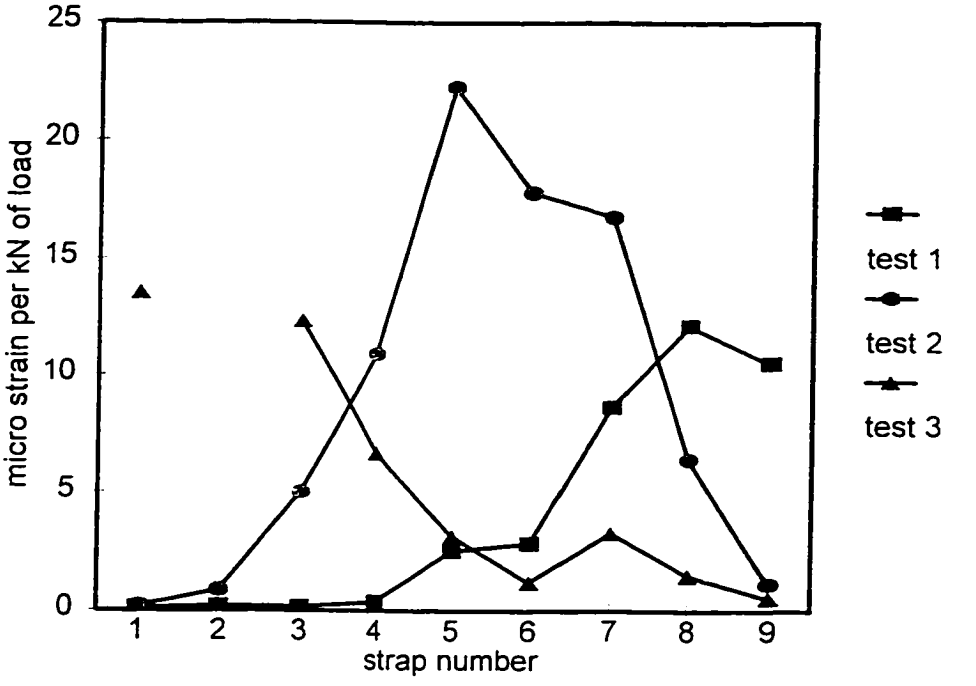

Figure 4.23 Distribution of strap strains at ultimate

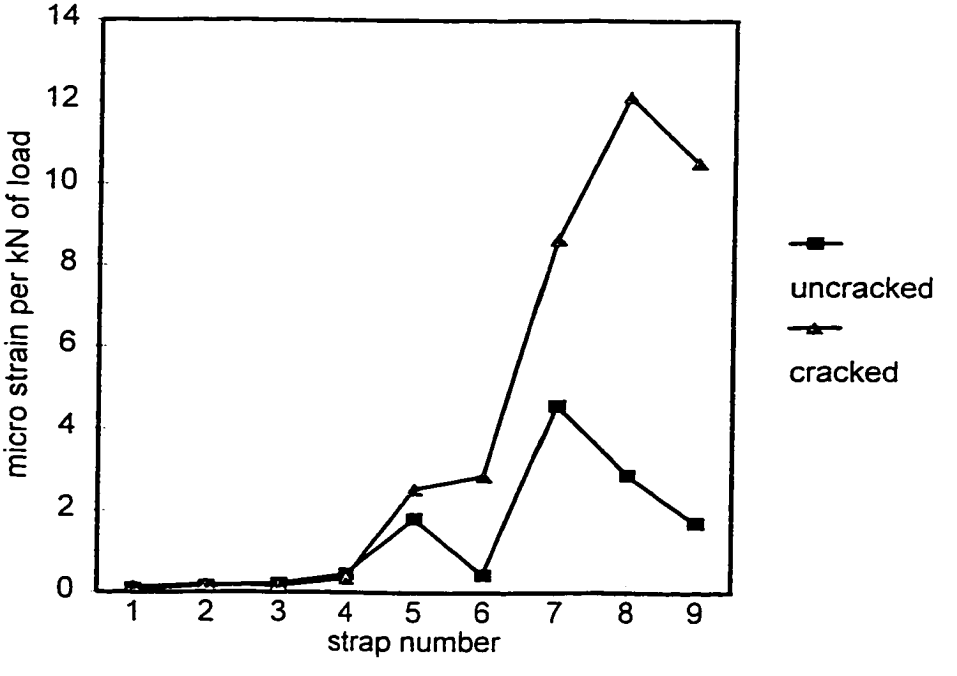

Figure 4.24 Comparison of strain distribution for uncracked and cracked deck slab

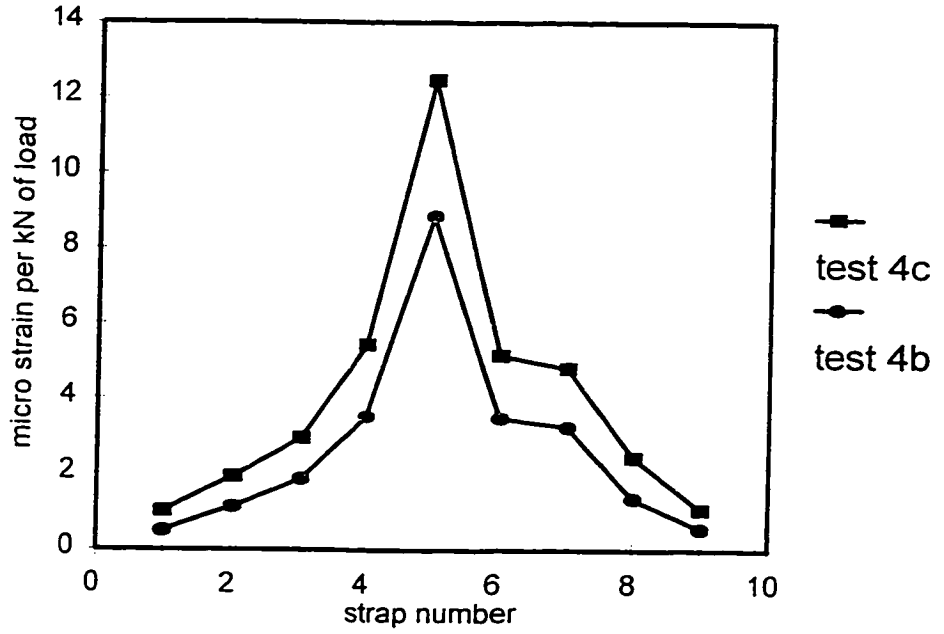

Figure 4.25 Strain distributions at mid-span (4c) and quarter-span (4b) of deck

4.2.6 Shakedown

Selvadurai and Bakht (1995) reported a load deflection response of a steel-free deck which changed slightly after each cycle of loading and unloading. The load deflection curve for a complete cycle forms a hysteresis loop which continues to be reduced with the number of load cycles until it reaches a stable state. Bakht (1996) refers to this process as shaking down to a stable state or simply shakedown.

To examine this effect, five cycles of loading to 40 tonnes and unloading were applied at the location of ultimate load test 1. The deflections and strap strains were recorded for each cycle.

The load-deflection curves for all five cycles are shown in Figure 4.26. For load cycle one, the change in response is quite large but by load cycle four the structure has stabilized considerably. For clarity, the hysteresis loops for cycle one and cycle four are

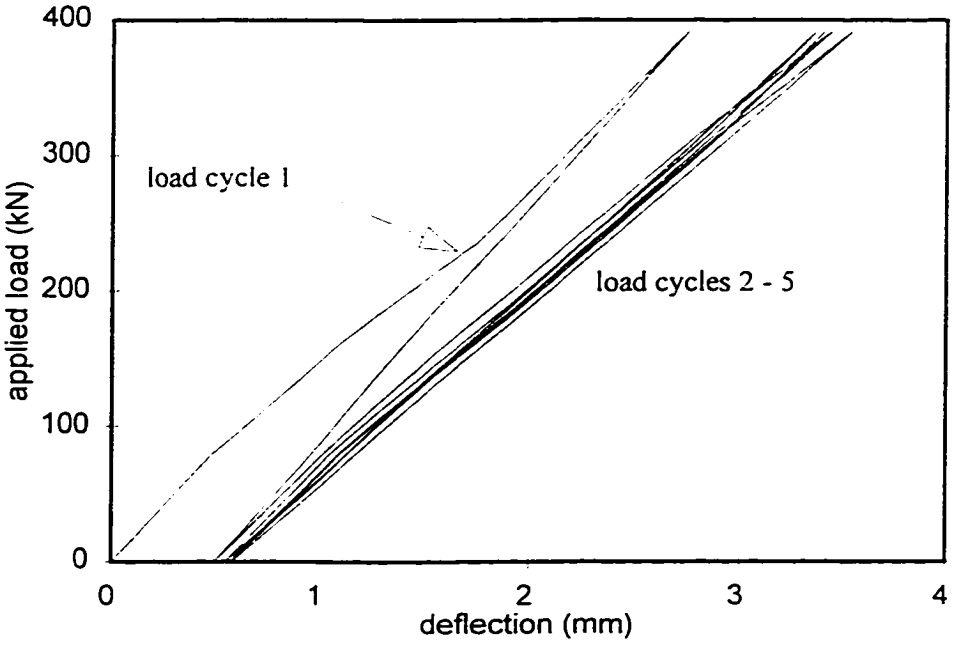

Figure 4.26 Load-deflection curves for load cycles 1 to 5

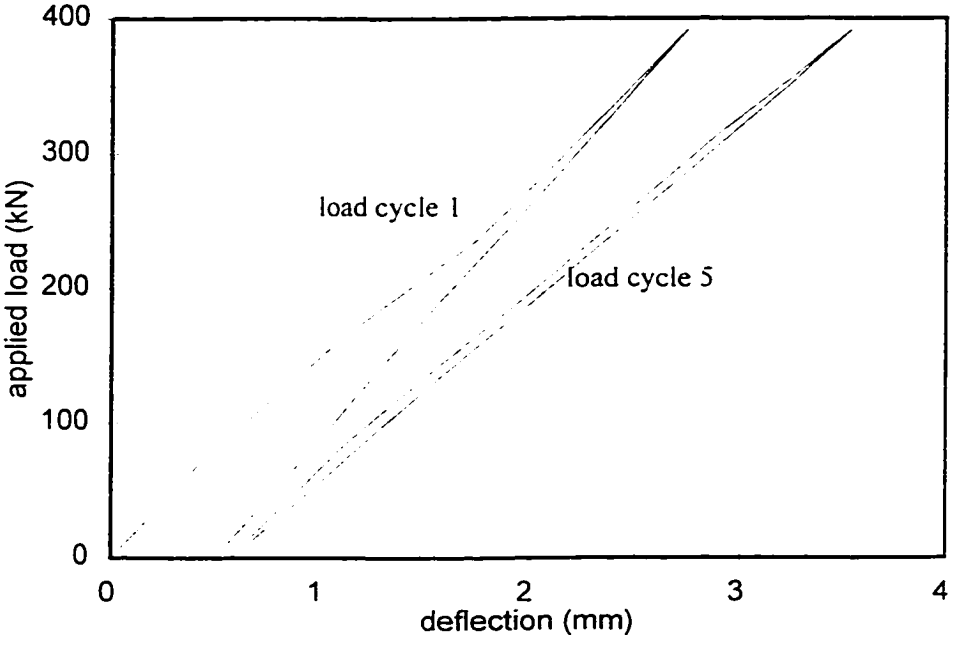

Figure 4.27 Load-deflection curves for load cycles 1 and 5

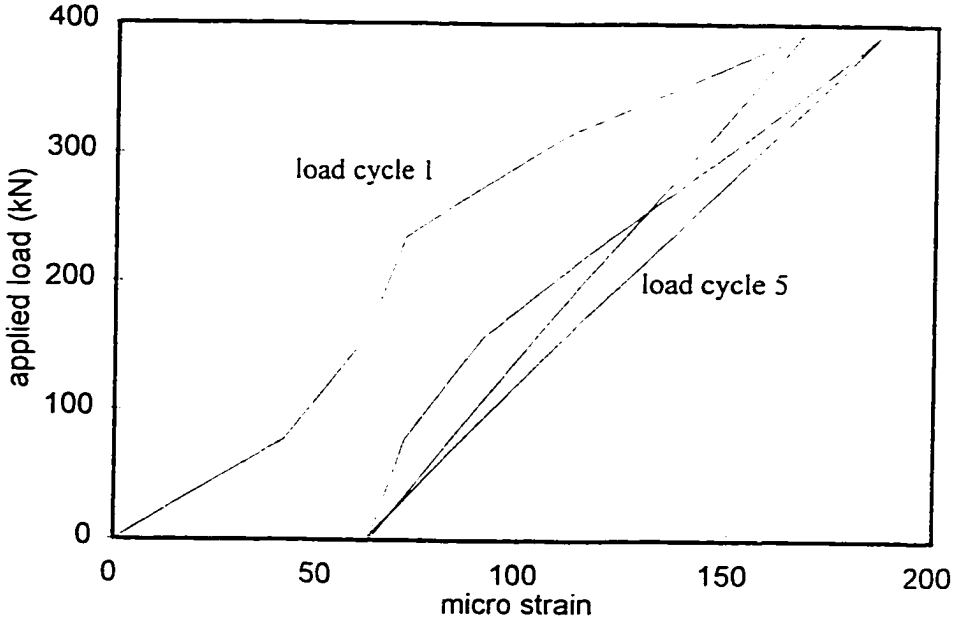

Figure 4.28 Load versus strap strains for load cycles 1 and 5

shown in Figure 4.27. The shakedown effect can be clearly seen, even for a low number of load cycles. The hysteresis loops for the strain values in strap 8 are also shown for load cycles one and four. Again the shakedown effect can be seen, Figure 4.28.

4.2.7 Effect of Haunches on Ultimate Load Behaviour

As shown in Figure 4.1b, the model bridge deck was constructed with 100 mm haunches over each girder. This model was the first such steel-free deck constructed and tested with haunches. The assumptions made in the rational model regarding the mechanics of the wedge rotation would indicate that the lever arm for rotation is based on the difference between the top surface of the slab where the load is applied and the point at which the lateral restraint is applied over the girders. Although 75% of the deck is only 200 mm thick, the effective depth for the PUNCH program would actually be 300 mm. Using the beam on springs analogy, the restraint stiffness for this location is determined to be 251 N/mm/mm, see Table 2.9. (Newhook and Mufti, 1996, had reported the stiffness to be 243 N/mm/mm for this same location. The difference is due to the level of sophistication

of the software used for the beam-on-springs model. The work in this thesis is based on the finite element analysis and is believed to be more accurate; but, the overall difference is less than 3%.) The Punch program is used to model the system with depths of 200, 250 and 300 mm. Four key parameters are selected for comparison to the experimental results. These are failure load, deck deflection, lateral deflection and strap strain, Table 4.7.

Table 4.7. Actual versus Predicted Behaviour

		Theoretical (PUNCH)		
Parameter	Actual	d = 200 mm	d = 250 mm	d = 300 mm
Failure Load (kN)	1275	728	1015	1306
Deck Deflect. (mm)	12.3	19.8	15.7	12.65
Lateral Defl. (mm)	3.0	2.38	2.64	2.58
Strap Strain (μstrain)	1555	1415	1500	1500

From this comparison, it can be seen that the deck behaviour corresponds very closely to that of a theoretical deck thickness of 300 mm. Therefore, the effect of the haunch is to increase the effective thickness of the deck and thus increase ultimate load capacity. This confirms the assumptions of the rational model. From pure mathematical considerations, the restraint force acts at the depth equal to thickness of the slab available at the support (above the girders), see Figure 4.1a; therefore, the thickness assumed as input data should be the full depth of the deck including the haunch.

4.2.8 Load-Deflection Behaviour

The data from ultimate load test 1 is used to study the load-deflection behaviour of the steel-free system as the deck progresses from an uncracked condition through to failure. The deflection of the deck under the load point as well as the deflection of the girders is shown in Figure 4.29. It is observed that the deflection curve for the deck exhibits an abrupt change of slope at about 470 kN and the behaviour of the deck is substantially different after this point. During the testing, it was observed that the first crack on the underside of the deck occurred at 470 kN load increment. The behaviour of the deck

before cracking is governed by flexural behaviour of the concrete slab and the behaviour after cracking is governed by the rotation of the wedges or arching action. The theoretical deck deflection is also shown in Figure 4.29. The theory assumes that cracks are present from initial loading. The experimental curve therefore begins with a much stiffer behaviour due to flexure but meets up with the theoretical curve at failure. The deflection behaviour of the girders remains unchanged throughout the load history as the load sharing between girders remains unaffected by the cracking.

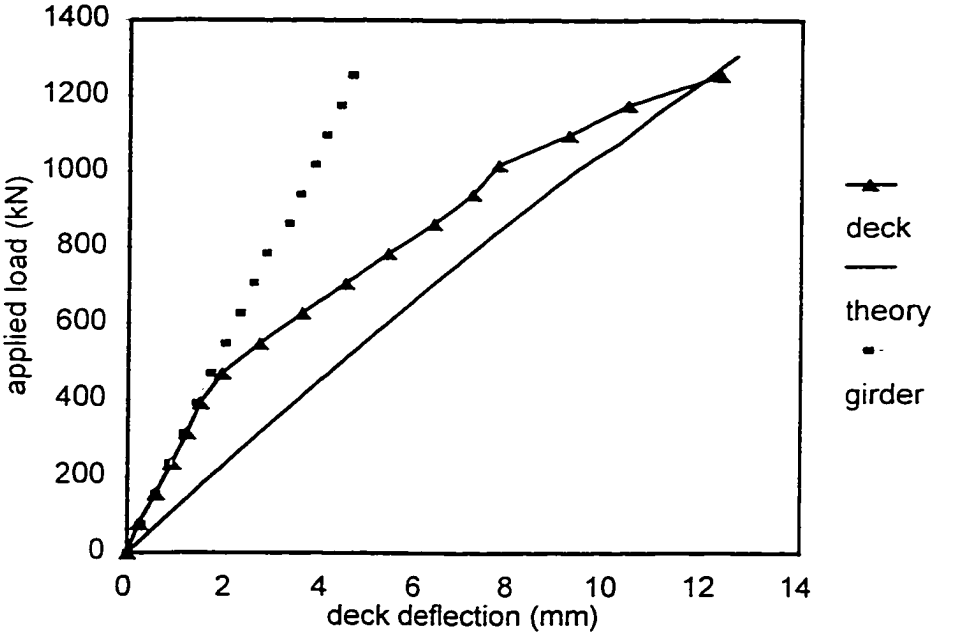

Figure 4.29 Vertical deflections for ultimate load test 1

The lateral deflection curve is given in Figure 4.30 along with the theoretical curve from the PUNCH analysis. This curve exhibits the same basic behaviour as the vertical deck deflection. Initially the response is quite stiff with a substantial change in slope after cracking occurs. The experimental curve eventually meets the theoretical curve near failure.

Finally, the experimental and theoretical strap strains are compared in Figure 4.31. Again the strap strains exhibit the same behaviour as the deflection curves. Initially governed by bending behaviour, the slope changes after cracking and the experimental values coincide with the theoretical values at failure.

All three plots indicate that a substantial change in behaviour occurs after cracking and that the after-cracking behaviour is governed by arching action and not flexure.

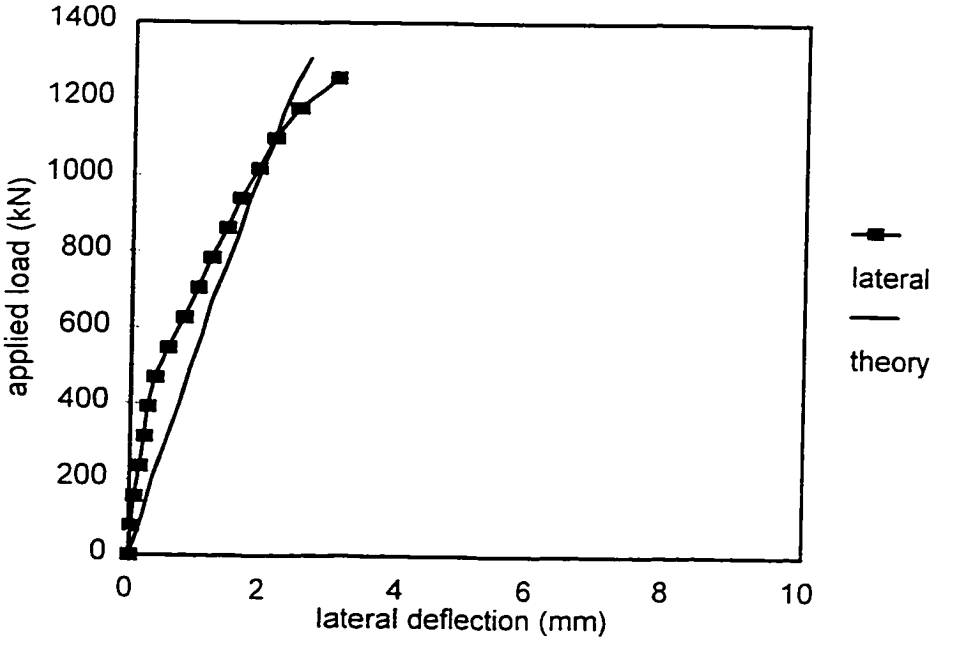

Figure 4.30 Lateral deflections for ultimate load test 1

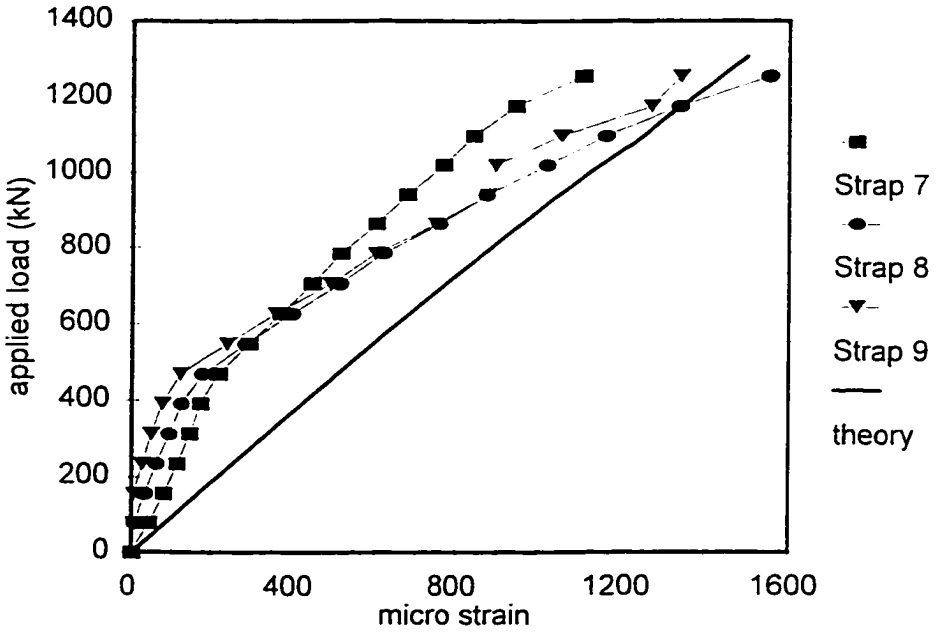

Figure 4.31 Strap strains for ultimate load test 1

4.2.9 Multiple Load Points

Vehicle loads on bridges are caused by large, heavily loaded trucks. These trucks come in a variety of configurations but most significant is the spacing and number of axles. Punching capacity of a deck is determined in terms of a single wheel load; however, the effect of closely spaced adjacent axles is important. While the exact mechanics of the interaction is complicated a simple method can be developed for predicting the effect of adjacent loads (Mufti and Newhook, 1997).

Consider Figure 4.32 in which a line of loads is moving on the bridge. We assume that interaction between two wheels is based on the outer diameter of the wedges which would be formed during the punching failure. The diameter of these circles is approximately equal to the girder spacing. Thus if the two circles do not overlap then the individual loads do not effect each other. If the circles do overlap then the amount of influence can be quantified by the percentage of overlapping area. The circular fields of influence can be further simplified to rectangular fields of influence at failure, as shown

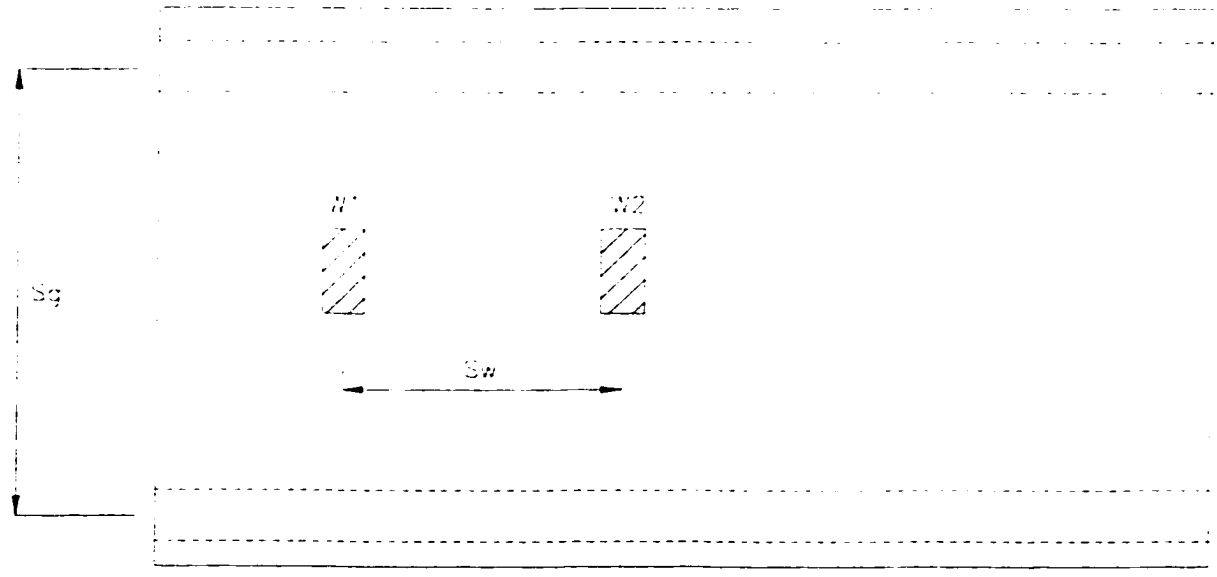

Figure 4.32 Multiple wheel loads

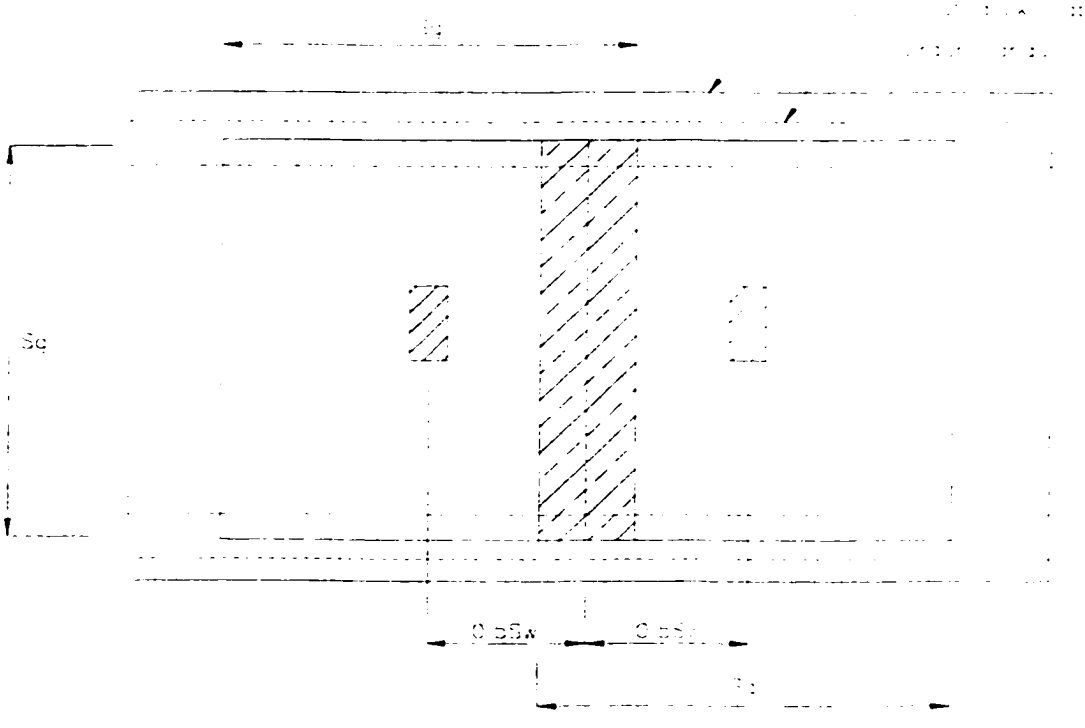

Figure 4.33 Fields of influence of multiple loads

in Figure 4.33. The reduction in the ultimate punch load can be calculated as follows:

$$\text{Reduction in the area of one wheel} = \frac{S_g - S_w}{2} \times S_g \qquad (45)$$

where S_g is the spacing between adjacent girders and S_w is the spacing between adjacent loads.

$$\text{Total reduced area} = S_g \times S_g - \frac{S_g - S_w}{2} \times S_g \qquad (46)$$

$$\text{Ratio with total area} = \frac{1}{2}\left[1 + \frac{S_w}{S_g}\right] \qquad (47)$$

Thus the reduction in the load will be given by

$$P_u' = P_u\left(1 + \frac{S_w}{S_g}\right) \qquad (48)$$

where P_u is the ultimate punch load due to a single load and P'_u is the ultimate punch load due to the total load.

For test 2 the loads were spaced at 600 mm apart and the girder spacing was 2700 mm. From load test 1 the ultimate capacity of a single wheel load was 130 tonnes. Substituting into equation (48) we get

$$P_u' = 130\left(1 + \frac{600}{2700}\right).$$

This gives a predicted total load of 160 tonnes or 1570 kN. The load-deflection plot for the tandem wheel load test is shown in Figure 4.34. Data was only available up to a load of 1020 kN after which the deflection values exceeded the stroke of the gauges. The load was applied up to a value of 1422 kN and then stopped for safety reasons. Before the loading was stopped, the deck was sustaining the load and showing no signs of failure. While it is unfortunate that the deck could not be taken to failure the test did demonstrate that the total failure load was in excess of a single wheel failure load and the deck appeared to be capable of sustaining the predicted load.

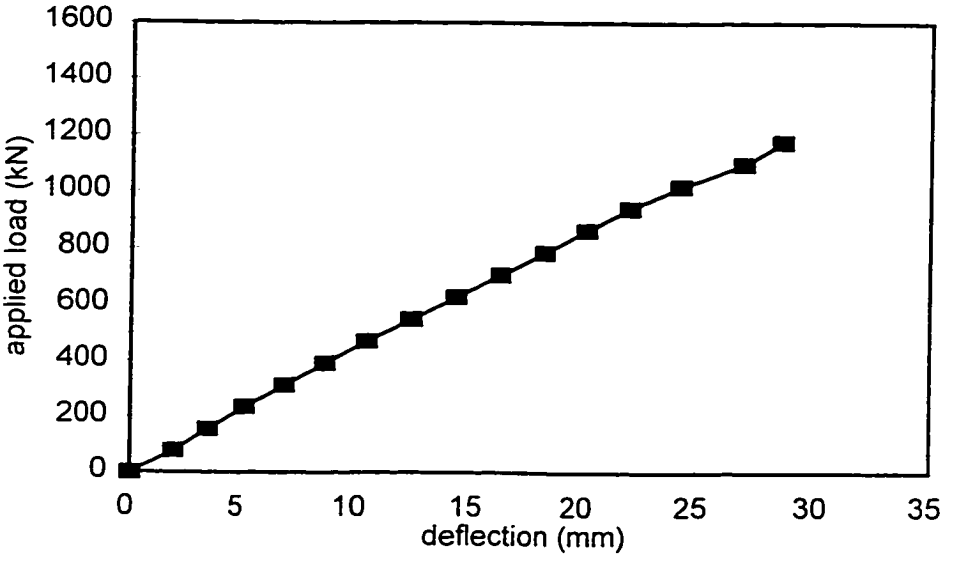

Figure 4.34 Load-deflection curve for ultimate load test 2

To examine the validity of this formula further, we investigate the test results of an isotropically reinforced deck. Fang et al. (1986) tested an isotropically reinforced deck by applying tandem loads a girder spacing of $S_g = 2133$ mm and an axle spacing of $S_w = 1220$ mm. The ultimate load for the tandem loading was 907 kN, the single load capacity was 631 kN. Substituting these values in Equation (48)

$$P_u' = 631 \left(1 + \frac{1220}{2133} \right) = 992 \ kN \ .$$

This compares well with the experiment results of $P_u = 907$ kN.

When the load was removed from the two wheel loads at test 2, a single wheel load was reapplied at the midpoint of the previous two load pads. A full crack pattern was already formed on both the topside and underside from the tandem wheel loading. The deck failed at a single wheel load of 1020 kN. It is interesting to note that this value is approximately 20% less than that for load test 1. The crack pattern for the tandem wheel load was approximately 22% bigger than that of a single wheel load crack pattern. It is believed therefore that the pre-existing crack pattern from the double wheel load influenced the failure of the single wheel load.

4.2.10 Reserve capacity of the system

As described previously, load test 3 was performed to determine the reserve capacity of the system in a deteriorated condition. Two of the most likely modes of deterioration are the corrosion or failure of a strap and the severe cracking of the deck. Both these conditions were simulated by the test. To establish the initial behaviour the deck was loaded up to 36 tonnes with the deck and strap in good condition. The strap was then removed and the deck loaded to 85 tonnes and the load removed. This achieved a condition whereby the strap beneath the load was ineffective and the concrete surrounding the load patch was severely cracked. In addition, the deck in general was cracked throughout and most of the remaining straps

showed visible plastic deformation from having yielded during previous tests. The deck in this condition was then tested to failure. The deck sustained a maximum load of 1118 kN before failing at a load of 951 kN. Using the beam on springs model, the lateral restraint stiffness for this test was 86 kN/mm^2 and the predicted failure load from PUNCH using a 300 mm thick deck was 951 kN.

The load-deflection curves for all three stages of the load test as well as the theoretical curve are shown in Figure 4.35. The curves indicate that the load-deflection behaviour is not significantly changed in the initial load portion by either the removal of a strap or the cracking of the deck. This may be due to the fact that the initial loading with the strap still in place was not taken to a high enough value to see the full effects of the arching behaviour. The final loading path does; however, exhibit more linearity than the first load cycle with the strap removed. It also shows a reduction in stiffness of about 30% from the initial two load curves. This illustrates that the cracking during the first load cycle with the strap removed eliminated much of the flexural capacity of the slab. Therefore, arching was the main behavioural characteristic during the final loading. As demonstrated by the theoretical curve the load-deflection relationship for pure arching behaviour (pure wedge rotation and no bending) is linear. The experimental curve for the final load cycle tends toward the theoretical curve at the end of the loading. The theoretical predicted failure load is reasonably close to the actual mode of failure demonstrating that the rational model can still be used as an analysis tool even in this less-than-ideal condition. A comparison of theoretical versus experimental strain is not so favourable with the maximum theoretical value being 830 micro strain and the maximum experimental value being 1500 micro strain.

The test does clearly demonstrate that the steel-free bridge deck system has substantial reserve capacity even in a severely deteriorated condition. Even in the event of the failure of a primary load carrying member, such as the strap directly beneath the load point, the system is able to sustain load through a redistribution of loads to the remaining straps. This fact is of great importance when considering the design safety of such a system.

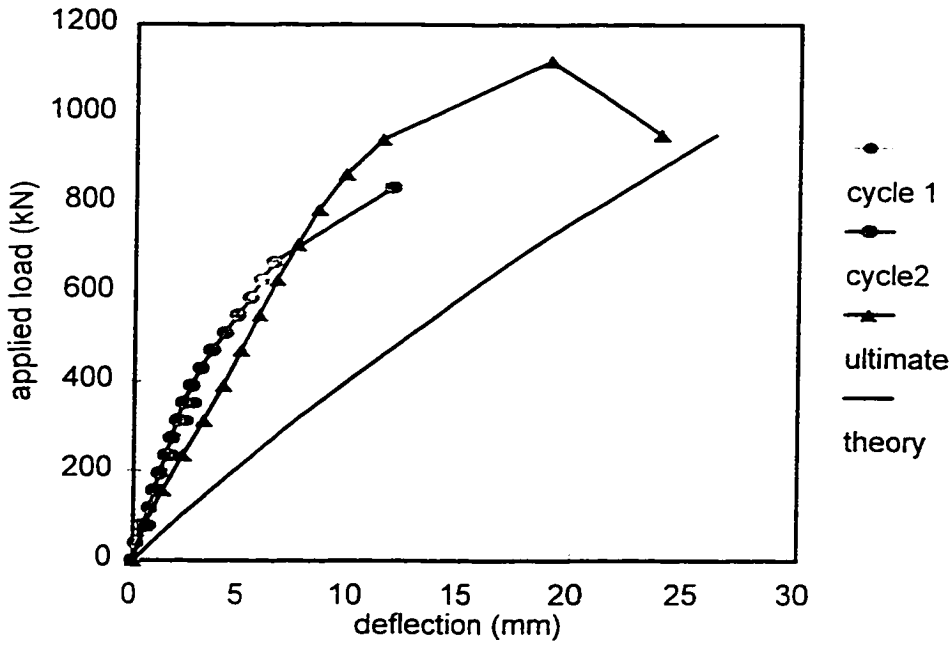

Figure 4.35 Load-deflection curves for ultimate load test 3

5 FIELD APPLICATION

Construction of a steel-free bridge deck on the Trans Canada Highway 104 was completed and opened to traffic on 5th December 1995. This project represents the world's first field application of the steel-free bridge deck technology. The design was undertaken by a five person design team consisting of Dr. Aftab A. Mufti, Dr. Leslie G. Jaeger, Dr. Baidar Bakht, Dr. Gamil Tadros and Mr. John Newhook. Much of the experimental work described herein was conducted to verify the design of the field structure.

5.1 General Arrangement

The general form is that of concrete slab-on-steel-girder construction with two simply supported spans of 31 200 mm each. One of the spans was designed using the steel-free bridge deck technology. A plan view of the bridges is shown in Figure 5.1.

Both structures are located on a vertical and horizontal curve in the road alignment. The radius of curvature of the horizontal curve was such that the girders could be designed as straight, not curved, girders with the centerline of the road offset from the centerline of the structure. Both structures were designed with a skew angle of 22° 15' 0". The deck was also super-elevated with a 4.8% cross-slope. To compensate for the vertical curve alignment both the conventional and the steel-free concrete deck were haunched over the girders. The haunch of the steel-free concrete deck was increased slightly to allow for removal of the deck formwork. The average haunch dimension was 130 mm.

At the abutments, the reinforced concrete footings rested on reinforced earth backfill. Because of the potential for settlement at these abutments, the bridges were constructed as two simple spans with a deck joint at the central pier rather than as continuous over the pier.

The typical cross-section and elevation of the Salmon River Bridge is shown in Figure 5.2.

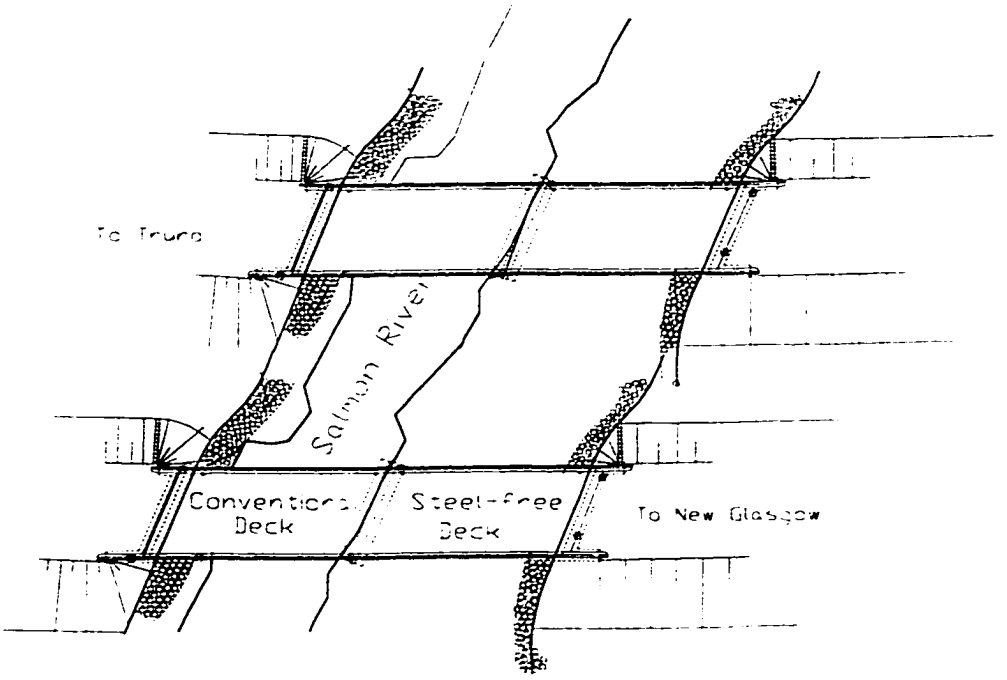

Figure 5.1 Plan view of Salmon River Bridge

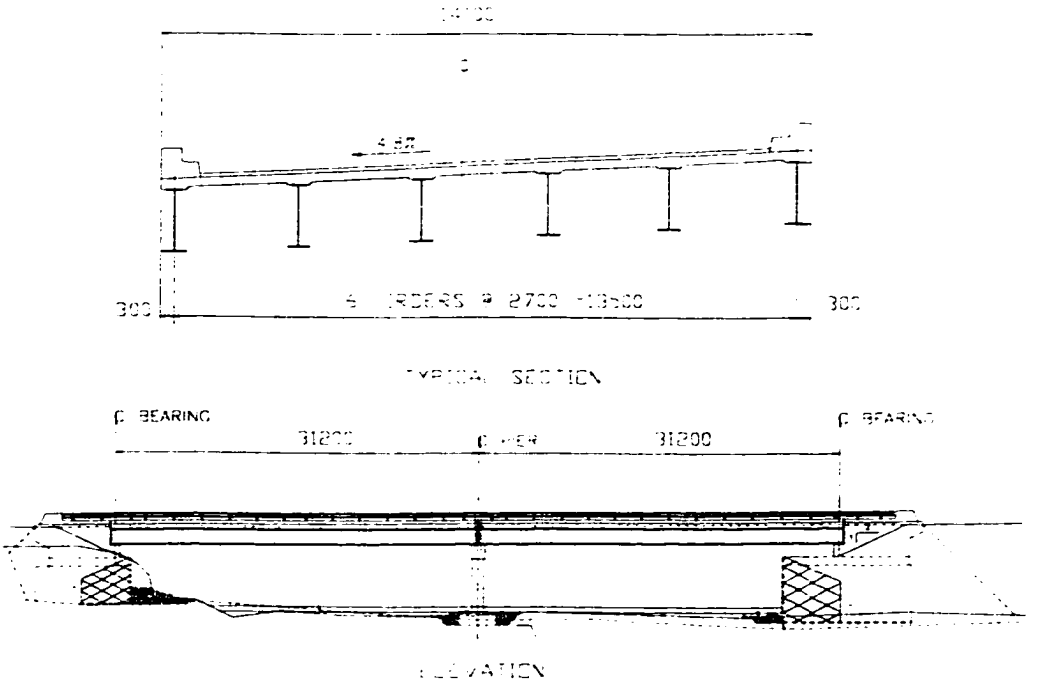

Figure 5.2 Typical section and elevation of Salmon River Bridge

The design of girders, piers and footing was done according to CAN/CSA-S6-88 Design on Highway Bridges (CSA-S6) using dead and live load provisions. The conventional deck was also designed according to the CSA-S6 Standard.

A partial cross-section of the steel-free concrete bridge deck is shown in Figure 5.3. In both systems the concrete deck was made composite with the steel girders using the shear connector requirements of CSA-S6. The size and spacing of shear studs is sufficient for both longitudinal shear and internal arching forces. The general details of both bridge deck designs are given in Table 5.1 and the mix design is given in Table 5.2.

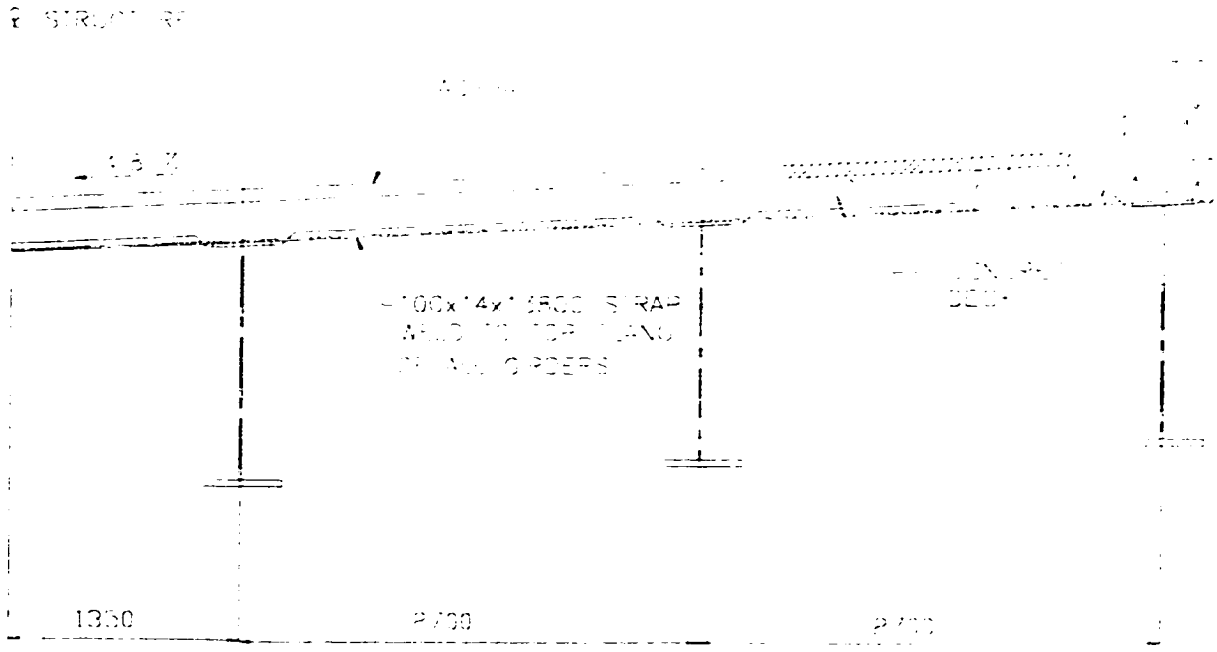

Figure 5.3 Partial elevation of steel-free deck

Table 5.1. General Design Details

Item	Conventional Design	Steel -Free Design
Girder Spacing	2 700 mm	2 700 mm
Slab Thickness	200 mm	200 mm
Concrete Strength	35 MPa	35 MPa
Steel Reinforcement	1.9%	0 %
Steel Straps	0 %	0.5%

Table 5.2. FRC Concrete Mix

Component	Mix Design
Type 10 Cement	415 kg/m3
Water	160 kg/m3
Coarse Aggregate	980 kg/m3
Fine Aggregate	754 kg/m3
Fibres	5.0 kg/m3
Low Range Water Reducer	1 L/m3
High Range Water Reducer	3.5 L/m3
Air Content	6%

5.2 Experimental Verification of Ultimate Strength

Considering only the restraint stiffness of the straps the theoretical ultimate load for this configuration was 550 kN. As demonstrated by ultimate load test 1, described in Section 4.2.7, the ultimate load capacity of the system was 1275 kN. If one considers the maximum permissible wheel load to be 49 kN and the factored design wheel load to be 196 kN then the actual failure load represents factors of safety of 26 on permissible loads and 6.5 design loads respectively. It was determined that the first cracking load of the concrete in the lab model was approximately 470 kN. If this is considered as the serviceability limit state for this system then there is a serviceability safety factor of 4.8 on the maximum observed unfactored wheel load of 98 kN. However, it should be noted that after 4 months of service,

cracking was observed on the underside of the deck on the Salmon River Bridge. The testing in the lab was performed only 1800 mm from the end of the slab. In this case, the transverse edge beam and diaphragm act as a fixed support. The flexural behaviour in the lab, therefore, closely resembled that of a two way slab. In the field, the cracking occured close to midspan of the structure. The precracking flexural behaviour in the field closely resembled a one way slab in bending. Considering a 1000 mm wide strip, a deck thickness of 200 mm, and a flexural modulus of rupture of the concrete of 6.0 MPa, the cracking load of the field slab is calculated as 6 tonnes for simply supported end conditions and 12 tonnes for fully fixed end conditions. The actual cracking load can be assumed to be between these two limits. In addition, it is believed that a series of load effects including impact, dynamic loading, thermal stresses and shrinkage stresses all combined to make the actual stress range in the field significantly higher than that of just static wheel loading alone. These effects were not present in the laboratory testing. The combination of different precracking flexural behaviour and increased stress range leads to the cracking of the field slab under ordinary vehicle loads whereas the laboratory deck cracked under a much higher monotonic static load.

The tandem wheel load test (Section 4.2.9) demonstrated that the proof load for an axle spacing of 600 mm was 1422 kN. For a typical design truck, as given by the Ontario Highway Bridge Design Code, the minimum axle separation is 1200 mm. The lab test can be considered to be a much more severe condition then would occur on the actual structure. The corresponding single wheel proof load is 711 kN. Considering that the ultimate factored wheel load is 200 kN, this corresponds to a factor of 3.6 for the proof load.

It was discussed in Section 4.2.10 that the system has a reserve capacity of at least 951 kN even in a deteriorated condition where the straps have yielded or failed and the deck is severely cracked. Therefore, even at the lower bound of failure loads, the system has a factor of 4.75 on the ultimate single wheel design load.

5.3 Design of Connections and Barrier Wall

The steel-free bridge deck system at Salmon River involved two important connection details, the first was the welded connection of the straps to the girder flanges and the second was the connection of the crash rail to the bridge superstructure. In the case of the welded strap connection, two considerations were important: design of the weld for ultimate strength and design for fatigue. For ultimate strength design, the critical load was determined from the yield strength of the strap. For fatigue, the stress range in the weld was limited to 48 MPa as per CSA-S6 requirements for a class W connection detail with over 2 million cycles of load reversal. The program PUNCH was used to predict the stresses in the welds due to service loads. Fatigue criteria were found to govern the weld design. From the testing performed in the lab, typical values of strap strain for various load locations under a service load of 90 kN are presented in Table 5.3. It is seen that the assumed fatigue strain for design is well above any of the corresponding strain values recorded.

Table 5.3. Maximum Strain (micro strain) in Straps at a Load of 90 kN

Test #	Strap	Distance to Load	Micro Strain
1	8	600	33
1	9	1 800	63
2	5	300	113
3	2	0	68
3	1	1 200	106
4c	5	0	94
design	-	0	257

The connection of the aluminum crash rail post to the deck curb and parapet required a unique design detail. Standard practice with this system is to anchor the posts to the curb/parapet which is in turn anchored to the deck with steel rebar. A crash causes an overturning moment on the system which is resisted by the top steel in the bridge deck. A deck devoid of reinforcement therefore cannot be used as the principal load resisting system

for this type of loading. An alternate connection was designed (Figure 5.4) where the post anchor bolts, which are in tension, are extended through the curb and deck concrete and anchored to cross-members connected to the girders. The anchor bolts are encased in PVC tubes to prevent forces being transferred to the concrete by bond with the bolts. The structural steel is then the primary load resisting system for tension. The deck and curb concrete resists only compressive and secondary forces which may arise in the event of a crash.

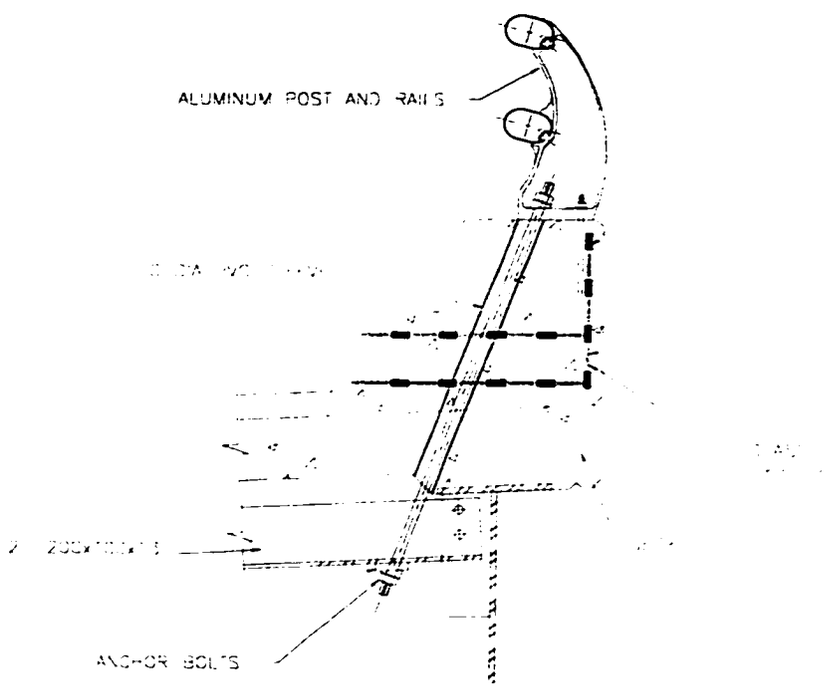

Figure 5.4 Typical curb and railing detail

5.4 Design of Curb Using NEFMAC

Steel reinforcement in curbs is a primary location for deterioration caused by de-icing salts. To provide durability similar to the steel-free deck, a fibre-reinforced plastic reinforcement was used in the curbs and parapets. Because the curbs are not participating in the tension forces from the crash rail, reinforcement in the curbs resist only secondary load effects from

a crash and shrinkage effects under normal conditions. Therefore, glass fibre reinforcement was chosen for the curbs. In particular three layers, two horizontal and one vertical, of NEFMAC (type G10) were used, see Figure 5.4. This is a two-way reinforcement with individual bars of 35 mm^2 cross-section in a 150 x 150 mm grid.

5.5 Construction of the Steel-Free Bridge Deck

After completion of the substructure, the six girders were simply supported at the free ends. The girders were fabricated with the top flanges at 4.8% slope, rather than perpendicular to the girder web, to match the cross slope of the deck. This allowed the steel straps to be continuous across all six girders with no gaps between the top of the girder and the strap. This reduced the amount of welding and simplified the girder strap connection detail. The cost of fabrication of the girders was not significantly affected by this detail. To provide composite action with the deck, rows of three 22 mm diameter shear studs were used. In the conventional design, these rows were spaced at 300 and 250 mm, at the midspan section and end sections respectively. This spacing was adhered to in the steel-free design; however, some local adjustments to spacings were made to accommodate placement and welding of the straps. During erection of the girders a standard system of diaphragms were installed according to the provision of CSA-S6. This consisted of two end diaphragms and four intermediate diaphragms spaced at approximately 7200 mm. At each end diaphragm, a C380 x 50 channel was welded to the top flanges of adjacent girders and made composite with the deck, which was thickened at these edges. In a conventional design, this channel would be installed with its strong axis in the vertical plane. However, in the steel-free design, the strong axis was placed in the horizontal plane (Figure 5.5) to provide in-plane restraint in the longitudinal direction of the slab. This type of edge beam is necessary to achieve punching failure behaviour at the free edge of the deck slab (Newhook et al., 1995). In addition, C200 x 28 channels (see Figure 5.5) were welded between the C380 x 50 edge beams and adjacent girders to compensate for the effect of the skew angle on the lateral restraint of the slab near the edge, (Bahkt and Agarwal, 1995).

Figure 5.5 View showing edge beam and channels

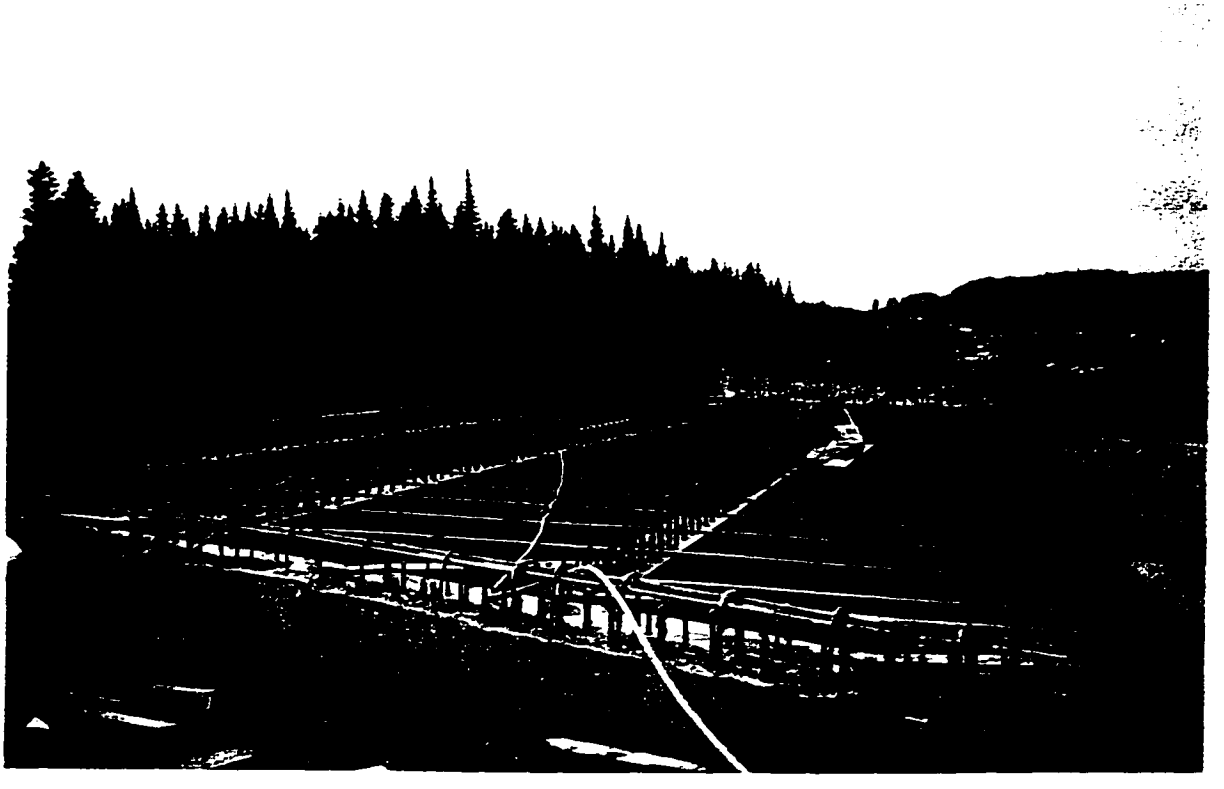

Figure 5.6 View showing welding of steel straps

The straps (100 x 14) were welded to the top of the girder and spaced at an average spacing of 1200 mm. Because the straps were uncoated weathering steel, a strap size of 100 x 14 was considered to be only a size of 100 x 12 in design. This was to allow for a 2 mm loss of section thickness due to the weathering process (Figure 5.6).

After the completion of the steel supporting frame system shown in Figure 5.6, the polypropylene fibre- reinforced concrete was placed. Figures 5.7 and 5.8 show the concrete deck being constructed. The absence of the steel reinforcement which would be present in a conventional bridge deck is immediately noticeable.

Although in the lab, 0.8% fibre content by volume was mixed with the concrete, this amount was not user-friendly in field conditions using large quantities of concrete. A slight reduction to 0.55% fibre content made the workability of concrete easier for the concrete suppliers and for placement by the contractor. The fibres are essentially being used for shrinkage crack control and the reduction in the fibre volume fraction did not affect the design.

After completion of the asphalt wearing surface, the Salmon River bridge was opened to traffic (Figure 5.9).

Figure 5.7 View of concrete placement

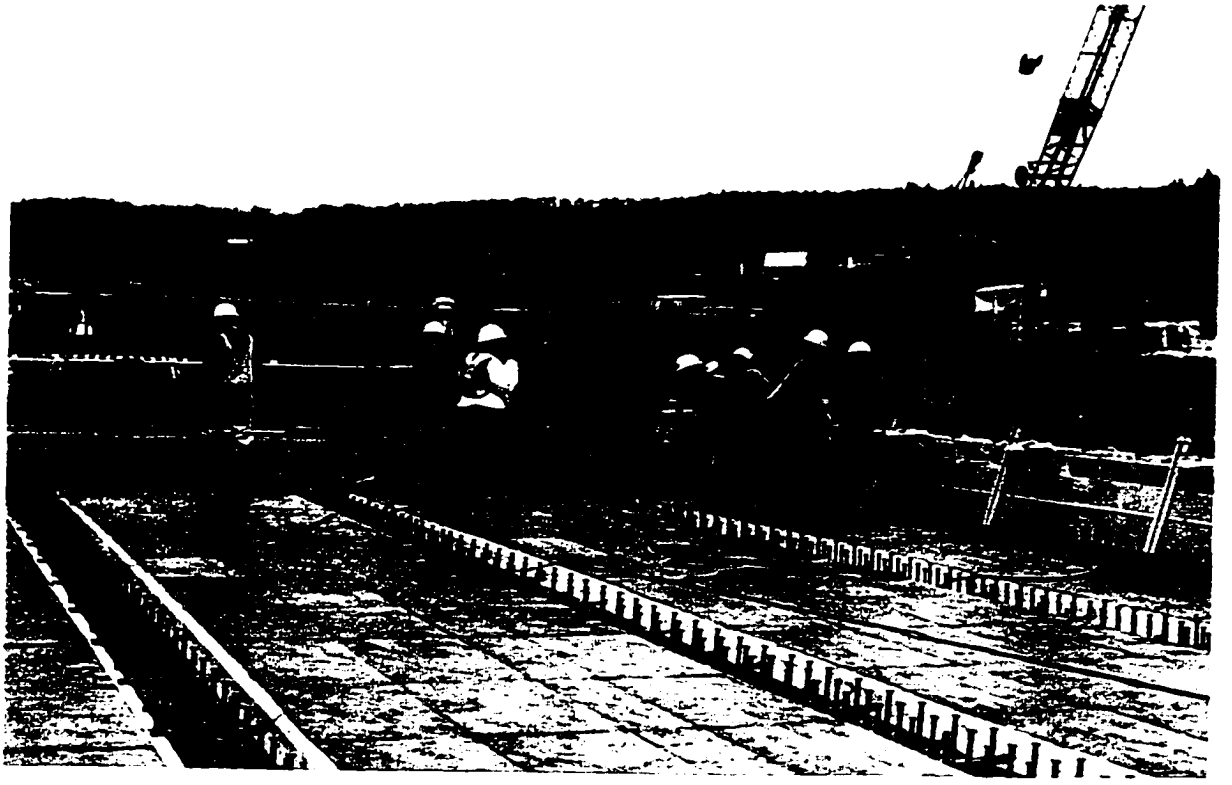

Figure 5.8 View showing no internal reinforcement in deck slab

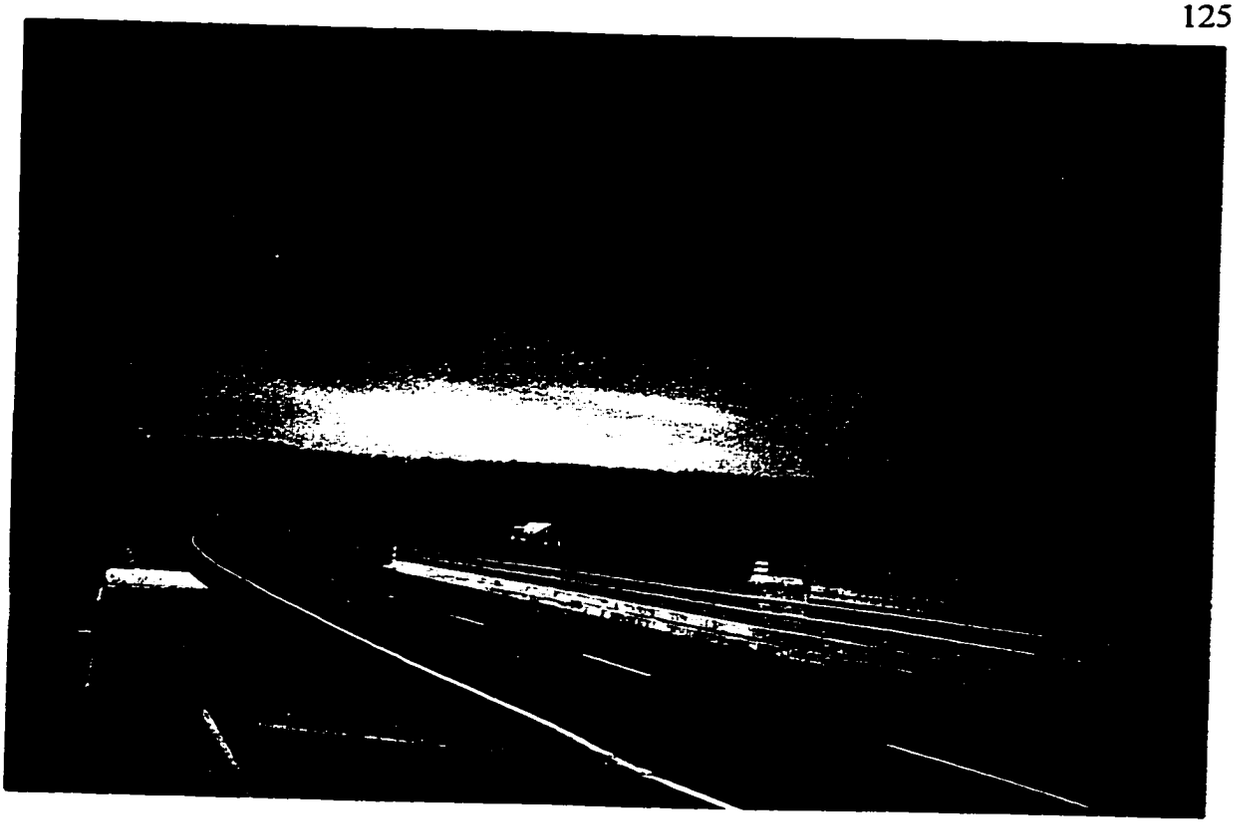

Figure 5.9 Salmon River Bridge Trans-Canada Highway 104

5.6 Economic Analysis

The total cost, in 1995 Canadian funds, of the two bridge structures at Salmon River was $2,300,000. The cost of each of the four spans, including deck, girders, foundations and abutments, is estimated to be $575,000. For comparisons based on square metres of bridge deck, the area of the deck on each span is taken as 440 m^2. The total cost of the conventional deck construction alone was $63,000 or $143/$m^2$. The total cost of the steel-free deck construction alone was $66,850 or $152/$m^2$. It should be noted that, while both styles of construction used the same volume of concrete, the cost of the conventional bridge deck concrete was $420/$m^3$ whereas the cost of the fibre reinforced bridge deck concrete, with 0.55% polypropylene fibre, was $542/$m^3$. It is cautioned that the quoted prices are based on the negotiated unit prices between the contractor and the owner for the Salmon River Project. As such, they must be scrutinized in light of three considerations: 1) the prices are based on pre-construction estimates not actual post-construction costs; 2) the prices are based on one

project only not the average of a number of projects; 3) the prices undoubtedly include some level of contingency as this was the first ever usage of this system and the contractor had no previous experience. Based on experience gained from this project, the designers feel that capital cost savings can be realized in future projects by:

- reducing the concrete deck thickness from 200 mm to 175 mm, giving a unit cost of $\$138/m^2$.
- reducing the polypropylene fibre content from 0.55% to 0.4%, giving a unit cost of $\$134/m^2$

These two changes would represent a 6.3% capital cost savings for the steel-free deck technology compared to conventional technology. A further cost savings can be realized by eliminating the waterproofing membrane and asphalt wearing surface on the steel-free deck for a savings of about $\$26/m^2$. This can be replaced by a 10 mm thick concrete wearing coarse costing $\$5/m^2$ for a net savings of $\$21/m^2$. In this case the cost of the steel-free deck can be reduced to as low as $\$115/m^2$.

The most significant savings with the steel-free deck system is in operation, maintenance and repair costs. A recent study by the US National Institute of Standards and Technology (Ehlen and Marshall, 1996) estimates that the typical cost of these three factors is $\$51/m^2$. Approximately 80% of these costs are user costs. The steel-free deck has the potential to eliminate almost all of these costs. In Salmon River Bridge design, the only maintenance item should be the external steel straps. These straps are accessible from beneath the structure and should be on the same maintenance cycle as the steel girders. The required maintenance, if any, will not disrupt traffic flow and therefore the user costs will be eliminated. The agency costs for materials and labour, which makes up the other 20% of the maintenance costs, should be substantially less than that required for concrete deck repair or replacement as is often required for reinforced concrete bridge decks.

The unique curb connection shown in Figure 5.4 also merits discussion. The cost of this curb connection detail was $48,500 compared to a conventional connection detail costing $11,700

for one span. If we now include the cost of the curb connection with the deck costs given above, we see that the conventional design cost $\$170/m^2$ while the steel-free design cost $\$262/m^2$. While the connection detail used may have substantially lower long-term maintenance cost compared to the conventional design, some owners may be concerned more with initial cost reduction. To address this situation, the designers suggest two alternatives:

- use a steel-free deck with conventional steel reinforced curbs, in which case the cost of the system will be approximately $\$167/m^2$.
- use the concrete barrier suggested by Bakht and Mufti (1996) at a total cost of $\$169/m^2$.

6 PARAMETRIC INVESTIGATION OF BEHAVIOUR USING THE RATIONAL MODEL

6.1 Deck Behaviour Investigation

The rational model, which was developed in Chapter 2 and validated in Chapters 3 and 4, can be used to theoretically investigate the effect of the key parameters on the system behaviour. The key parameters are identified as the girder spacing, S_g; the effective depth of the deck, **d**; the restraint stiffness, **K**, the yield strain of the straps, ϵ_y; the compressive strength of the concrete, f'_c; and the ultimate failure load, P_u . The tire print is taken to a constant size of 250 x 500 as given by the OHBDC. In addition, the concrete confinement constant, **k**, is also taken to be a constant with a value of 10 as demonstrated in Section 2.4. The range investigated for each of these parameters is given in Table 6.1.

Table 6.1 Parameters and Range of Values for Investigation

Parameter	Range				
S_g (mm)	1500	2000	2500	3000	3500
d (mm)	175	200	225	250	275
f'_c (MPa)	25	30	35	40	50
P_u (kN)	400	500	600	1000	
ϵ_y	0.0015	0.00175	0.002		

A base case representing a typical bridge deck, given in Table 6.2, was chosen. One parameter was then selected and varied over the range given in Table 6.1. The Punch program was used to analyse each new configuration and predict the change in behaviour of the system or the effect on other parameters.

Table 6.2 Base Case Bridge Deck Parameters

Parameter	Value	Parameter	Value
S_g (mm)	2500	tire print (mm x mm)	250 x 500
d (mm)	200	strap to load spacing (mm)	0
f'_c (MPA)	30	β	0.85
ϵ_y	0.0015	confinement constant	10

6.1.1 Restraint Stiffness

Holding all other values constant, the restraint stiffness is varied from 80 N/mm/mm to 700 N/mm/mm. Assuming the ultimate design wheel load to be 200 kN, the values of strap strain ,ϵ_s, and central deflection, Δ, at 200 kN are recorded for each increment of restraint stiffness. The strap strains are converted to an equivalent restraining force, F in unit of force per metre of circumference of the wedge, by equation 49.

$$F = \epsilon_s \cdot \frac{S_g}{2} \cdot K \tag{49}$$

This comparison demonstrates the effect of changing the restraint stiffness on the system behaviour for the same value of applied load.

Table 6.3 System Response for Varying K at an Applied Load of 200 kN

K (N/mm/mm)	P (kN)	ϵ_s	Δ (mm)	F (kN/m)
80	200	0.00136	11.43	136
100	200	0.00109	9.14	136
200	200	0.00054	4.57	135
300	200	0.00036	3.04	135
400	200	0.00027	2.29	135
500	200	0.00022	1.81	137
600	200	0.00018	1.51	135
700	200	0.00015	1.30	131

The results of Table 6.3 are plotted in Figure 6.1, **K** versus Δ, and Figure 6.2, K versus ϵ_s. As expected the increase in restraint stiffness causes a decrease in central deflection. The relationship is exponential with the most significant decrease occurring up to 400 N/mm/mm. After this point, the change in the absolute value of deflection is small. A similar trend applies to the change in strap strain. An increasing value of **K** results in an exponentially decreasing value of strap strain. The most interesting comparison, however, is the value of restraining force. It is a constant value of about 135 kN/m for all values of restraint stiffness. The slight variations in Table 6.3 are presumably due to round-off errors in the strain values. Therefore, for the configuration given in Table 6.2, the restraining force for an applied load of 200 kN is constant and independent of the value of restraint stiffness. In more general terms, for a given deck configuration, each value of applied load has a characteristic value of restraining force which is not dependant upon the magnitude of restraint stiffness. This has an implication on understanding the function of the straps in the system. The influence of the straps on system behaviour is not in the amount of force developed by an individual strap for a unit displacement but rather in the stiffness of the strap. The strap stiffness will actually determine the amount of lateral deflection which must occur to develop the restraining force for the applied load.

Extending the evaluation of the restraining stiffness on the behaviour of the system, Table 6.4 presents the failure data for the deck configuration given in Table 6.2. Again the restraining force F is calculated for each failure. The failure is designated as *concrete* when crushing of the concrete initiates punching failure and *strap* when yielding of the strap initiates punching failure (Section 2.3.6).

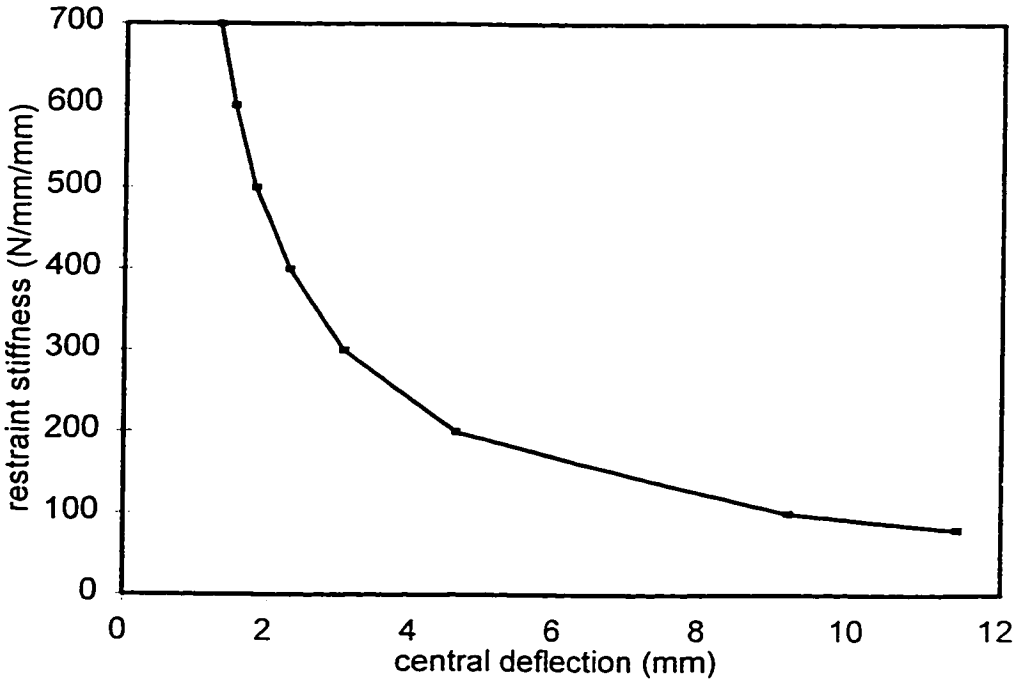

Figure 6.1 Restraint stiffness versus deflection, Table 6.3

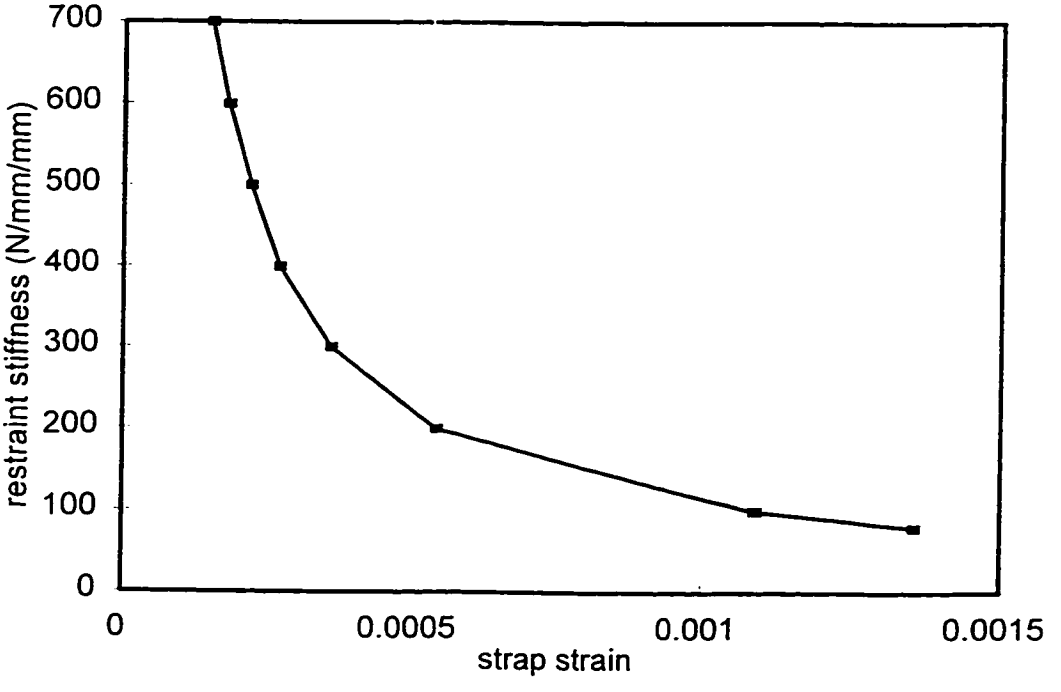

Figure 6.2 Restraint stiffness versus strap strain, Table 6.3

Table 6.4 System Response for Varying K Values at Failure

K (N/mm/mm)	P (kN)	ϵ_s	Δ (mm)	F (kN/m)	failure mode
80	215	0.0015	12.69	150	strap
100	265	0.0015	12.87	188	strap
200	506	0.0015	13.71	375	strap
300	720	0.0015	14.29	563	strap
400	920	0.0015	14.86	750	strap
500	1100	0.00149	15.17	936	concrete
600	1210	0.00139	14.49	1042	concrete
700	1310	0.00132	13.94	1155	concrete

As expected, the failure load increases as the restraint stiffness increases. The relationship is plotted in Figure 6.3. It is noted that when the mode of failure switches from strap yielding to concrete crushing, the slope of the line also changes to become flatter. When the failure is determined by strap yielding, the benefit of increasing the restraint stiffness is much greater than when the failure is controlled by concrete crushing. Also, strap yielding dominates at low values of restraint stiffness while concrete crushing dominates at higher values.

A curve of deflection at failure versus restraint stiffness is plotted in Figure 6.4. Again the curve changes as the failure mode switches from strap yielding to concrete crushing. For strap failure, the deflection at ultimate will increase with increasing values of restraint stiffness. However, the ultimate deflection decreases as the restraint stiffness increases for conditions in which the concrete crushing dominates.

The restraining force is calculated and presented in Table 6.4. Unlike Table 6.3, where the restraining force was invariant with respect to restraint stiffness, the restraining force in this case increases with an increase in restraint stiffness. This is undoubtedly due to the increase in failure load. A plot of failure load versus restraining force, Figure 6.5, shows a consistent relationship between the failure load and the restraining force. This relationship is not

affected by the failure mode and appears to be quite linear. Based on the information in Tables 6.3 and 6.4, it can be concluded that for a given girder spacing, deck thickness and concrete strength, there is a characteristic value of restraining force associated with each value of applied load that is independent of the value of restraint stiffness.

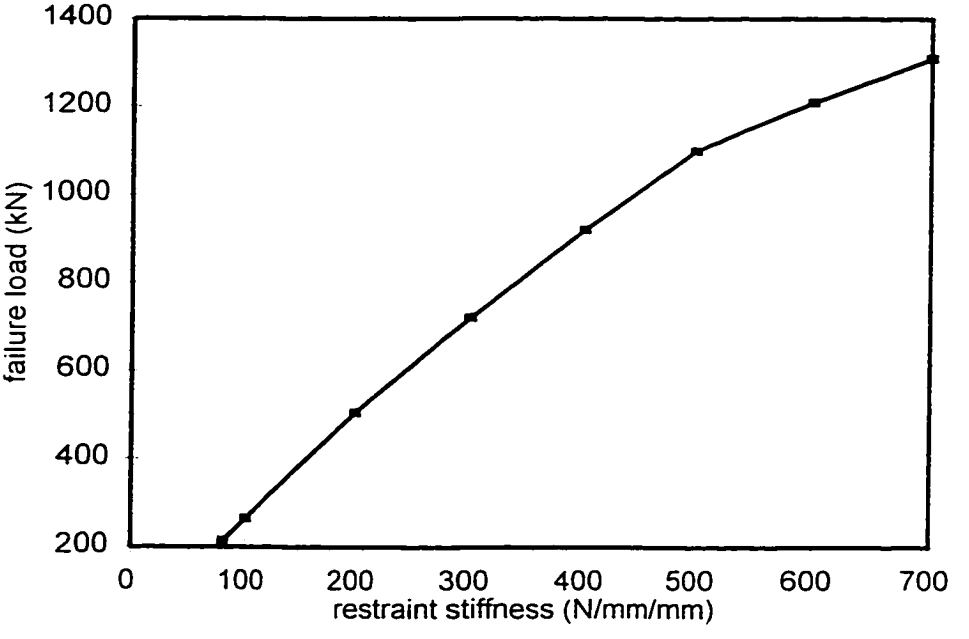

Figure 6.3 Failure load versus restraint stiffness, Table 6.4

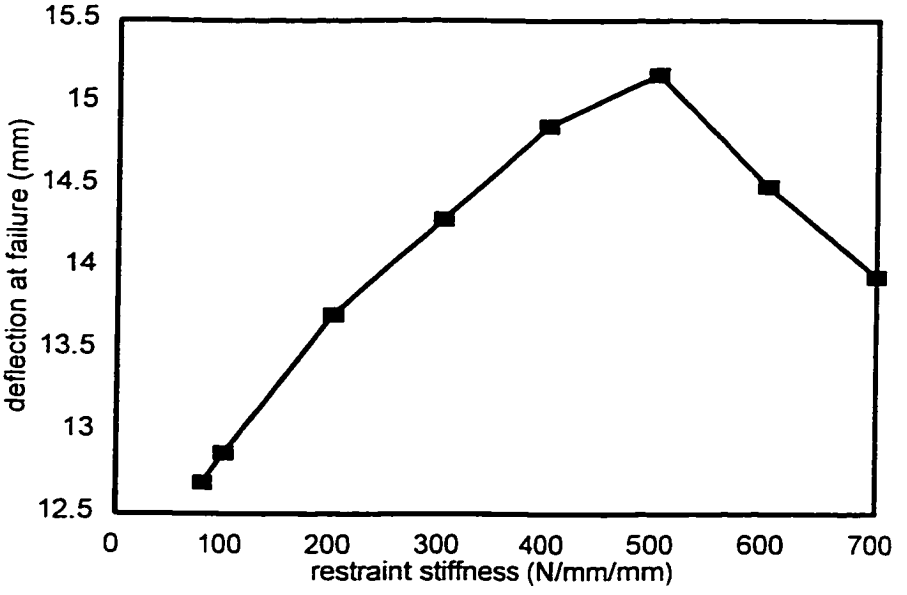

Figure 6.4 Deflection at failure versus restraint stiffness, Table 6.4

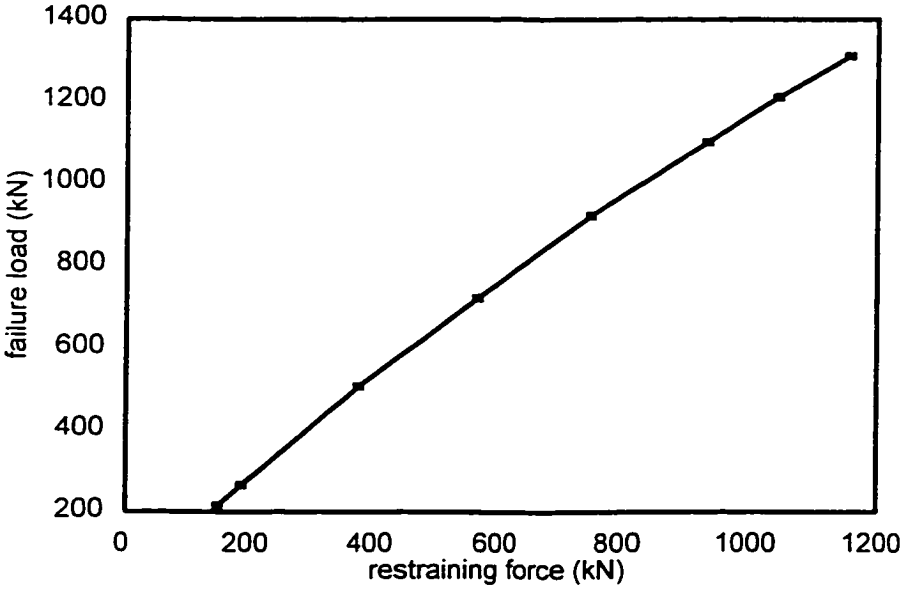

Figure 6.5 Failure load versus restraining force, Table 6.4

6.1.2 Yield Strain of the Straps

The next parameter to be investigated is the yield strain of the straps. The deck configuration given in Table 6.2 is used as the base model and the restraint stiffness is varied as in Table 6.1. However, the yield strain of the strap is changed from 0.0015 to 0.002. Table 6.5 presents the same investigation as Table 6.4 except that the yield strain of the strap is higher. Changing the yield strain is obviously a failure criteria consideration only and the behaviour exhibited in Table 6.3 at a constant applied load of 200 kN will be unaffected.

Table 6.5 System Response at Failure for $\epsilon_y = 0.002$

K (N/mm/mm)	P (kN)	ϵ_s	Δ (mm)	F (kN/m)	failure mode
80	277	0.002	17.26	200	strap
100	342	0.002	17.57	250	strap
200	637	0.002	18.86	500	strap
300	826	0.00178	17.42	667	concrete
400	971	0.00161	16.10	805	concrete
500	1100	0.00149	15.17	936	concrete
600	1210	0.00139	14.49	1042	concrete
700	1310	0.00132	13.94	1155	concrete

With a yield strain value of 0.002, the concrete failure mode dominates at a much lower value of restraint stiffness. Figures 6.3, 6.4 and 6.5 are repeated in Figures 6.6, 6.7 and 6.8 respectively; however, the data from Table 6.5 is added for comparison. The failure load versus restraint stiffness follows the same behaviour as before except that the magnitude of the failure loads is much higher up to a restraint stiffness value of 500 N/mm/mm. The change in curve is again noticeable when the failure mode switches from strap yielding to concrete crushing.

Figure 6.7 clearly shows that the deflection values at failure decreases with increasing restraint stiffness when the concrete crushing dominates. The relationship between failure load and restraining forces is consistent with that presented in Figure 6.5.

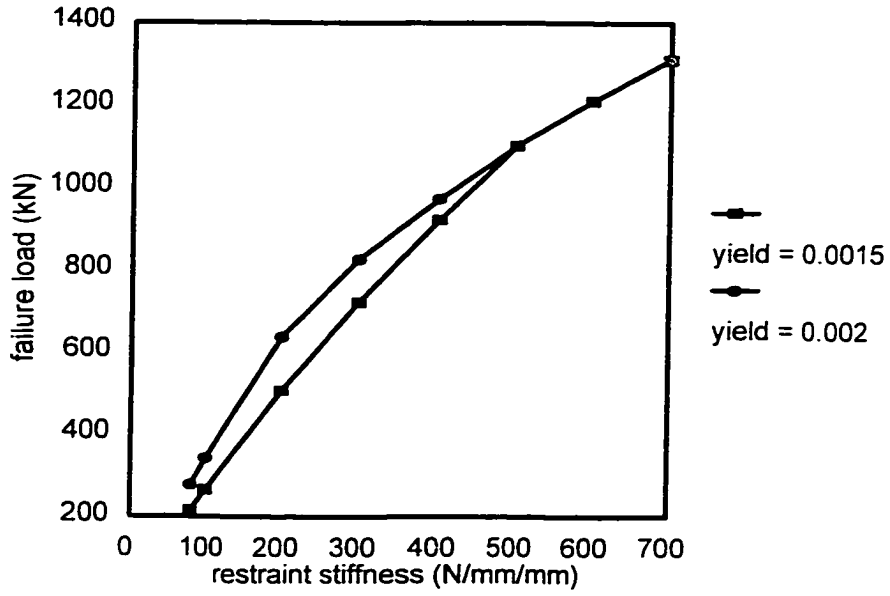

Figure 6.6 Failure load versus restraint stiffness for varying yield strains

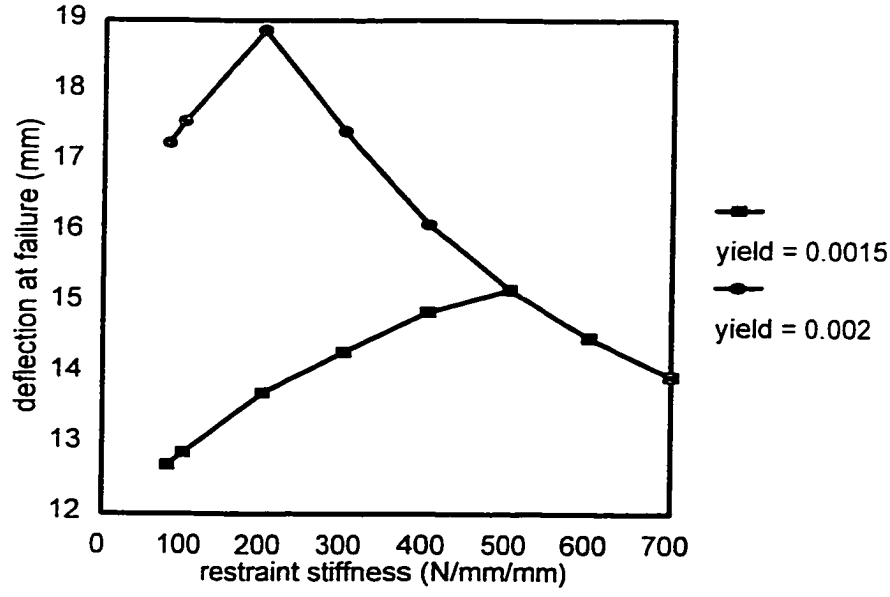

Figure 6.7 Deflection at failure versus restraint stiffness for varying yield strains

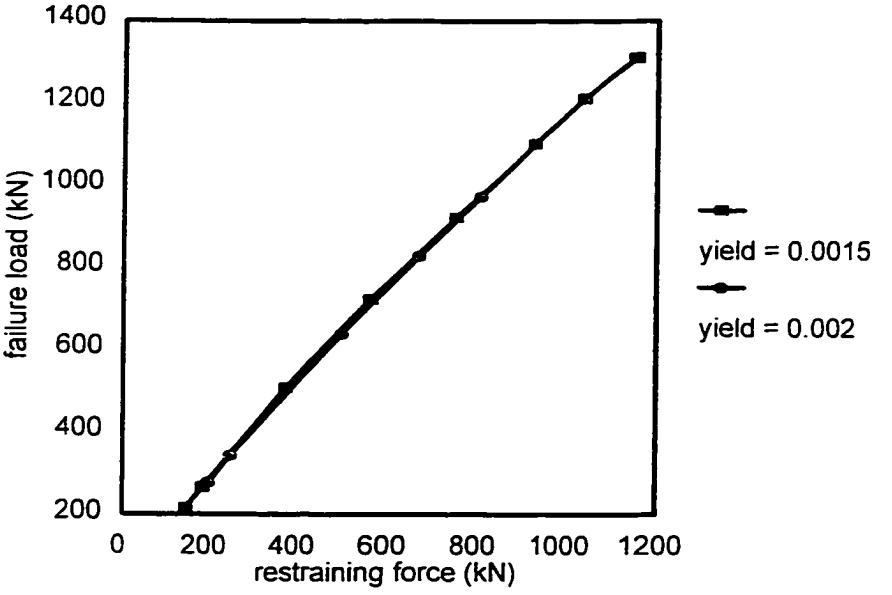

Figure 6.8 Failure load versus restraining force for varying yield strains

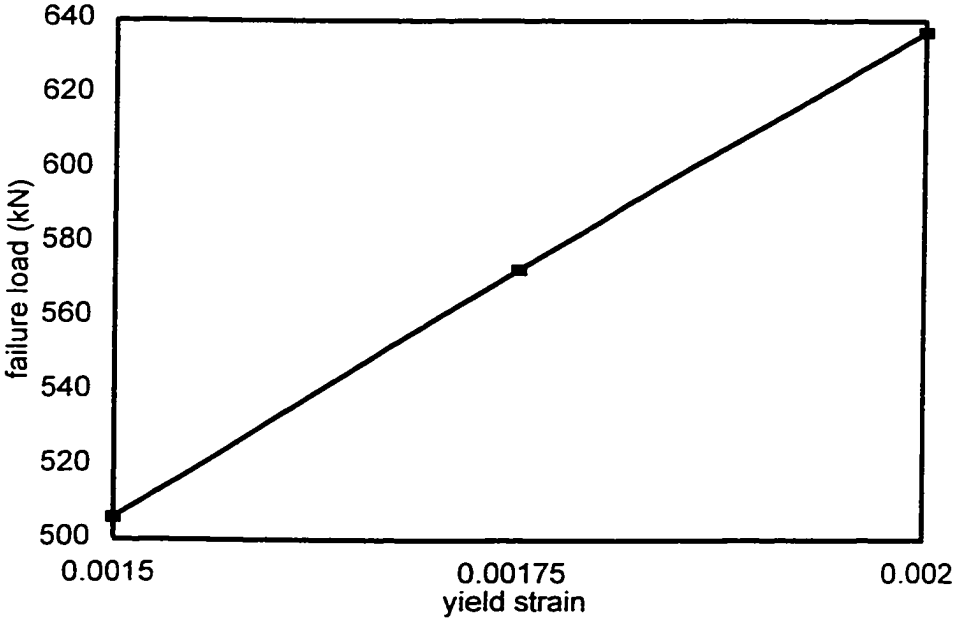

Figure 6.9 Failure load versus yield strain

It is noted that $\epsilon_y = 0.0015$ (Table 6.4) gives mostly strap yielding failure while $\epsilon_y = 0.002$ (Table 6.5) gives mostly concrete crushing failure. This fact will be used in subsequent studies to help assess the behaviour of the system for both failure modes.

By way of further investigation, the configuration in Table 6.2 is used with a constant restraint stiffness value of 200 N/mm/mm. The yield strain of the strap is varied from 0.0015 to 0.00175 to 0.002. The results are given in Table 6.6.

Table 6.6 System Response for Varying ϵ_y

ϵ_y	P (kN)	Δ (mm)	failure mode
0.0015	506	13.71	strap
0.00175	573	16.23	strap
0.002	637	18.86	strap

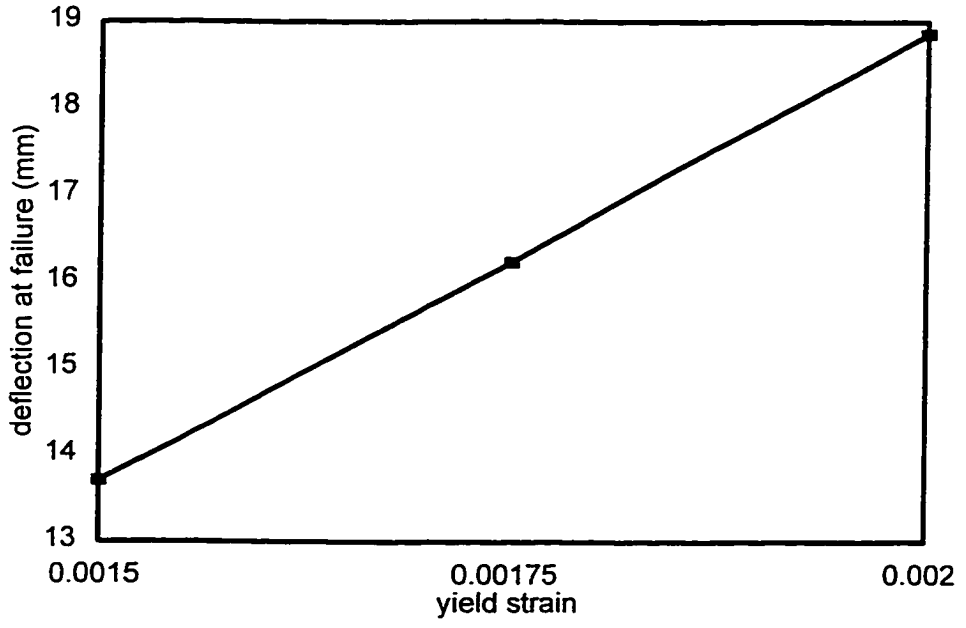

Figure 6.10 Deflection at failure versus yield strain

A plot of failure load versus yield strain, Figure 6.9, and deflection versus yield strain, Figure 6.10, reveal a nearly linear increase in values with respect to yield strain. The case presented is for conditions which lead to failure by strap yielding. In cases where the failure is initiated by concrete failure, the yield strain of the straps has no effect.

6.1.3 Girder Spacing

The configuration in Table 6.2 is used with a constant restraint stiffness of 400 N/mm/mm. The spacing of the girders is varied according to the values given in Table 6.1. The resulting failure data is given in Table 6.7 for a yield strain of 0.0015 and Table 6.8 for a yield strain of 0.002.

Table 6.7 System Response for Varying Girder Spacing and $\epsilon_y = 0.0015$

S_g (mm)	P (kN)	ϵ_s	Δ (mm)	F (kN/m)	failure mode
1500	749	0.0015	4.64	450	strap
2000	845	0.0015	8.79	600	strap
2500	920	0.0015	14.86	750	strap
3000	811	0.00117	17.48	702	concrete
3500	704	0.00090	18.90	630	concrete

Table 6.8 System Response for Varying Girder Spacing and $\epsilon_y = 0.002$

S_g (mm)	P (kN)	ϵ_s	Δ (mm)	F (kN/m)	failure mode
1500	969	0.002	6.29	600	strap
2000	1070	0.002	12.05	800	strap
2500	971	0.00161	16.10	805	concrete
3000	811	0.00117	17.48	702	concrete
3500	704	0.00090	18.90	630	concrete

As in previous examples, the behaviour of the system is affected not only by the girder spacing but also by the failure mode. The deflection at failure versus girder spacing, Figure 6.11, appears to be the most consistent relationship with a general trend of increasing

deflection for increasing girder spacing. The behaviour of the failure load is very much influenced by the failure mode, Figure 6.12. With all other parameters held constant, the failure load will increase with an increase in girder spacing provided that strap yielding initiates failure. The failure will decrease with increasing girder spacing if concrete crushing initiates punching. The relationship between restraining force and failure load, Figure 6.13, is not as well-behaved as in Figure 6.5 or 6.8. It does however indicate that the relationship is not only a function of girder spacing as the same failure load has more than one possible value of restraining force based determined by the girder spacing.

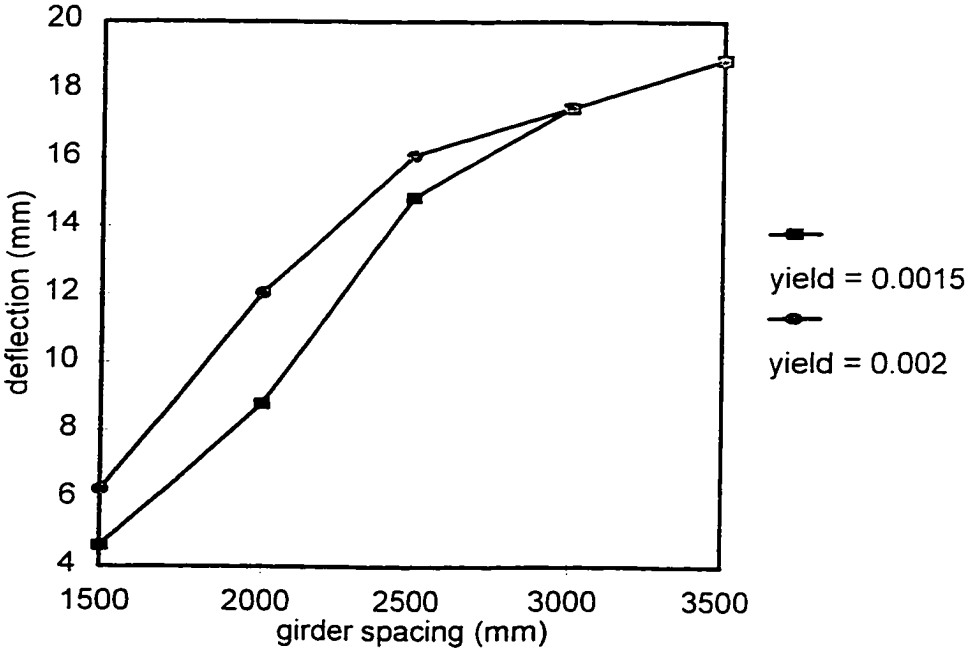

Figure 6.11 Deflection versus girder spacing

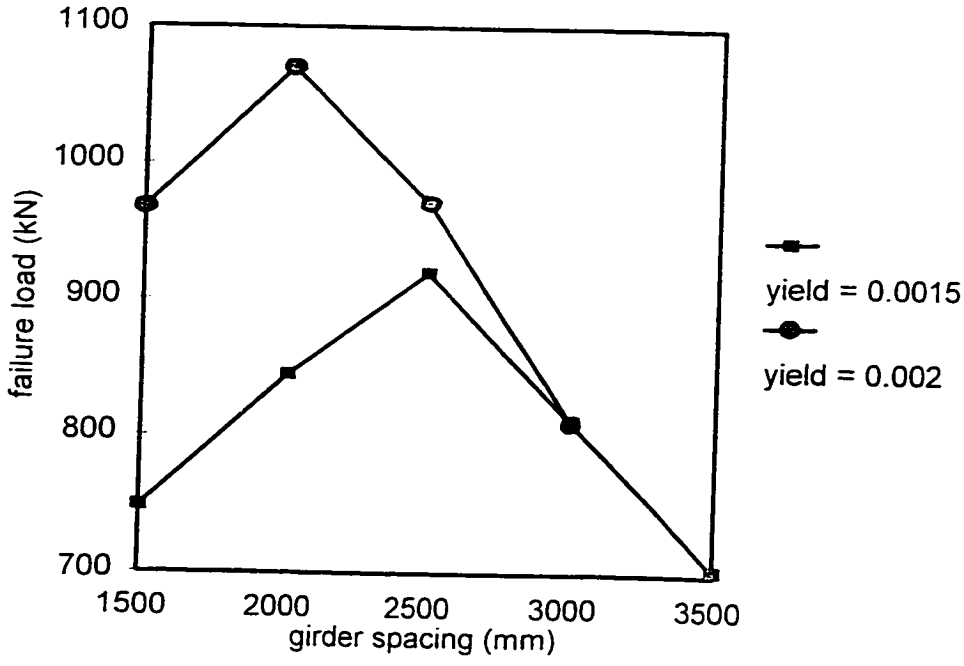

Figure 6.12 Failure load versus girder spacing

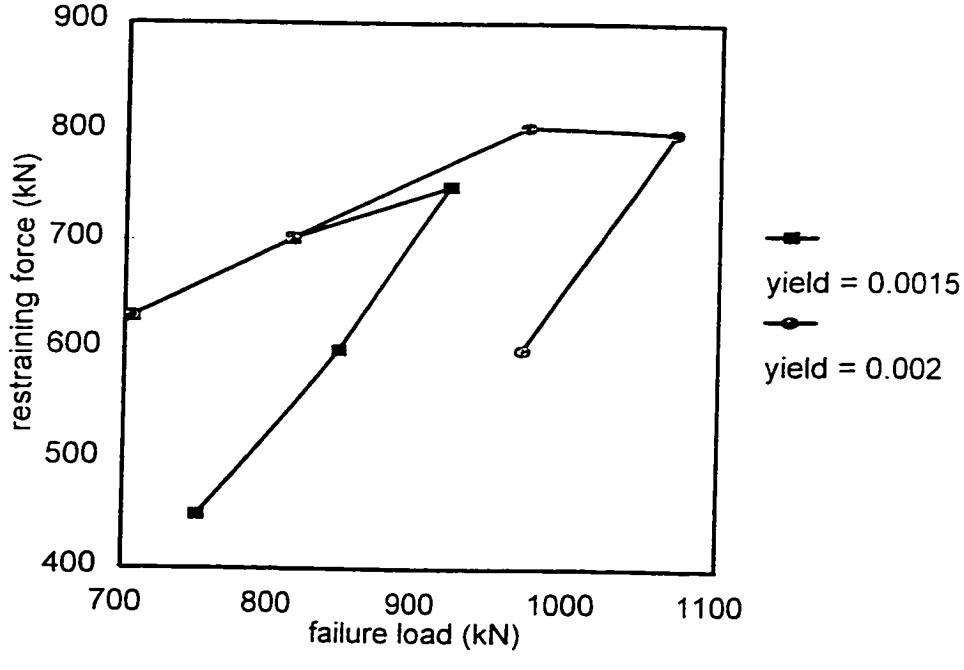

Figure 6.13 Restraining force versus failure load for varying girder spacings

6.1.4 Deck Thickness

The deck configuration given in Table 6.2 is used as a basis with a constant value of restraint stiffness of 400 N/mm/mm. The thickness of the deck is varied according to the range given in Table 6.1. The results of the study are given in Table 6.9 for a yield strain of 0.0015 and Table 6.10 for a yield strain of 0.002.

Table 6.9 System Response for Varying Deck Thickness and $\epsilon_y = 0.0015$

d (mm)	P (kN)	ϵ_s	Δ (mm)	F (kN/m)	failure mode
175	700	0.00135	16.08	675	concrete
200	920	0.0015	14.86	750	strap
225	1084	0.0015	12.56	750	strap
250	1242	0.0015	10.92	750	strap
275	1398	0.0015	9.67	750	strap

Table 6.10 System Response for Varying Deck Thickness and $\epsilon_y = 0.002$

d (mm)	P (kN)	ϵ_s	Δ (mm)	F (kN/m)	failure mode
175	700	0.00135	16.08	675	concrete
200	971	0.00161	16.10	805	concrete
225	1307	0.00190	16.34	950	concrete
250	1581	0.002	14.89	1000	strap
275	1785	0.002	13.03	1000	strap

It is interesting to note that in this case, the smaller thickness leads to punching initiated by crushing of the concrete and the larger thickness leads to punching initiated by yielding of the straps. The failure load follows a clear trend of increasing failure load for increasing deck thickness, Figure 6.14. The deflection values decrease with increasing deck thickness except when concrete failure initiates punching. In this case, the deflection increases marginally as deck thickness increases, Figure 6.15. The restraining force remains constant when strap yielding controls, even though the failure load increases, Figure 6.16. The restraining force does however change with deck thickness when concrete crushing controls.

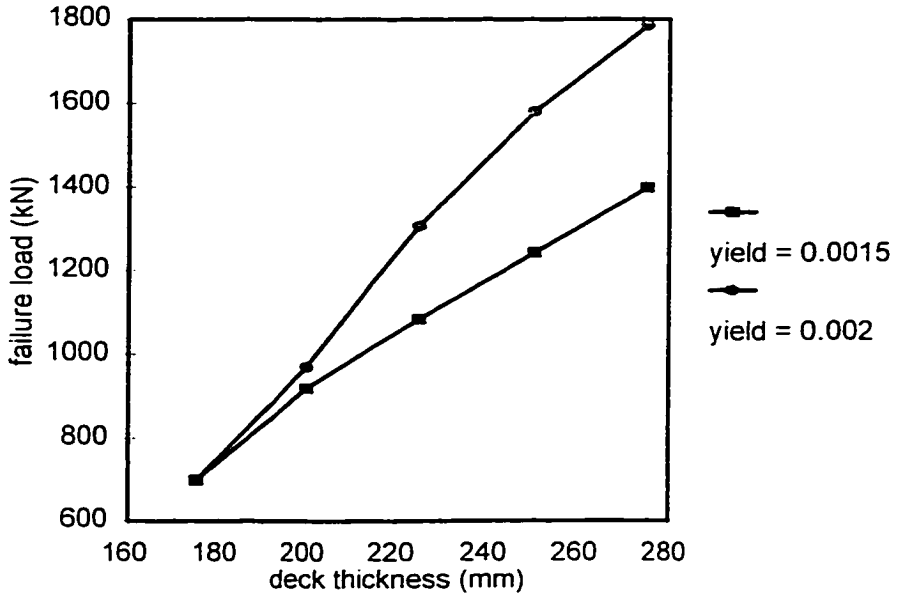

Figure 6.14 Failure load versus deck thickness

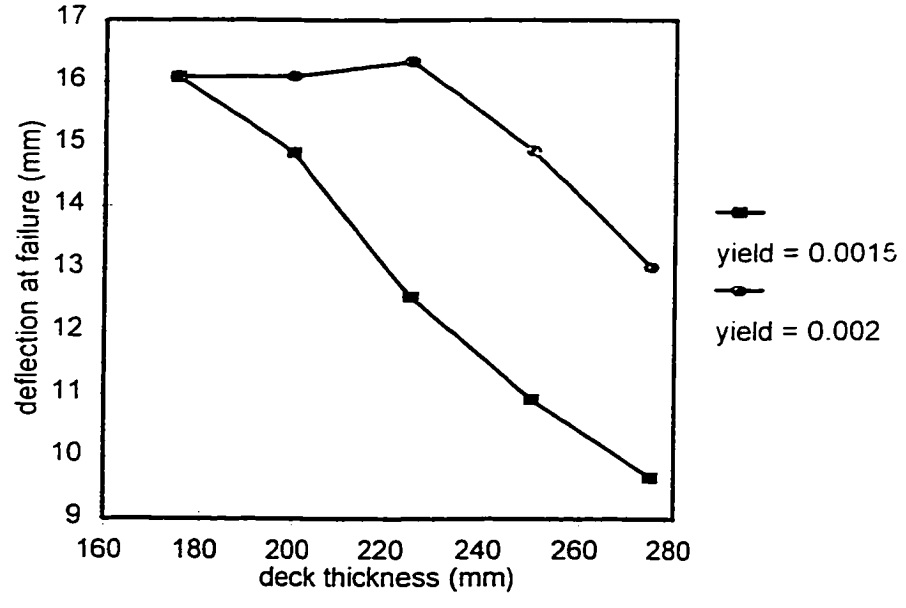

Figure 6.15 Deflection at failure versus deck thickness

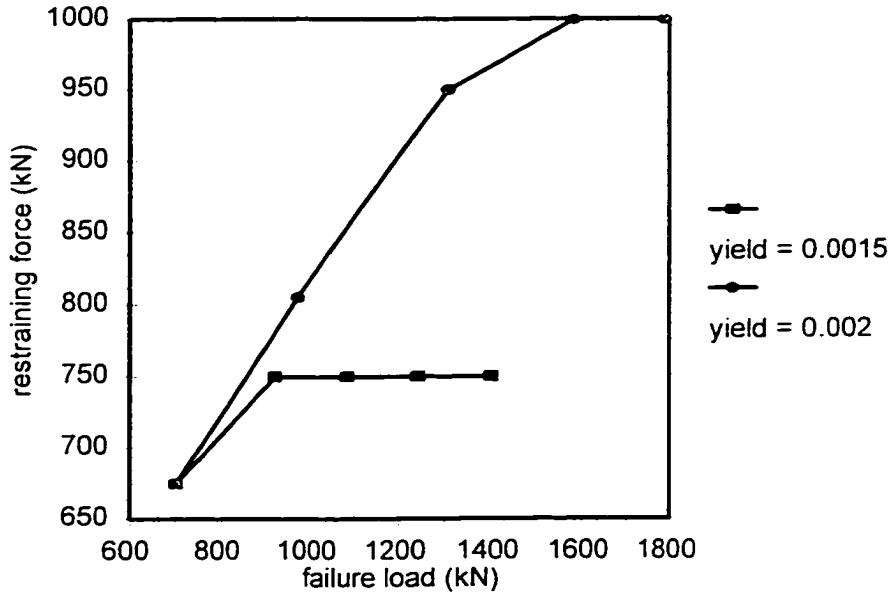

Figure 6.16 Restraining force versus failure load for varying deck thicknesses

6.1.5 Concrete Strength

The deck configuration in Table 6.2 is used as a basis with the restraint stiffness being held constant at 400 N/mm/mm. The concrete compressive strength is varied according the range given to Table 6.1. The results of the study are given in Table 6.11 for a yield strain of 0.0015 and Table 6.12 for a yield strain of 0.002. Table 6.11 produces results in which the failure is controlled by yielding of the strap. Table 6.12 produces results in which the failure is controlled by crushing of the concrete.

Table 6.11 System Response for Varying f_c' and $\epsilon_y = 0.0015$

f'_c (MPa)	P (kN)	ϵ_s	Δ (mm)	F (kN/m)	failure mode
25	897	0.0015	15.19	750	strap
30	920	0.0015	14.86	750	strap
35	946	0.0015	14.76	750	strap
40	961	0.0015	14.67	750	strap
50	984	0.0015	14.77	750	strap

Table 6.12 System Response for Varying f_c' and $\epsilon_y = 0.002$

f_c' (MPa)	P (kN)	ϵ_s	Δ (mm)	F (kN/m)	failure mode
25	905	0.00152	15.48	760	concrete
30	971	0.00161	16.1	805	concrete
35	1009	0.00164	16.34	820	concrete
40	1038	0.00166	16.5	830	concrete
50	1078	0.00168	16.66	840	concrete

Both sets of data follow the same general trend, an increase in concrete compressive strength results in an increase in failure load. In this case however the increase is only marginal. Doubling the concrete strength from 25 MPa to 50 MPa results in only a 10% increases in the failure load when strap yielding controls and a 19% increase in failure load when concrete crushing controls, Figure 6.17. Therefore, merely increasing the concrete compressive strength to a medium or high strength concrete does not appear to be an efficient way to achieve extra strength for the bridge deck system. Studying the strap strain and the deflection values, the effect of increasing the concrete compressive strength is only marginal. Figure 6.18.

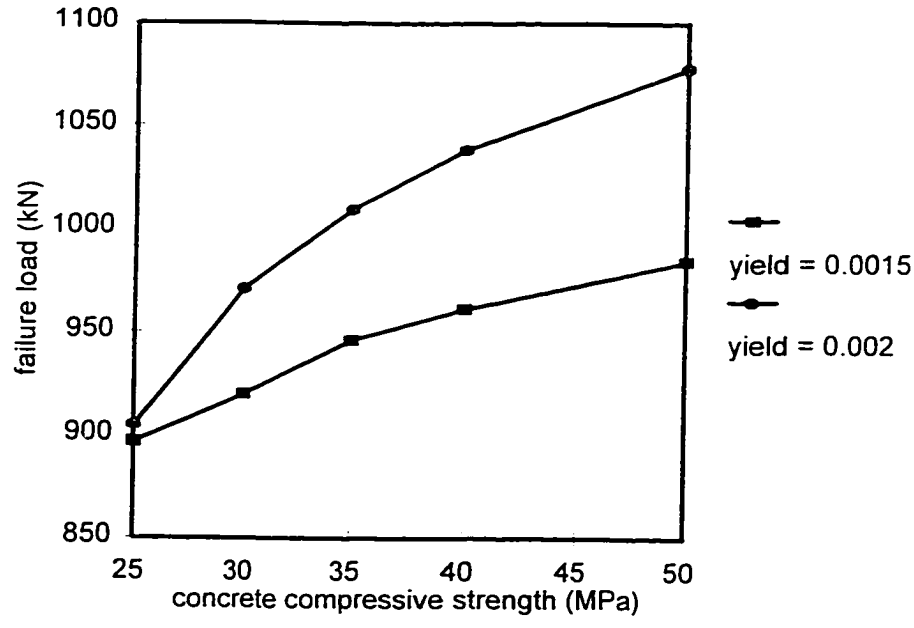

Figure 6.17 Failure load versus concrete strength

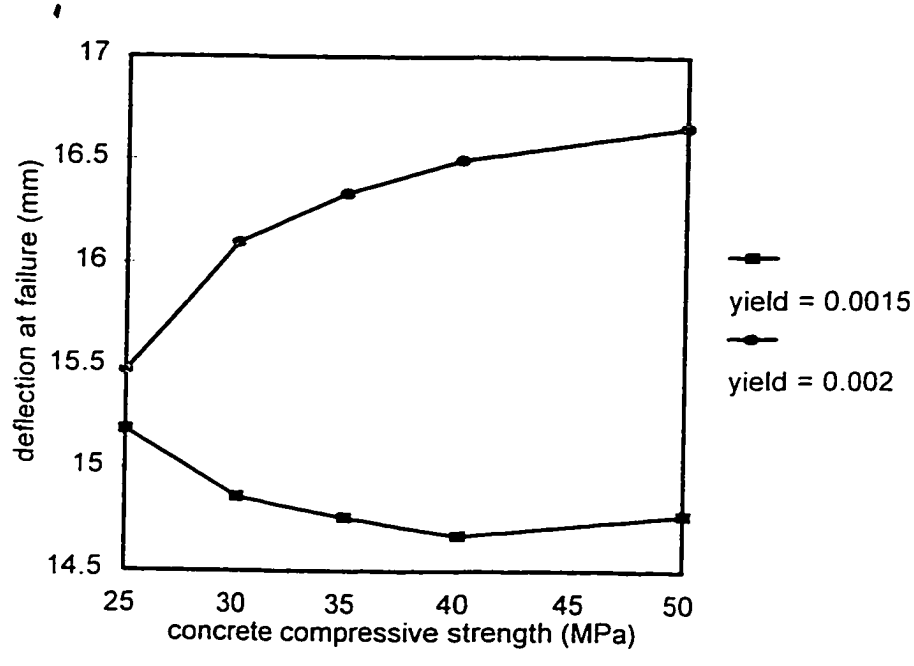

Figure 6.18 Deflection at failure versus concrete strength **6.1.6**

6.1.6 Girder Span / Deck Thickness Ratio

The data compiled in Tables 6.7 through 6.10 is re-organized in Tables 6.13 and 6.14 to reflect the span to thickness ratio for each configuration.

Table 6.13 System Response for Varying Span/Thickness Ratio and $\epsilon_y = 0.0015$

S_g/d	S_g (mm)	d (mm)	P (kN)	ϵ_s	Δ (mm)	F (kN/m)	failure mode
7.5	1500	200	749	0.0015	4.64	450	strap
9.0	2500	275	1398	0.0015	9.67	750	strap
10	2000	200	845	0.0015	8.79	600	strap
10	2500	250	1242	0.0015	10.92	750	strap
11.1	2500	225	1084	0.0015	12.56	750	strap
12.5	2500	200	920	0.0015	14.86	750	strap
14.3	2500	175	700	0.00135	16.08	675	concrete
15	3000	200	811	0.00117	17.48	702	concrete
17.5	3500	200	704	0.00090	18.90	630	concrete

Table 6.14 System Response for Varying Span/Thickness Ratio and $\epsilon_y = 0.002$

S_g/d	S_g (mm)	d (mm)	P (kN)	ϵ_s	Δ (mm)	F (kN/m)	failure mode
7.5	1500	200	969	0.002	6.29	600	strap
9.0	2500	275	1785	0.002	13.03	1000	strap
10	2000	200	1070	0.002	10.92	800	strap
10	2500	250	1581	0.002	14.89	1000	strap
11.1	2500	225	1307	0.0019	16.34	950	concrete
12.5	2500	200	971	0.00161	16.10	805	concrete
14.3	2500	175	700	0.00135	16.08	675	concrete
15	3000	200	811	0.00117	17.48	702	concrete
17.5	3500	200	704	0.00090	18.90	630	concrete

From Figure 6.19 it can be seen that no clear relationship exists between the S_g/d ratio and the failure load. The values are very much affected by the combination of girder spacing and deck thickness that lead to that S_g/d value. The relationship between

deflection and S_g/d is also not consistent, although it generally increases as the ratio increases, Figure 6.20. A plot of restraining force versus applied load, Figure 6.21, does not yield any discernable correlation to the S_g/d ratio. Therefore, S_g/d by itself is not a good indicator of system behaviour unless it is considered in conjunction with other parameters.

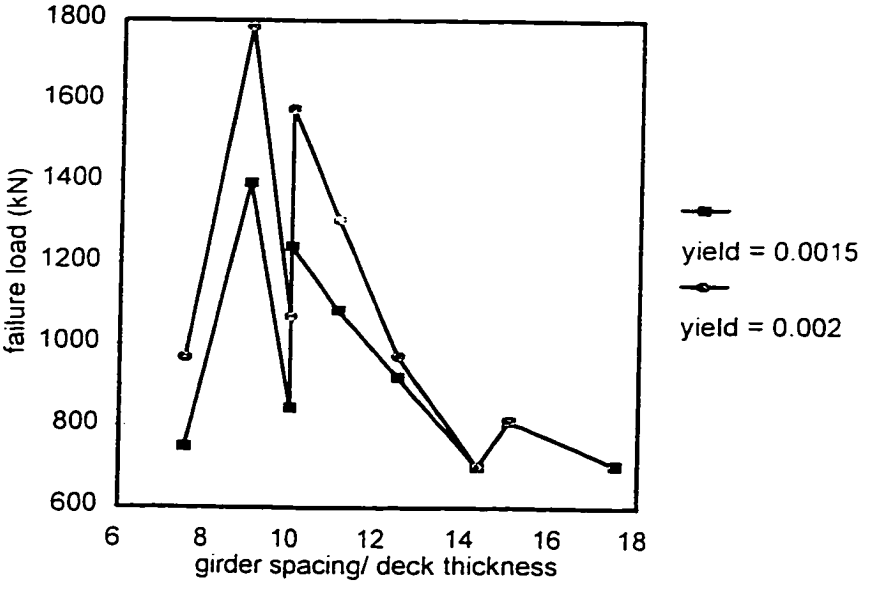

Figure 6.19 Failure load versus S_g/d

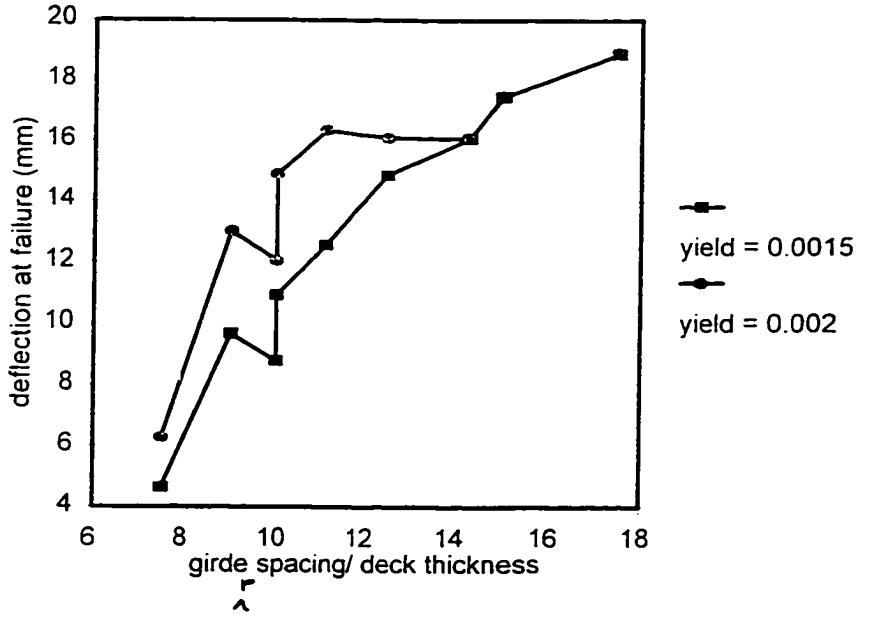

Figure 6.20 Deflection at failure versus S_g/d

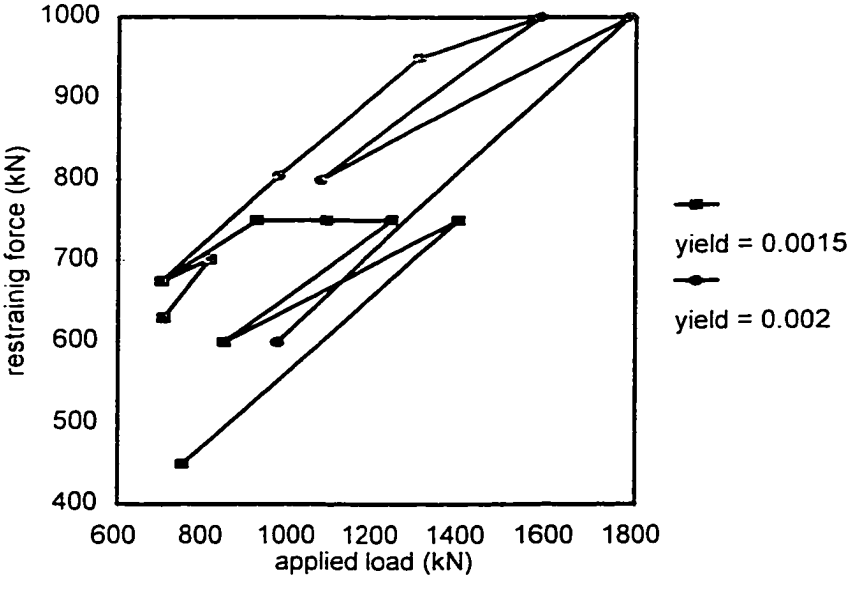

Figure 6.21 Restraining force versus failure load for varying S_g/d ratios

6.1.7 Summary

The parametric study revealed several basic behavioural characteristics of the steel-free bridge deck behaviour. They can be summarized as follows:

- All other parameters being held constant, at the same value of applied load, an increase in restraint stiffness leads to a decrease in deflection and strap strain.
- An increase in the restraint stiffness causes an increase in the failure load.
- The basic system behaviour is affected by whether the failure mode is initiated by yielding of the straps or crushing of the concrete.
- The restraining force developed by the system is closely linked to the applied load and is independent of restraint stiffness. It does however, depend heavily on the geometry of the system including girder spacing and deck thickness.
- The contribution of the straps is most significant in the stiffness they provide and not the amount of force developed by an individual strap.
- Strap yielding initiates failure at lower values of restraint stiffness, girder spacing. S_g/d ratios and higher values of deck thickness. Concrete crushing initiates failure at higher values of restraint stiffness, girder spacing, S_g/d ratios and lower values of deck thickness.
- Concrete compressive strength has only a marginal influence on deck behaviour and increasing concrete strength is not an effective means of increasing capacity.
- Increasing the yield strain of the straps has the general effect of increasing the failure load; however, a higher yield strain also produces lower values for the transition from failure initiated by strap yielding to failure initiated by concrete crushing.
- Ranking the parameters in order of their influence on the failure load, from greatest to least, we have restraint stiffness, deck thickness, girder spacing, yield strain and concrete strength.

6.2 Restraint Stiffness Investigation

6.2.1 Strap Size and Spacing

The magnitude of the restraint stiffness provided to the bridge deck system is affected by several parameters: girder spacing, strap spacing, strap size, strap material and the top flange of the girder. If we assume that the girder spacing is determined by other considerations and the strap material will always be steel then the designer has control over only three parameters. The top flange of the girder is also largely determined by other design consideration such that restraint stiffness design is essentially a choice of strap size and spacing. Placing issues of constuctability aside, the optimum strap configuration is one which provides the highest level of restraint. The restraint, as demonstrated in Section 2.5, can be calculated using a beam on elastic springs model. In this analogy, the best situation is one in which the beam is continuously supported an the elastic continuum. Considering only the elastic modulus of the supporting material, the interaction of the beam and the supports is typical called a Winkler beam (Den Hartog, 1952) and its behaviour is well studied. For a beam of infinite length or conversely for a loading situation which is free from end effects, the deflection under an applied point load can be calculated from the following Equation:

$$\delta = \frac{P \cdot \lambda}{2 \cdot k} \quad where \quad \lambda = \left(\frac{k}{4EI} \right)^{\frac{1}{4}} \tag{50}$$

Similar to the method developed for interpreting the beam on springs results in Section 2.5, the restraint stiffness K is calculated as

$$K = \frac{P}{\delta}, \quad such\ that \quad K = 2\frac{k}{\lambda} \tag{51}$$

where **k** is the spring modulus which can be found from equation (44). The values **E** and **I** correspond to the modulus of elasticity of the beam and the moment of inertia of the beam. If we consider the laboratory model shown in Figure 4.1, then

$$k = \frac{200{,}000 \cdot 1{,}250}{2{,}370/2 \cdot 1{,}200} = 176 \ N/mm/mm$$

and

$$\lambda = \left(\frac{176}{4 \cdot 200{,}000 \cdot 92 x 10^{6}} \right)^{\frac{1}{4}} = 0.0012456$$

Substituting into equation (51) yields **K** = 284, 200 N/mm per metre length of circumference or **K** = 284 N/mm/mm.

The effective spring modulus **k** was calculated based on a strap size of 1250 mm^2 every 1200 mm. This converts to 1.0417 mm^2/mm spacing. This same effective spring modulus can be achieved by an infinite combination of strap sizes and associated spacings. However, the implication is that the more discrete and farther spaced the support springs, the less the structure behaves like a beam on a continuous support. To examine this effect in terms of the lab model, the finite element procedure was employed to analysis the beam on spring model for a variety of strap spacings and sizes and to determine the effective restraint stiffness. For each case an upper and lower bound for stiffness was determined based on the load being directly over a strap or directly between two straps. The results are presented in Table 6.15.

It can be seen that up to a strap spacing of 1000 mm the effective restraint stiffness is very close to the ideal restraint stiffness value of 284 N/mm/mm as calculated in equation (51). At a strap spacing of 1200 mm there is a noticeable difference in the lower and upper bound values, however, there is still only a 10% variation from the ideal value. At a spacing of 1500 mm, the variation is large, approximately 25% less for the lower bound. While this example is specific to the beam size chosen (**I** = 92 x 10^6 mm^4), it is indicative of a typical design configuration. It should also be noted that below a strap spacing of 800

mm no noticeable improvement can be seen. It is concluded therefore that the strap spacing should be between 800 and 1200 mm.

Table 6.15 Effect of Strap Spacing on Restraint Stiffness

	Strap		Upper Bound		Lower Bound	
Spacing (mm)	As (mm^2)	k_{strap} (N/mm)	δ (mm)	K (N/mm/mm)	δ (mm)	K (N/mm/mm)
200	210	35,443	3.514	285	3.514	285
400	415	70,042	3.544	282	3.550	282
500	520	87,763	3.535	283	3.547	282
800	830	140,084	3.510	285	3.611	277
1000	1050	177,215	3.421	292	3.690	271
1200	1250	210,970	3.339	299	3.929	254
1500	1560	263,291	3.108	322	4.556	219

6.2.2 Girder Size

The girder size will obviously have an influence on the effective restraint stiffness value. The largest influence is due to the moment of inertia of the top flange of the girder. While the size of the girder is determined largely from the bending stresses in the girder, the designer does have some control over its dimensions. It is therefore important to know the relative importance of the magnitude of this moment of inertia on the magnitude of the restraint stiffness. Equation (51) is a useful tool in assessing this parameter. Table 6.16 summarizes the calculated restraint stiffness value for a range of top flange moments of inertia. The model tested in the lab has a value of 92×10^6 mm^4 while the girder at Salmon River has a value of 485×10^6 mm^4.

Table 6.16 Effect of Varying Moment of Inertia

Moment of Inertia (x 10^6 mm4)	λ	K (N/mm/mm)
92	0.0012456	284
200	0.0010255	345
300	0.0009267	382
500	0.0008156	434
600	0.0007792	454
1000	0.0006858	516

In relative terms, it can be seen that the restraint stiffness is only marginally sensitive to the value of the moment of inertia. Considering the two extremes given in Table 6.16, a ten times increase in moment of inertia does not even double the restraint stiffness value.

7 DESIGN RECOMMENDATIONS

A sub-committee of the new Canadian Highway Bridge Design Code (Bakht et al., 1996) charged with creating Section 16-Fibre Reinforced Structures has included, for the first time in any bridge code, clauses pertaining to the design of Fibre Reinforced Concrete Deck Slabs. Fibre reinforced concrete deck slabs are synonymous with the steel-free bridge deck structural system described through this thesis. Based on involvement in research work, the design and construction of the Salmon River bridge and the findings of this thesis, this author provides a series of design recommendations for the steel-free deck system. These recommendation are evaluated against the proposed clauses for the CHBDC. The author's recommendation are based on the current state of the art. With increased laboratory testing and in particular, increased field experience some of the recommendation may prove to be too conservative.

7.1 General Discussion

7.1.1 Bridge Superstructure

The work of this thesis and all of the work recorded to date has been performed on concrete slab on steel girder system. With the exception of the most recent testing, not completed at the time of writing this thesis, all of the work was performed on simple span structures. The technology however is by no means limited to this particular superstructure type. Indeed the system may be even more effective if used with concrete girder bridges. The rational model and other theoretical tools would apply equally well to concrete bridge deck slabs on all girder types. The defining behavioural element of the technology is the lateral restraint provided to the deck. The challenge with other girder types is to design the construction details such that proper interaction between the straps, the girders and the deck is achieved. It is therefore recommended that the steel-free deck technology can be used with any girder system if testing is performed to demonstrate that the connection details achieve the proper level of lateral restraint.

The system is not limited to simple span structures but may also be used in continuous bridge structures. The technique is to design the girders themselves to carry all the negative moment for ultimate strength design and to establish adequate crack control for the concrete deck over the piers for service load design. Testing is currently underway to address the latter issue. The current draft of CHBDC states:

> *For continuous span bridges, the deck slab contains longitudinal negative moment reinforcement in at least those segments in which the flexural tensile stresses in the concrete due to bending in the SLS are larger than* $0.6f_{cr}$...

The steel-free technology is not limited to only new construction or cast-in-place construction. The principle of arching action can be employed in deck replacement projects or in precast deck projects. Again, the challenge is not in whether or not the technology is applicable but in the design of proper details to achieve the lateral restraint and arching behaviour.

It is noted that extensive experimental work has been performed for cast-in-place decks on steel girder systems. Use of the steel-free deck with other systems will require some further testing, not to establish the technology or behaviour, but to test the effectiveness of the design details employed.

7.1.2 Concrete Strength

It was demonstrated in Section 6.1.5 that the concrete compressive strength has only a marginal effect on the ultimate load capacity of the system. It is therefore recommended that concrete compressive strengths of 30 MPa or 35 MPa be used as required by the standard practices of the agencies responsible for the structure. The use of concrete strengths higher than these values will not adversely affect behaviour. The decision to use higher strengths however should be based on other considerations, such as durability, and not on improving

the ultimate capacity of the system. A slight increase in strap size is a much more efficient means of attaining increased capacity.

7.1.3 Transverse Negative Moments

The steel-free system relies on the development of compressive stresses in the concrete through lateral restraint and arching action. Due to certain possible load situations, portions of the deck may be subjected to tensile stresses due to negative transverse bending moments. Two examples of this are the bending stresses created by the cantilever overhangs and the bending stresses caused by crash loads on the barrier rails or walls. Two design options are possible.

The first option is to design the superstructure such that these stresses do not develop. This approach was chosen for the Salmon River Bridge Project. Initially the bridge was designed with six girders and a cantilever overhang of approximately 500 mm on either side of the bridge. The spacing of the girders was increased such that the overhang was eliminated (Figure 5.3). In addition the connection detail between the crash rail and the deck was modified such that the crash rails was anchored to the structural steel girders and not the concrete deck, see Figure 5.4 This eliminated the need to design for tensile concrete stresses due to a crash load.

The second option is to design for these stresses in the usual manner and reinforce the deck in the tensile regions. Mahue and Bakht (1993) have demonstrated that it is possible to design the barrier wall and the overhang using fibre reinforced plastic reinforcement instead of steel reinforcement. In this manner, the deck still has a high level of durability even though it contains reinforcement. While use of steel reinforcement is not prohibited. transverse negative moments require that the steel be placed near the top of the deck and in the zone where the curb or barrier wall meets the deck. This is the most corrosion susceptible area of the deck and therefore use of steel reinforcement may lead to essentially the same maintenance problems as with standard reinforced concrete construction. It may be argued

that the lowest capital solution should prevail and that steel reinforcement should be used in the negative moments regions regardless of the corrosion problems. The design will be less expensive than the conventionally designed deck and will have at least the same level of durability. While this may be a valid approach, the author believes that a marginal increase in capital costs due to the use of FRP reinforcement is justified based on the significant reduction in life cycle costs which may be achieved. In many cases, the steel-free design with FRP reinforcement may actually be less expensive on a capital costs basis than the conventional design. Use of the non-corrosive FRP reinforcement is recommended.

These recommendations are consistent with the current draft of CHBDC which states:

> *A deck slab of fibre reinforced concrete .... need not be analyzed except for negative moments due to loads on the overhang and barrier walls; ...*
>
> *The deck contains appropriate tensile reinforcement for transverse negative moments, resulting from loads on deck slab overhangs and loads on railings or barrier walls.*

7.1.4 Deck Geometry

The general geometry of the bridge superstructures which can be used with the steel-free bridge deck technology should be limited. The CHBDC draft suggests the following:

> *The spacing of the supporting beams, S, does not exceed 3.0 m.*
>
> *The deck slab thickness, t, is at least 175 mm, and not less than S/15.*

These limits are reasonable and it is recommended that they be followed. Testing to date has demonstrated that a girder spacing of 2 700 mm is feasible; therefore, a spacing of 3 000 is consistent with the current state of knowledge. Wider girder spacing may be possible but

these systems would require further experimental verification before they could be adopted for construction.

If we consider the test model shown in Figure 4.2 to have **S** = 2700 mm and **t** = 200 mm, then **S/t** = 13.5 . Therefore **S/15** is a reasonable limit. Designs not meeting this limit will require further testing. However, in Section 4.2.7. It was demonstrated that the effective thickness of this deck was actually **t** plus the thickness of the haunch or 300 mm. It is recommended that, given the present state of the art and limited field experience, the actual value of **t** be used for code purposes in establishing geometric limits. This will add a level of conservatism to the design. For analysis; however, the effective depth should be used in determining the capacity of the system.

The use of haunches over the girders has been demonstrated to be an effective means of increasing the performance of the system. Again, limitations need to be placed on the size and configuration of the haunch such that it does not have an adverse effect on the structure. Obviously a haunch of large height will not be beneficial to the system . In addition, an abrupt change in deck thickness from the haunch area to the remainder of the deck is not recommended. The CHBDC draft makes the following recommendation:

> *...the height of the haunch between the deck and the top of a supporting beam is between 25 and 125 mm ..*

This recommendation is endorsed. The lab testing has been performed with a height of 100 mm and the Salmon River Bridge has an average haunch depth of 130 mm. The height of the haunch used will be affected by two parameters, the straps should remain external to the concrete and adequate breathing room must be present between the top of the strap and the underside of the deck such that moisture is not trapped causing rapid and undetectable corrosion. Also, the formwork used to construct the deck will generally be above the strap

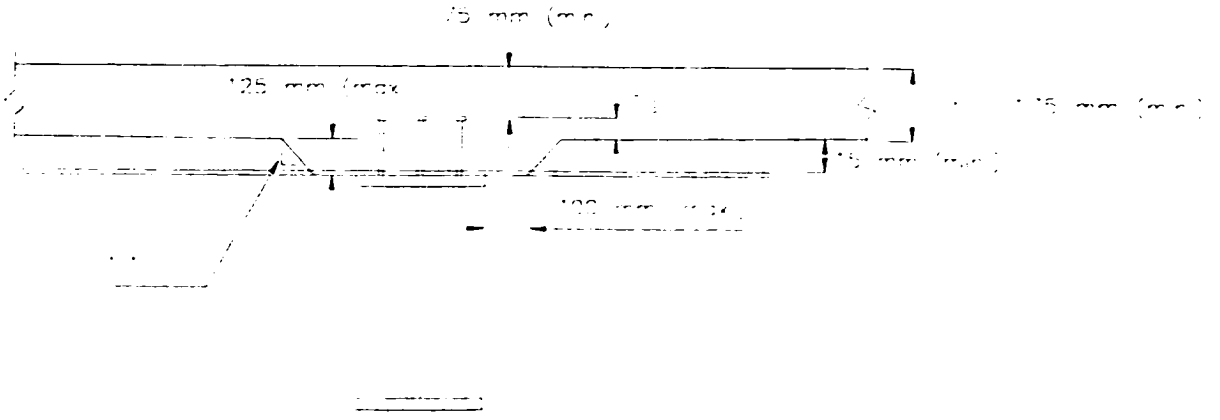

Figure 7.1 Typical haunch detail

and will have to be removed. The height of the haunch will have to be great enough to allow its removal. In general, the height of the haunch will be closer to the upper limit for constructability.

Careful thought must also be given to the transition in depth. As a minimum, the transition should be made at a 1:1 slope as shown in Figure 7.1. Figure 7.1 is based on Figure 16.7 (a) of the draft CHBDC. The author makes a further recommendation that if a load is applied at the mid-span of the deck, then a clear line of arching must be able to be made from the load point to the top of the girder. In other words, the geometry of the haunch must be such that the imaginary line arching forces does not exit the deck before it reaches the girders which support the deck. While it can be argued that the shape of this imaginary line is curved, it is conservative to assume that it is linear. Using this principle the geometry shown in Figure 7.2a would be unacceptable while the geometry shown in Figure 7.2b would be acceptable. This philosophy is based on the idea of having to maintain a continuous compression field within the concrete. The linear arching force rule is simple and conservative; however a designer may chose to use engineering judgement provided the designer believes that the compression field can be maintained. The impact of this recommendation is that the width of the haunch may have to extend a short distance past the edge of the girder flanges. If this

extension exceeds 100 mm, then the designer should consider making some overall changes to the deck geometry such as increasing the deck thickness. Another possibility is to make an even smoother transition from the haunch to the deck. While more expensive to construct, a circular or parabolic profile for the underside of the slab may be the geometric optimum. In general, very thin decks with deep haunches and abrupt transitions should be avoided.

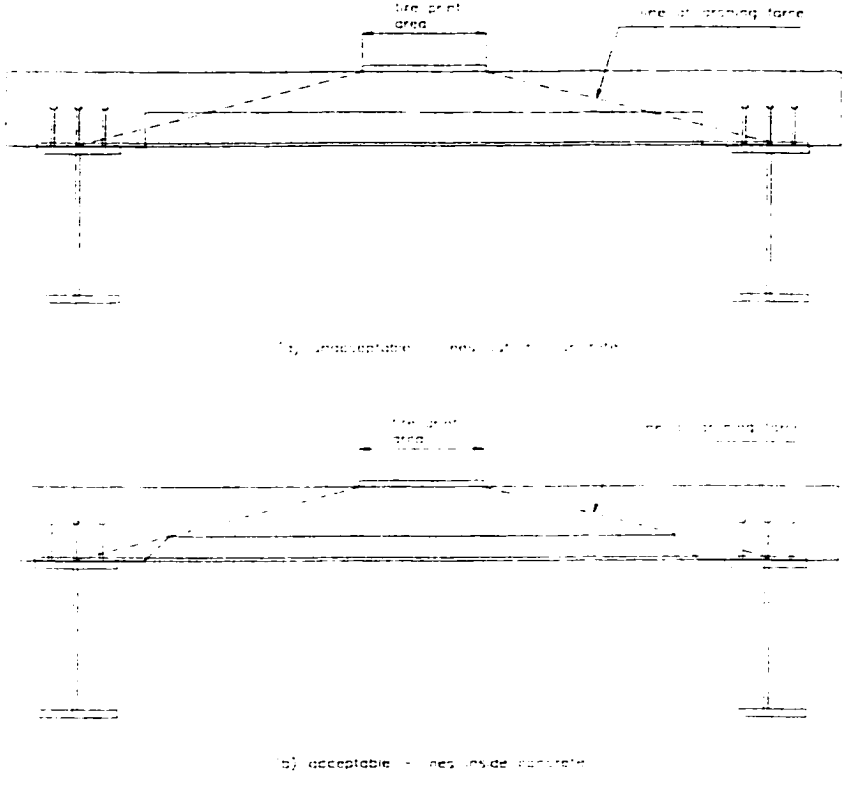

Figure 7.2 Geometry of haunch and arching forces

Equally important to the development of arching action is the effectiveness of the studs on the top of the girders. The CHBDC draft requires that:

> *... the projection of the shear connecting devices in the deck slab, t_s is at least 50 mm; in addition the distance between the top of the shear connecting devices and the top surface of the deck slab is a minimum of 75 mm.*

Figure 7.1 provides an illustration of this requirement. The author supports this requirement as a means of ensuring effective shear connection and arching action.

7.1.5 Restraint Strap Configuration

Most testing to date has been performed with steel straps welded to the top flanges of the girders. This need not always be the case and in some instances, such as concrete girders, may not even be readily possible. Bakht (1996) and the CHBDC provide some alternative strap connection details. The recommendation for the strap connection is that it be designed for adequate interaction such that lateral restraint is provided by both the girders and the straps. The top flange of the girder is the most important element in providing continuous lateral support to this system whereas the straps provide restraint at a series isolated points along the girder. A girder without straps may not provide the required lateral restraint. Likewise, series of widely spaced straps may be effective only when the load is applied close to a strap and ineffective when the load is applied a some distance from a strap. The girder-strap interaction can be considered to be mutually dependent in that the straps enhance the restraint of the girders through beam on spring behaviour and the girders enable lateral forces to be transferred to straps not directly adjacent to the load. Connection with the deck must be made such that the restraining forces can be transferred from the concrete to the girder-strap system.

It is recommended that strap connections exist between all adjacent beams. The straps used in the Salmon River Project were continuous across all six girders; however, the welded connection was made at each girder. In interior panels, it can be argued that the deck has a high degree of global lateral stiffness due to the girders and the deck. While this may be true, the punching behaviour has specific local influence and global stiffness should not be relied as the sole lateral restraint. At every location of the deck, a clear system of a compressive arch in the deck with and a tension tie must be present. The CHBDC draft states that:

The top flanges of all adjacent supporting beams are connected by an external transverse confining system, comprising straps, which are perpendicular to the supporting beams, and which are either connected directly to the top flanges ... or

connected indirectly ... alternatively transverse confining systems comprises devices which have been proven through full-scale laboratory testing.

It should also be noted that the strap connection need be on the top surface of the top flange. In the Salmon River Project the straps were placed on top of the flanges to facilitate construction. The system works equally effective if the straps are welded to the underside of the top flange as shown in Figure 7.3. This method requires overhead welding and may be more expensive but it can be used as an effective repair technique.

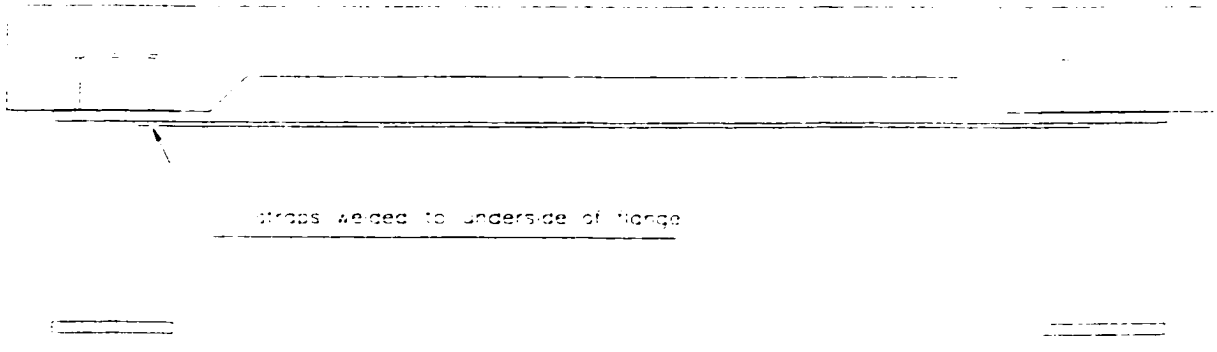

Figure 7.3 Cross-section of strap welded to underside of top flange

The CHBDC recognizes the increased global lateral stiffness of the superstructure in interior panels by reducing the minimum area of strap required by 20%. The author endorses this concept but recommends that the reduction not exceed 20%. Also a minimum cross-sectional area of strap always be provided. This minimum is discussed in Section 7.1.6. In addition, considering the lateral restraint provided by the straps only, the theoretical punching load should be at least twice the ultimate limit states design wheel load.

The CHBDC requires that:

The spacing of the straps, S_l, is not more than 1.5 m.

The author recommends that, except in special cases, the spacing of the straps should not exceed 1200 mm. As demonstrated in Table 6.15, a strap spacing of 1500 mm gives a 25% reduction in stiffness compared to the average restraint stiffness of the strap system. By comparison, the 1200 mm spacing gives only a 10% reduction. While testing demonstrated that a strap spacing of 2400 mm gave adequate strength performance, the deck suffered severe cracking at low loads for this test. Therefore, a large strap spacing may lead to serviceability and fatigue problems even though it meets ultimate strength requirements.

The experimental testing described in Chapter 4 and the parametric study of Chapter 6 demonstrated that yielding of the straps can occur and that it is most likely at low values of lateral restraint. It is recommended that a design philosophy be adopted such that the strap connection strength should not be less than the strength developed in the strap. Considering that yielding is a possible failure mode, the ultimate limit states strength of the strap connection should be greater than the yield strength of the strap. This is very important for two reasons. Firstly, the connection between the strap and the girder can not be visually inspected such that failure of a connection can only be detected by failure of the system. Strap yielding on the other hand, can be detected by visual inspection. Secondly, if a connection fails, and more importantly, if more than one connection fails, then the capacity of the deck is substantially reduced and wide-spread catastrophic failure of the deck can occur. If a strap yields, punching may occur but this is a more local effect. A yielded strap can still provide a lateral restraining force equivalent to is yield strength and once the loading is removed it continues to function with only a slight reduction in overall capacity. In the event that the fundamental behaviour of the system is modified due to exceptional loads, or other unforseen circumstances, then the presence of straps which can sustain loads up to their yield strength provides the deck with a reserve capacity. Therefore connection failures can

lead to disaster, whereas strap yielding may lead to serious problems but less likelihood of catastrophic failure. The CHBDC draft requires that;

> *The direct or indirect connection of a strap to the supporting beams is designed to have a strength in Newtons of at least 200A.*

The connection strength in this case is less than the factored yield strength of the strap, taken to be 270A for 300 MPa steel. The philosophy behind the code approach is that structure will not see loads high enough to cause yielding of the straps and therefore the system should not be penalized with the expense of connection strengths greater than that of yielding of the strap. This reasoning has merit especially if the failure load of the deck is in the order of magnitude of 1000 kN for a single wheel load. With time however the design capacity of this deck may be substantially reduced to a value much closer to the ULS design wheel load. In the case of the Salmon River Bridge Project, the design of the welded strap connection was governed by fatigue design requirement such that the ULS of the connection was much greater than the yield strength of the strap at no addition expense to the project. It is this author's recommendation that, as safety measure against unforseen failure or problems, the strap connection be designed with a strength in excess of that of the yield strength of the strap. In situations where this may provide undue expense to the construction of the system then a lesser connection strength may be considered if no other alternative is possible. If the connection has to be reduced then it should be no less than that recommended by the CHBDC requirements and should still provide a ultimate capacity which is acceptable to the design engineer.

The straps on the Salmon River Bridge were 14 x 100 mm in size. It was found that these straps will vibrated as heavy vehicles passed over the structure. Preliminary calculation revealed that the natural frequency of the strap is very close to the natural frequency of the structure. While this does not pose any apparent problems, it is recommended that this

situation be avoided in the future. The strap cross-section should be closer to a 2:1 ratio rather than a 8:1 ratio as was used in the Salmon River Bridge Deck system.

7.1.6 Lateral Restraint Value

Section 2.5 demonstrated that a beam on elastic spring analogy is necessary to accurately predict the amount of lateral restraint provided by the girder-strap interaction. While this is a useful tool for analysis and leads to a better understanding of the influence of each component, a simpler procedure is recommended for design. Equation (43) which accounts only for the restraint provided by straps is a very fast and useful design tool. The designer should use this equation to determine the lateral restraint of the system. The rational model, through the PUNCH program, can then be used to predict the ultimate capacity of the system. The effective depth of the concrete slab including the height of the haunch should be used. Where a variable depth haunch is constructed, the haunch height used to calculate the effective depth should be the minimum guaranteed height. In addition, the effective depth used in design should not exceed 1.33 times the actual depth or 300 mm. Using this method, the designer should have a target design capacity of not less than 3.0 times the ULS design wheel load. It is well known that conventionally reinforced concrete bridge decks have reserve capacity in excess of twice the ULS design wheel load. The use of a minimum of 3.0 times ULS will be consistent with current deck capacities. This method is simple and sufficiently conservative, such that a designer inexperienced with this technology can have a level of comfort with the design process.

Some designers may wish to take full advantage of the lateral restraint provided by the girder strap interaction and, through a more rigorous analysis, reduce the strap requirements calculated from the above method. While this is a valid design approach, care must be taken not to attribute too much of the lateral restraint to the girder, unless the lateral restraint has been verified by testing. In lieu of specific test results, a minimum value of restraint stiffness should be provided in all cases. To address the issue of minimum lateral restraint the CHBDC draft proposes a minimum area of strap which must be provided:

Each strap has a minimum cross-sectional area, A, in mm², given by

$$A = \frac{F \cdot S^2 \cdot S_l}{E \cdot t} \times 10^9$$

where the factor F_s is 6.0 for outer panels and 5.0 for inner panels.

The CHBDC values of minimum strap area per metre length of girder is presented in Table 7.1 for a range of standard design configurations. It should be noted that the depth refers to the actual depth of the slab, **t**, and not the effective depth.

Table 7.1 CHBDC Minimum Strap Area (mm²)*

Girder Spacing (mm)	Depth of Deck (mm)					
	175	200	225	250	275	300
1500	386	338	300	270	245	225
2000	686	600	533	480	436	400
2500	1071	938	833	750	682	625
3000		1350	1200	1080	982	900

* These values can be reduced by 20% for interior panels.

The use of a minimum strap area is a simple guideline to follow; however, there is one main drawback. The function of the strap is to provide stiffness. The spring constant of an individual strap is based both on its cross-sectional area and its length. Depending upon the type of strap connection detail, the length of the strap could be up to 20% shorter than the girder spacing, 20% longer than the girder spacing or equal to the girder spacing. Obviously the same cross-sectional area will not give the same level of restraint in all three cases. To be conservative, the minimum area requirement should be increased by the ratio of the effective length of the strap over the spacing of the girders in cases where the effective length is longer than the value of S_g.

Using the simple design method proposed by the author leads to the cross-sectional areas given in Table 7.2. It was assumed that the length of the strap was approximately equal to the spacing of the girders and that the strap had a yield strain of 0.0015. A design load of 400 kN was used for spans up to and including 2500 mm and a design load of 500 kN was used for spans in excess of 2500 mm. It is believed that the larger girder spacings should have a higher design load particularly when considering minimum values.

Table 7.2 Proposed Minimum Strap Area (mm^2)

Girder Spacing (mm)	Depth of Deck (mm)					
	175	200	225	250	275	300
1500	900	790	675	600	550	525
2000	1050	900	775	750	625	600
2500	1200	940	850	720	660	650
3000		1350	1200	1020	900	900

It is noted that the value for spans lengths of 2500 mm and 3000 mm are in close agreement with the CHBDC values; however, the values below a span 2500 mm are much higher than the CHBDC values. The depth in Table 7.2 is, however, the effective depth of the slab including the height of the haunch. In addition, these values would be reduced by 10% if the designer were to use steel straps with a yield strain of 0.00175 and 20% if the designer were to use steel straps with a yield strain of 0.002, provided that strap yielding governed the failure. Furthermore, these values are based on the use of steel straps with a modulus of elasticity of 200, 000 MPa. If another material is used for the strap, then these values would obviously change.

For comparison, the results of full-scale experimental testing are compiled in Table 7.3 to illustrate the parameters tested to date.

Table 7.3 Summary of Experimental Punch Tests

Girder Spacing (mm)	Depth (mm)	Area of Strap (mm^2/ m)	Punch Load (kN)
2000	175	2500	1127
2000	175	1250	923
2000	175	950	911
2000	175	650	844
2000	175	650	576
2000	175	650	715
2700	200+100 haunch	1040	1275

Of particular interest are the results for a deck thickness of 175 mm and strap area of 650 mm^2. The failure load for this case ranged between 576 kN and 844 kN. Table 7.2 would have suggested that a strap area of 1050 mm^2 needed to be used. This would have resulted in a failure load of approximately 900 kN according to Table 7.3. It can be demonstrated that the combination of the effective length of the strap being 15% shorter than the centre to centre spacing of the girders and the contribution of the girder flanges to the lateral restraint leads to an actual restraint stiffness that is almost twice that of calculated for Table 7.2. This illustrates the conservative nature of the proposed method.

It is evident from this discussion that the selection of an appropriate minimum strap area is not a straight forward process. Many elements have to be considered including the type of strap provided, the connection detail and the complex interaction of the system. However, in design, a simple approach should prevail. It is therefore recommended that, in lieu of specific test results which demonstrated the safety and serviceability of a particular design, Table 7.2 be adopted as the minimum required area of strap with a further requirement that the area of an individual strap not be less than 625 mm^2. The values in this table should be increased for straps made from materials with lower values of modulus of elasticity or straps with effective lengths in excess of the centre to centre spacing of the girders.

7.1.7 Edge Beam

Mufti et al. (1993) and Newhook et al. (1995) demonstrated the need for in plane lateral stiffness at the free edge of the concrete deck slab. This has been achieved in the past by using an edge beam which is made composite with the concrete deck and has high bending stiffness in the plane of the deck. The CHBDC code states that:

> *The transverse edges of the deck slab are stiffened by composite edge beams having a minimum flexural rigidity, EI, in the plane of the deck slab, of 3.5 x L_u^4 MN-m^2, where L_u is the unsupported length of the edge beam.*

The CHBDC draft also presents a number of possible design alternatives from steel channels or beam sections connected to the deck with shear studs to a thickened slab with reinforcement. The author supports these recommendations.

7.1.8 Fibre Content

Design of an optimum fibre content was beyond the scope of this thesis. Work is currently underway to establish the optimum fibre content and proper engineering guidelines for selecting the appropriate fibre types and fibre volume fractions. The CHBDC draft is proposing a simple procedure for determining the minimum fibre volume fraction based on a ratio of post-cracking strength to nominal cracking strength. The use of fibre is for the primary purpose of controlling shrinkage and thermal cracking in the deck slab. The fibres are not believed to have any effect on the ultimate load capacity of the deck.

The fibre content used in the Salmon River Bridge Project was 5.0 kg/m^3 or a volume fraction of 0.55% of collated fibrillated polypropylene fibres approximately 40 mm in length. The author can only recommend that this volume fraction is acceptable for design. Other fibre types or volume fractions may be used but they should meet the requirements of the CHBDC draft and should be selected in consultation with an expert in the field of fibre reinforced concrete.

7.2 Design Clauses

For clarity, the design recommendations are summarized below. The recommendations are presented as code clauses as this will be a familiar style for design engineers. Clauses marked by an asterisks are taken in whole or in part from the CHBDC draft without revision. Clauses marked by a cross are taken from the CHBDC draft but contain some revisions. Some clauses refer to other sections of the CHBDC code dealing with conventional design requirements, fibre reinforced plastic reinforcement requirements or fibre reinforced concrete material requirements. These references are highlighted in italic font and are not discussed in detail as they are beyond the scope of this work. Where the specific CHBDC clause numbers are not known, the clauses are referred to in general terms.

X. Steel-Free Bridge Deck Structural Systems

X.0 Notation

S_g = centre to centre spacing of girders (mm)

S_l = centre to centre spacing of straps (mm)

A = cross-section area of straps (mm^2)

E = modulus of elasticity (MPa)

t = thickness of deck (mm)

t_s = project of shear connectors into the deck slab (mm)

t_e = effective thickness of deck for analysis (mm); X.

L_s = effective length of strap (mm); X.

K = lateral restraint stiffness (N/mm/mm)

t_h = height of haunch (mm)

I = moment of inertia (mm^4)

L_u = unsupported length of edge beam (mm)

F_c = strength of strap connection (kN)

f_y = yield stress of strap (MPA)

k_g = lateral restraint reduction factor for support system stiffness

X.1 General

a) A steel-free bridge deck structural system shall be comprised of a concrete deck slab on supporting girders with a system of external straps between girders. The system shall be designed such that the girders and straps interact to produce an adequate level of lateral restraint such that the deck carries applied loads through arching action and its principle failure mode is that of punching of the deck under a concentrated load.

b) The concrete shall contain randomly distributed synthetic fibres to control cracking due to shrinkage and thermal effects. The fibres shall be added in accordance with *Clause 16.6 of CHBDC.*

c)† The deck slab shall be made composite with the supporting beams in both the positive and negative moment regions. In the negative moment region the shear connectors shall be designer to transfer the maximum lateral restraining forces which can be developed by the straps.

X.2 Concrete Strength

The compressive strength of the fibre reinforced concrete shall be at least 30 MPa.

X.3 Analysis

X.3.1 Transverse Moments*

The deck slab of a steel-free bridge decks satisfying the conditions of clauses X.1 through

X.12 need not be analyzed for transverse moments except where loads on the overhang or barrier walls will cause transverse negative moments in the deck slab.

X.3.2 Composite Action

The steel-free bridge deck system shall be assumed to provide full composite action with the supporting girders. Design of the composite section for longitudinal bending shall be done in accordance with *the appropriate CHBDC design clauses for composite beam behaviour.*

X.3.3 Ultimate Load Behaviour

The steel-free deck slab shall be analysed by assuming the deck derives its capacity from the lateral restraint provided by the girders and straps. This restraint causes arching forces in the deck which leads to punching of the deck under wheel load as the ultimate failure mechanism.

X.3.4 Wheel Load

Unless otherwise specified, the design wheel load shall be assumed to have a tire print area of 250 x 500 mm with the shorter dimension in the longitudinal direction of the structure.

X.3.5 Load Sharing

The calculation of load sharing between girders shall be done in accordance with *the CHBDC clause for load sharing for reinforced concrete deck slab construction.*

X.4 Edge Stiffening*

The transverse edges of the deck slab are stiffened by composite edge beams having a minimum flexural rigidity, EI, in the plane of the deck slab, of $3.5 \times L_u^4$ MN-m^2, where L_u is the unsupported length of the edge beam.

X.5 Deck Thickness

X.5.1* Minimum Thickness

The deck slab thickness, t, shall be at least 175 mm, and not less than S/15.

X.5.2 Haunch Dimensions

a)† As illustrated in Figure X.5.2 (a), the height of the haunch, t_h, shall not be greater than 125 mm.

b) The transition from the thickness of the deck at the haunch, $t + t_h$, to the deck thickness, t, shall be made over a lateral distance not less than t_h.

c) The haunch shall have sufficient width such that an imaginary line of force drawn from the top of the deck at the mid-span to the top flange of the girders at the centre line of the girders remains entirely within the concrete, Figure X.5.2 (c).

d) The haunch width shall not extend beyond the edge of the girder flange more than 100 mm.

e) The height of the haunch shall be such that a minimum clearance of 15 mm is provided between the top of the strap and the underside of the concrete deck.

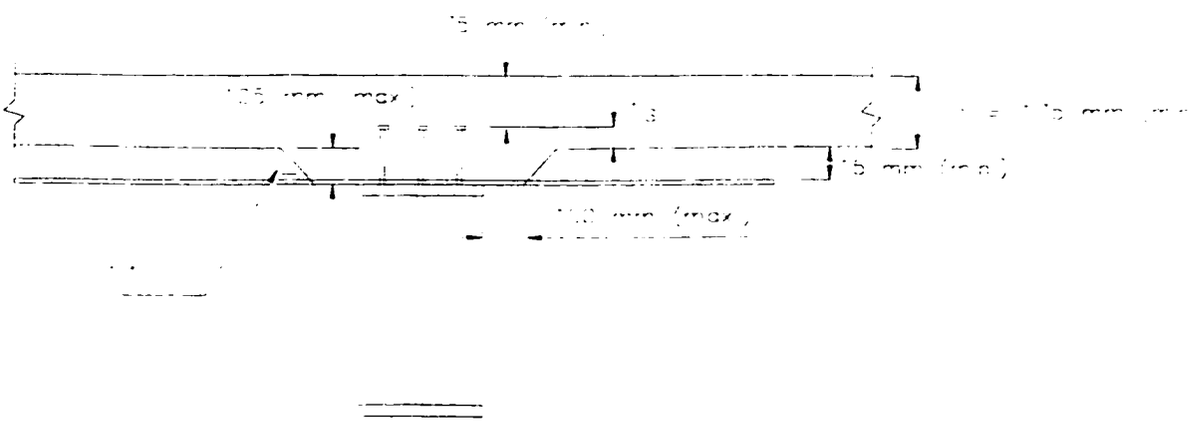

Figure X.5.2(a) Typical Haunch and deck details

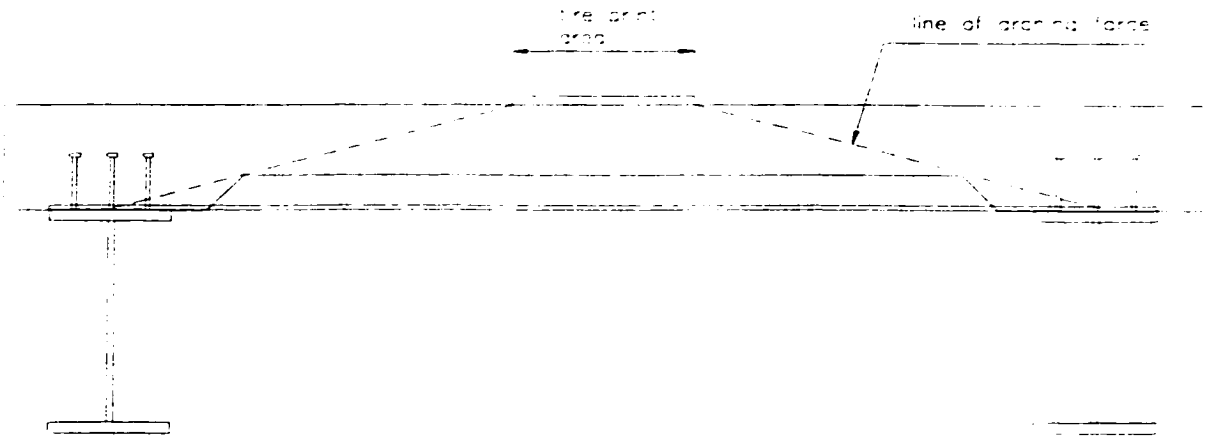

Figure X.5.2(c) Geometry of arching forces

X.5.3 Effective Depth

For analysis of deck slabs with haunches over the girders, the effective depth of the slab, t_e, may be increased to account for increased thickness at the haunch by

a) $t_e = t + t_h$,

b) except that t_e shall not be greater than 1.5t or 300 mm

X.6 Height of Shear Connectors†

The height of the shear connecting devices shall be such that

a) the projection in the deck slab above the haunch is at least 50 mm; and

b) the distance between the top of the deck and the top of the shear connectors is a minimum of 75 mm.

X.7 Girder spacing*

The centre to centre spacing of supporting beams, S_g, shall not exceed 3000 mm.

X.8 Strap Size and Spacing

X.8.1 Maximum Strap Spacing

The spacing of straps, S_t, shall not exceed 1200 mm.

X.8.2

The minimum size of an individual strap shall not be less than 625 mm^2 unless the strap spacing is less than 500 mm.

X.8.3 Minimum Strap Size

The dimension of the straps should be proportioned such that

a) rectangular straps will have an approximate width to depth ratio of 2:1

b) the natural frequency of the strap is greater than the natural frequency of the structure.

X.9 Effective Strap Length

a) The effective strap length, L_s, shall be the length of the continuous prismatic section of strap which is free to elongate under axial load.

b) In general, L_s will be equal to the distance between the centre of the connection of the straps to the girder flanges.

c) For welded connections, L_s may be taken as the clear distance between the ends of the welds on adjacent girders.

X.10 Strap Connection

X.10.1†

The top flanges of all adjacent supporting beams shall be connected by external transverse restraint system, comprising straps, which are perpendicular to the supporting beams, and

which are either connected directly to the top flanges through welding, or connected indirectly through shear connectors on both the strap and surrounding girder flange.

X.10.2*

Alternative connection details may be used if proven by full-scale laboratory testing.

X.10.3

The direct or indirect connection of a strap to the supporting beams shall be designed such that the factored strength of connection

a) $F_c \geq \phi_s f_y A$.

X.10.4

For welded connections, the weld must be designed to meet *the fatigue requirements of CHBDC* for the axial stresses in the strap due to live loads.

X.11 Lateral Restraint

X.11.1 Simplified Method

X.11.1.1

The lateral restraint system should be designed using the assumptions and procedures developed for the PUNCH program.

a) In lieu of specific experimental testing, the level of lateral restraint provided by the external straps, K, should be such that the failure load is at least 3 times the ULS design wheel load.
b) t_e is calculated according to X.5.3
c) the tire print area is as given in X.3.4

X.11.1.2 Strap Area

a) The cross-sectional area of the strap is calculated by

$$A = \frac{K \cdot L_s \cdot S_l}{2 \cdot E}$$

b) L_s is calculated according to X.9.

c) This area may be reduced by 20 % for interior panels.

d) The strap area shall not be less than that given in X.8.2 and X.11.1.3.

X.11.1.3 Girder Lateral Restraint

When the system of supporting girders and diaphragms has a demonstrated high level lateral restraint, A as calculated from X.11.1.2 may be reduced to $(1-k_g)A$, where

a) $k_g = 0.0002(3000-S_g)$; and

b) k_g is not greater than 0.25

X.11.2 Minimum Strap Area

a) The minimum cross-section area of strap per metre length of deck shall not be less than given in Table X.11.2

b) The area in Table X.11.2 shall be increased by 200 000/E for strap material other than structural steel.

c) The area in Table X.11.2 shall be increased by L_s/S_g when L_s is greater than S_g.

Table X.11.2 Minimum Strap Cross-Section Area per Metre Length of Slab (mm^2/m)

Girder Spacing (mm)	effective depth of deck, t_e (mm)					
	175	200	225	250	275	300
1500	900	790	675	600	550	525
2000	1050	900	775	750	625	600
2500	1200	940	850	720	660	650
3000		1350	1200	1020	900	900

X.11.3 Full-Scale Testing

X.11.3.1

The requirements of X.11.2 may be waived if the ultimate load capacity and serviceability performance of a transversely restrained bridge deck system is proven through full-scale laboratory testing under static and dynamic loading conditions.

X.11.3.2

Design criteria include, but are not limited to. the following:

a) The ultimate load capacity of the system shall not be less than 3.0 times the ULS design wheel load.

b) The system must have proven arching behaviour and the failure mode must be that of punching failure of the concrete.

c) Under service loads, the concrete must not crack or otherwise deteriorate to the extent that the ultimate capacity of the deck is reduced.

d) The system must not be susceptible to failure or reduction of ultimate load capacity due to fatigue of either the concrete or the transverse restraint system.

X.12 Tensile Stresses in the Deck Slab

X.12.1 Overhangs and Barrier Walls†

Where the deck slab is subjected to tensile stresses due to loads on overhangs or barrier walls or railings, the deck shall contain tensile reinforcement sufficient to resist the transverse negative moments. This reinforcement may be

a) steel reinforcement, designed to meet *the CHBDC clauses on reinforced concrete structures*.

b) fibre reinforced plastic reinforcement, designed to meet the requirements of *Section 16 of the CHBDC.*

X.12.2 Continuous Bridge Deck Structures†

For continuous span bridges, the deck slab shall contain longitudinal negative moment reinforcement in at least those segments in which the flexural tensile stresses in the concrete due to longitudinal bending in the SLS are larger than $0.6f_{cr}$.

8 CONCLUSIONS AND RESEARCH NEEDS

8.1 Conclusions

The behaviour of the steel-free bridge deck structural system under static loading conditions was investigated and a rational model developed to theoretically predict the behaviour of the system. The conclusions which can be derived from this research are summarized into the following points.

1) The capacity of the deck is derived from arching forces arising from the lateral restraint of the supporting girders. Both the girders and the external steel straps connected to the adjacent girders act together to produce the lateral restraint. The contribution of the diaphragms to this lateral restraint can be ignored. A beam on elastic springs analogy can be used to directly determine the level of lateral restraint in the system.

2) The fundamental behaviour of the deck is not flexural bending but rather compressive arching with the ultimate capacity of the system being governed by punching failure and not flexural strength.

3) The concrete surrounding the wheel load is in a state of three-dimensional compressive stress such that the compressive stresses in the concrete reach values well in excess of the uniaxial compressive strength of the concrete. A new triaxial confinement relationship is established for the particular application of a bridge deck under punching loads.

4) The failure of the deck can be initiated by either crushing of the concrete around the wheel load or yielding of the transverse restraint straps.

5) The rational model was verified by comparison with existing experimental test results. A method was developed for applying the rational model to reinforced concrete deck slabs and demonstrated by two examples. The key element of this approach is to assume that the bottom layer of transverse reinforcing steel is acting as restraining straps.

6) The rational model was also used to identify the key parameters which affect the ultimate capacity and behaviour of the system. The key parameters, listed in order of decreasing influence or sensitivity, are restraint stiffness which includes the strap size and material, deck thickness, girder spacing, yield strength of the strap and concrete compressive strength. A summary of basic behavioural characteristics is presented in Chapter 6.

7) It was demonstrated experimentally that the girder flanges displace lateral away from the point of load application as predicted by the theory.

8) The system performs adequately for a girder spacing of 2700 mm, a deck span to depth ratio of 13.5 and a girder spacing of 1200 mm.

9) The haunches over the girders increase the effective depth of the concrete slab to the sum of the deck thickness plus the haunch height.

10) The system has substantial reserve capacity even in a deteriorated condition. The system capacity with a strap missing and the deck severely cracked is approximately 75% of the ultimate load capacity.

11) The global composite behaviour of the girders and deck is consistent with the guidelines of the OHBDC clause for composite section behaviour in reinforced concrete deck slabs and does not appear to be affected by the cracking of the deck.

12) The load sharing for the two girder system in an uncracked condition was found to be consistent with the level of load sharing predicted by a semi-continuum analysis of the structure.

13) The capacity of both steel-free and reinforced concrete bridge deck construction under multiple wheel loads can be predicted by a simple formula.

14) A series of design recommendations and guidelines are presented which can be used by engineers to design a steel-free bridge deck system. The recommendations of the author are compared to the draft recommendations proposed by the CHBDC sub-committee on Fibre Reinforced Structures and any differences in approach have been noted. The most important difference is the author's recommended minimum area of straps is more conservative than the draft CHBDC, particularly at smaller girder spacings.

8.2 Research Needs

The steel-free bridge deck system is still evolving as a technology and many different issues and concepts still need to be investigated. In general terms, more experience with field performance of these structures is required. This will lead to a better understanding of design requirements and may produce less conservative design guidelines. Also, experimental testing needs to be performed on a variety supporting girder systems, such as prestressed concrete girders. More experimental testing should also be undertaken to verify the minimum lateral restraint requirements, or produce new ones, over a wide range of girder spacings and deck thicknesses.

A list of specific research topics are identified as important to the further advancement of the technology in the near future. The list is by no means all inclusive.

- Development of a standard set of connection details for various types of straps and supporting girder configurations.
- Investigation of multi-girder laboratory models and field structures to exactly determine the level load sharing between girders and, in particular, is the load sharing affected by cracking of the deck slab.
- Determination of optimal design parameters for serviceability and fatigue in regions of longitudinal negative moment.
- Testing to establish the capacity of the system to resist longitudinal shears and associated transverse tensile stresses from composite action in longitudinal bending.
- Development of design and construction techniques for a precast steel-free deck structural system.
- Establishment of clear and concise design techniques for determining fibre volume fraction requirements for varying types of synthetic fibres.
- Development of a stay-in-place formwork system that will become part of the steel-free bridge deck and eliminate the need for formwork removal.
- Investigation of impact and dynamic loading and their effect on the behaviour of the system.

9. REFERENCES

Ahmad, S.H., Zia, P., Yu, T.J., and Xie, Y. 1994. Punching shear tests of slabs reinforced with 3-D carbon fibre fabric. Concrete International, June: 36-41.

Alexander, J., and Cheng, J.R.R. 1996. Shear strengthening of small scale concrete beams with carbon fibre reinforced plastic sheets. Proceedings of the Canadian Society for Civil Engineering Annual Conference, Edmonton, Vol. IIA..: 167-177.

Azad, A.K., Baluch, M.H., Abbasi, M.S., and Kareem, K. 1994. Punching capacity of deck slabs in girder-slab bridges. ACI Structural Journal, **91**(6): 656-662.

Azizinamini, A., Kathol, S., and Beacham, M. 1996. Effect of cross frames on behaviour of steel girder bridges. Proceedings of the Fourth International Bridge Engineering Conference: 117-124.

Bakht, B. 1996. Revisiting arching in deck slabs. Canadian Journal of Civil Engineering, **23**(4): 973-981.

Bakht, B., and Agarwal, A.C. 1995. Deck slabs of skew girder bridges. Canadian Journal of Civil Engineering, **22**(3): 514-523.

Bakht, B., and Mufti, A.A., 1996. FRC deck slabs without tensile reinforcement. Concrete International, V. 18, No. 2, pp. 50-55.

Bakht, B., Al-Bazi, G., Banthia, N., Cheung, M., Erki, M-A., Faoro, M., Machida, A., Mufti, A.A., Neale, K.W., Tadros, G. 1996. Design provisions for fibre reinforced structures in the Canadian Highway Bridge Design Code. Proceeding of the Second International Conference on Advanced Composite Materials in Bridges and Structures. Montreal, pp. 391-406.

Bakht, B., Mufti, A.A., and Tadros, G. 1996. Providing transverse confinement in deck slabs. Proceedings of the Canadian Society for Civil Engineering Annual Conference, Edmonton, Vol. IIA.: 443-454.

Bakht, B., and Markovic, S. 1986. Accounting for internal arching in deck slab design. Journal of the Institute of Engineers, 67(CII): 18-25.

Bazant, Z.P., and Cao, Z. 1987. Size effect in punching failure of slabs. ACI Structural Journal, **84**(1): 44-53.

Beal , D.B. 1982. Load capacity of concrete bridge decks. ASCE Journal of the Structural Division, **108**(ST4): 814-832.

Bickley, J.A., Neale, K.W., and Fabbruzzo, G. 1993. Market Potential and Identification of Suppliers of Advanced Industrial Materials for Construction of Bridges and Other Structures. Industry Science and Technology Canada.

Demers, M., and Neale, K.W. 1994. Strengthening of concrete columns with unidirectional composite sheets. Developments in Short and Medium Span Bridge Engineering '94, Canadian Society for Civil Engineering: 895-905.

Den Hartog, J.P. 1952. Advanced Strength of Materials. McGraw-Hill Book Company. New York.

Dunker, K.F., and Rabbat, B.G. 1993. Why America's bridges are crumbling. Scientific American, March: 62-72.

Ebeido, T., and Kennedy, J.B. 1996. Punching strength of deck slabs of skew composite bridges. ASCE, Journal of Bridge Engineering, **1**(2): 59-66.

Ehlen, M.A., and Marshall, H.E. 1996. The Economics of New-Technology Materials: a Case Study of FRP Bridge Decking. National Institute of Standards and Technology, Gaithersburg, MD, USA. NISTIR 5864.

Fang, I-K., Worley, J.A., Burns, N.H., and Klinger, R.E. 1986. Behaviour of Ontario-type bridge decks on steel girders. Research Report 350-1, Center for Transportation Research, the University of Texas at Austin.

Gardner, N.J. 1990. Relationship of the punching shear capacity of reinforced concrete slabs with concrete strength. ACI Structural Journal, **87**(1): 66-71.

Ghoneim, M.G., and MacGregor, J.G. 1994. Prediction of the ultimate strength of reinforced concrete plates under combined inplane and lateral loads. ACI Structural Journal, **91**(6): 688-696.

Hannant, D.J. 1974. Nomograms for the failure of plain concrete subjected to short-term multi-axial stresses. The Structural Engineer, **52**(5): 151-165.

Hewitt, B.E., and Batchelor, B. 1975. Punching shear strength of restrained slabs. ASCE, Journal of the Structural Division, **101**(STP9): 1837-1853.

Jaeger, L.G., and Bakht, B. 1989. Bridge Analysis by Micro-Computer. McGraw-Hill Book Company. New York.

Jiang, D-H., and Shen, J-H. 1986. Strength of concrete slabs in punching shear. ASCE Journal of Structural Engineering. **112**(12): 2578-2591.

Kinnunen, S., and Nylander, H. 1960. Punching of concrete slabs without shear reinforcement. Transactions, Royal Institute of Technology, Stockholm, Sweden, No. 158.

Kuang, J.S., and Morley, C.T. 1992. Punching shear behaviour of restrained reinforced concrete slabs. ACI Structural Journal, **89**(1): 13-19.

MacGregor, J. 1992. Reinforced Concrete Mechanics and Design. Prentice Hall, New Jersey.

Maheu, J., and Bakht. B. 1993. A new connection between concrete barrier walls and bridge decks. Proceedings of the Canadian Society for Civil Engineering Annual Conference, Winnipeg, Vol. II, pp. 224-229.

Malvar, L.J. 1992. Punching shear failure of reinforced concrete pier deck model. ACI Structural Journal, **89**(5): 569-576.

Marzouk, H., and Hussein, A. 1991. Punching shear analysis of reinforced high-strength concrete slabs. Canadian Journal of Civil Engineering, **18**: 954-963.

Mufti, A.A., and Newhook, J.P. 1997. Punching shear strength of restrained concrete bridge deck slabs. Submitted to ACI Structural Journal.

Mufti, A.A., Bakht, B., Mahesparan, and Jaeger, L.G. 1992. User Manual for Computer Program SECAN Semi-Continuum Method of Analysis for Bridges. Ministry of Transportation of Ontario, Research and Development, Structures Office.

Mufti, A.A., Jaeger, L.G., Bakht, B., and Wegner, L.D. 1993. Experimental investigation of FRC deck slabs without internal steel reinforcement. Canadian Journal of Civil Engineering, **20**(3): 398-406.

Newhook, J.P., and Mufti, A.A. 1996. A reinforcing steel-free concrete bridge deck for the Salmon River Bridge. Concrete International. 18(6): 30-34.

Newhook, J.P., and Mufti, A.A. 1995. Rational method for predicting the behaviour of laterally restrained concrete bridge decks without internal reinforcement. Proceedings of the Canadian Society for Civil Engineering Annual Conference, Ottawa, Vol. III, pp. 519-528.

Newhook, J.P., Mufti, A.A., and Wegner, L.D. 1995. Fibre reinforced concrete deck slabs without steel reinforcement: half-scale testing and mathematical formulation. Research Report No. 1-1995. Nova Scotia CAD/CAM Centre. Nova Scotia, Canada.

Newhook, J.P., Mufti, A.A., Jaeger, L.G., MacDonnell, R.E., and Hamilton, D. 1996. Steel-free concrete bridge deck - the Salmon River Project: design and construction. Proceedings of the Candian Society for Civil Engineering Annual Conference, Edmonton, Vol. IIA.: 203-214.

Ontario Highway Bridge Design Code (OHBDC) Addendum. 1995. Ministry of Transportation of Ontario. Ontario, Canada.

Regan, P.E. 1974. Design for punching shear. The Structural Engineer, **52**(6): 197-207.

Selvadurai, A.P.S., and Bakht, B. 1995. Simulation of rolling wheel loads on an FRC deck slab. Proceedings, 2nd University-Industry Workshop on FRC, Toronto, pp. 273-287.

Shehata, I. 1990. Simplified model for estimating the punching resistance of reinforced concrete slabs. Materials and Structures, **23**: 364-371.

Siao, W.B. 1994. Punching shear resistance of flat slabs: a beam-strip analogy. ACI Structural Journal, **91**(5):594-604.

Stallings, J.M., Cousins, T.E., and Stafford, T.E. 1996. Effects of removing diaphragms from a steel girder bridge. Transportation Research Board. 75th Annual Meeting, Preprint 960985.

Taylor, R., and Hayes, B. 1965. Some tests on the effect of edge restraint on punching shear in reinforced concrete slabs. Magazine of Concrete Research, **17**(50): 39-44.

Thorburn, J., and Mufti, A.A. 1995. Full-scale testing of externally reinforced FRC bridge decks on steel girders. Proceedings of the Canadian Society for Civil Engineering Annual Conference, Ottawa, Vol. II, pp. 543-552.

Wegner, L.D. 1993. Optimization of externally-reinforced FRC bridge decks on steel girders. Innovative Structural Technologies, Term Report. Massachusetts Institute of Technology, personal correspondence.

Wegner, L.D. 1992. An experimental and analytical investigation of the failure behaviour of fibre-reinforced concrete deck slabs without steel reinforcement. Master of Applied Science Thesis, Technical University of Nova Scotia. Halifax, Canada.

Wegner, L.D., and Mufti, A.A. 1994a. Finite element investigation of fibre-reinforced concrete deck slabs without internal steel reinforcement. Canadian Journal of Civil Engineering, **21**(2): 231-236.

Wegner, L.D., and Mufti, A.A. 1994b. Optimization of externally-reinforced FRC bridge decks on steel girders. Proceedings of the Canadian Society for Civil Engineering Annual Conference, Winnipeg: 551-562.

Appendix I - Fortran Program for Rational Model Solution

Fortran Program to automate the solution of the rational model presented in Chapter 2.

```
C
C  PROGRAM TO CALCULATE PUNCH SHEAR AND SNAP-THROUGH LOADS
C
C
      WRITE(6,*) 'START CALCULATION'
      OPEN(70,FILE='FPSFST.DAT')
      OPEN(80,FILE='FPSFST.RES')
      OPEN(90,FILE='FPSFST.PLT')
      WRITE(6,*) 'READING DATA'
      READ(70,*) C,B,FPC,SK,SL,D,B1,CK,A,SNY,IU
C
C  IU=0, STRESS IN PSI ; IU=1, STRESS IN MPA
C
C  THE 'FCTF' STRESS IN 'PSI' USED IN K&N MODEL
C
      ICOUNT=0
      IF(IU.EQ.1) FPC1=145.*FPC
      IF(IU.EQ.0) FPC1=1000.*FPC
        FCB=FPC1/(.75+.000025*FPC1)
        FCTF=1007.+0.392*FCB
      IF(IU.EQ.0) FCTF=FCTF/1000.
      IF(IU.EQ.1) FCTF=FCTF/145.
      IF(IU.EQ.0) WRITE(80,*) 'UNITS ENGLISH KIPS, INCHES, SECONDS'
      IF(IU.EQ.1) WRITE(80,*) 'UNITS METRIC  KN, MM, SECOND'
      WRITE(80,*) 'Clear Span Between Girders=',C
      WRITE(80,*) 'Diameter of Equivalent Circle for Load=',B
      WRITE(80,*) 'Maximum Compressive Stress of Concrete=',FPC
      WRITE(80,*) 'Elastic Axial Stiffness of Strap=',SK
      WRITE(80,*) 'Strap to Load Spacing=',SL
      WRITE(80,*) 'Depth Of Slab=',D
      WRITE(80,*) 'Beta to Define Rectangular Stress Block=',B1
      WRITE(80,*) 'Concrete Constant used for confinement=',CK
      WRITE(80,*) 'AREA of Load Patch=',A
      WRITE(80,*) 'Yield strain=',SNY
      WRITE(80,*)' DELTA  ASI    Y     R4      W  ALPHA       P
     1  EPS   PFAIL    STRN'
      WRITE(90,1000) DELTA,ASI,Y,R4,W,ALPHA,P,EPS,PFAIL,STRN
      WRITE(80,1000) DELTA,ASI,Y,R4,W,ALPHA,P,EPS,PFAIL,STRN
      IPFAIL=0
      DELTA=0.
      Y=D/100.
```

```
      FACT3=.5*(C-B)
    1 CONTINUE
      DELTA=DELTA+D/350.
      ASI=2.*DELTA/C
      ITER=1
    2 CONTINUE
      FACT0=LOG(.5*C/(.5*B+Y))
      IF(FACT0.LE.0) WRITE(80,*) 'FACT0.LT.0 PROGRAM STOPPED'
      IF(FACT0.LE.0) WRITE(6,*) 'FINISH CALCULATION'
      IF(FACT0.LE.0) STOP
      SS=2.*SL
      SSDC=SS/C
      CTHS=1.-SSDC**2
      STRNB=ASI*(D-Y)/(.5*C)
      STRN=CTHS*STRNB
      R4=0.5*(Y**2)*(0.5*B/Y+1.)*FCTF*FACT0
      W1=0.5*C*SK*ASI*(D-Y)
      IF(STRN.GE.SNY) ICOUNT=ICOUNT+1
      IF(ICOUNT.EQ.1) WC=W1
      IF(ICOUNT.GT.1) W1=WC
      W=W1-R4
      C2=SK*ASI*(D-Y)/(.85*FPC)
      FACT1=D-0.333333*Y-.5*C2
      FACT2=D-.5*B1*Y-.5*C2
      FACT4=FACT3+ASI*FACT2
      FACT5=FACT2-ASI*FACT3
      FACT=((R4/W)*FACT1+FACT5)/FACT4
      IF(FACT.LE.0) WRITE(80,*)'FACT.LE.0 PROGRAM STOPPED'
      IF(FACT.LE.0) WRITE(6,*) 'FINISH CALCULATION'
      IF(FACT.LE.0) STOP
      ALPHA=ATAN(FACT)+ASI
      P=2.*3.14159*W*TAN(ALPHA-ASI)
      SIGMA1=P/A
C
C     RITCHART FAILURE CRITERIA FOR 3-D STRESSES IN CONCRETE
C
      SIGMA3C=FPC*(1.+CK*SIGMA1/FPC)
C
C     ADINA FAILURE CRITERIA FOR 3-D STRESSES IN CONCRETE
C
C     SIGMA3C=FPC*(1.+1.5*SIGMA1)
C     IF(IU.EQ.1) SIGMA1=.145*(P/A)
C     IF(IU.EQ.1) SIGMA3C=FPC*(1.+1.5*SIGMA1)
```

```
      C1=P/(.85*3.14159*B*SIN(ALPHA-ASI)*SIGMA3C)
      Y1=C1*COS(ALPHA-ASI)/B1
      EPS=ABS(Y-Y1)
      IF(EPS.EQ.0.) GO TO 3
      IF(ITER.EQ.1000) WRITE(80,*) 'Y=',Y,'Y1=',Y1
      IF(ITER.EQ.1000) WRITE(6,*) 'FINISH CALCULATION'
      IF(ITER.EQ.1000) STOP
      IF(EPS.GT..00001) Y=Y1
      ITER=ITER+1
      IF(EPS.GT..0001) GO TO 2
    3 ESTH=Y*ASI/(.5*B+Y)
      PFAIL=.002-ESTH
      IF(PFAIL.LE.0.) IPFAIL=IPFAIL+1
      IF(IU.EQ.1) W=W/1000.
      IF(IU.EQ.1) R4=R4/1000.
      IF(IU.EQ.1) P=P/1000.
      DEG=180./3.14159
      ASI=DEG*ASI
      ALPHA=DEG*ALPHA
      IF(IPFAIL.NE.1) GO TO 100
      DELTAP=(DELTAP*PFAIL-DELTA*PFAILP)/(PFAIL-PFAILP)
      ASIP=(ASIP*PFAIL-ASI*PFAILP)/(PFAIL-PFAILP)
      YP=(YP*PFAIL-Y*PFAILP)/(PFAIL-PFAILP)
      R4P=(R4P*PFAIL-R4*PFAILP)/(PFAIL-PFAILP)
      WP=(WP*PFAIL-W*PFAILP)/(PFAIL-PFAILP)
      ALPHAP=(ALPHAP*PFAIL-ALPHA*PFAILP)/(PFAIL-PFAILP)
      PP=(PP*PFAIL-P*PFAILP)/(PFAIL-PFAILP)
      EPSP=(EPSP*PFAIL-EPS*PFAILP)/(PFAIL-PFAILP)
      STRNP=(STRNP*PFAIL-STRN*PFAILP)/(PFAIL-PFAILP)
      PFAILP=0.
      WRITE(80,1000) DELTAP,ASIP,YP,R4P,WP,ALPHAP,PP,EPSP,PFAILP,STRNP
      WRITE(90,1000) DELTAP,ASIP,YP,R4P,WP,ALPHAP,PP,EPSP,PFAILP,STRNP
      WRITE(80,*)'*******  Punch Load-Strain in concrete=.002  *******'
      STOP
  100 CONTINUE
      WRITE(90,1000) DELTA,ASI,Y,R4,W,ALPHA,P,EPS,PFAIL,STRN
      WRITE(80,1000) DELTA,ASI,Y,R4,W,ALPHA,P,EPS,PFAIL,STRN
      IF(ICOUNT.GT.1) WRITE(80,*)'*******  Punch Load-Yield Strain
     1  in Strap  *******'
      IF(ICOUNT.GT.1) STOP
 1000 FORMAT(1X,F5.2,1X,F5.2,1X,F5.2,2F8.2,F8.2,1X,F8.2,1X,F8.5,2(1X,F8.
     *6))
      DELTAP=DELTA
```

```
ASIP=ASI
YP=Y
R4P=R4
WP=W
ALPHAP=ALPHA
PP=P
EPSP=EPS
STRNP=STRN
PFAILP=PFAIL
write(6,*)' STILL COMPUTING AT DELTA=',DELTA,'ITERATION=',ITER
IF(DELTA.LE.D) GO TO 1
WRITE(6,*) 'FINISH CALCULATION'
STOP
END
```

Sample input data file

2000. 477.5 35. 190. 0. 175. .81 10. 125000. 0.0015 1

Sample output file

UNITS METRIC KN, MM, SECOND
Clear Span Between Girders= 2000.00
Diameter of Equivalent Circle for Load= 477.500
Maximum Compressive Stress of Concrete= 35.0000
Elastic Axial Stiffness of Strap= 190.000
Strap to Load Spacing= 0.000000
Depth Of Slab= 175.000
Beta to Define Rectangular Stress Block= 0.810000
Concrete Constant used for confinement= 10.0000
AREA of Load Patch= 125000.
Yield strain= 0.150000E-02

Δ	ψ	Y	R4	W	α	P	ϵ	PFAIL	STRN
0.00	0.00	0.00	0.00	0.00	0.00	0.00	0.00000	0.000000	0.000000
0.50	0.03	1.66	6.42	10.05	20.54	23.63	0.00007	0.001997	0.000087
1.00	0.06	3.19	12.36	20.29	20.12	46.54	0.00008	0.001987	0.000172
1.50	0.09	4.61	17.89	30.67	19.74	68.81	0.00007	0.001972	0.000256
2.00	0.11	5.93	23.07	41.17	19.39	90.47	0.00007	0.001952	0.000338
2.50	0.14	7.17	27.94	51.78	19.08	111.60	0.00007	0.001927	0.000420
3.00	0.17	8.34	32.53	62.46	18.79	132.21	0.00007	0.001899	0.000500
3.50	0.20	9.44	36.88	73.22	18.52	152.35	0.00009	0.001867	0.000579
4.00	0.23	10.48	41.00	84.03	18.28	172.04	0.00010	0.001832	0.000658
4.50	0.26	11.47	44.93	94.88	18.05	191.31	0.00007	0.001794	0.000736
5.00	0.29	12.42	48.68	105.77	17.84	210.17	0.00010	0.001753	0.000813
5.50	0.32	13.32	52.27	116.69	17.64	228.66	0.00007	0.001709	0.000889
6.00	0.34	14.18	55.70	127.63	17.45	246.78	0.00010	0.001664	0.000965
6.50	0.37	15.01	59.00	138.58	17.27	264.56	0.00008	0.001616	0.001040
7.00	0.40	15.81	62.18	149.55	17.11	281.99	0.00006	0.001565	0.001114
7.50	0.43	16.57	65.25	160.52	16.95	299.11	0.00009	0.001513	0.001188
8.00	0.46	17.31	68.20	171.49	16.80	315.91	0.00007	0.001459	0.001262
8.50	0.49	18.02	71.06	182.46	16.66	332.41	0.00005	0.001403	0.001334
9.00	0.52	18.71	73.83	193.42	16.52	348.61	0.00010	0.001346	0.001407
9.50	0.54	19.38	76.52	204.38	16.39	364.53	0.00008	0.001287	0.001478
10.0	0.57	20.08	79.35	216.33	16.26	381.70	0.00004	0.001224	0.001549

******* Punch Load-Yield Strain in Strap *******

IMAGE EVALUATION TEST TARGET (QA-3)

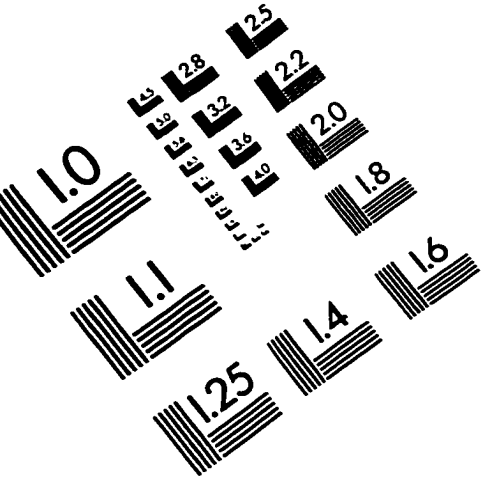

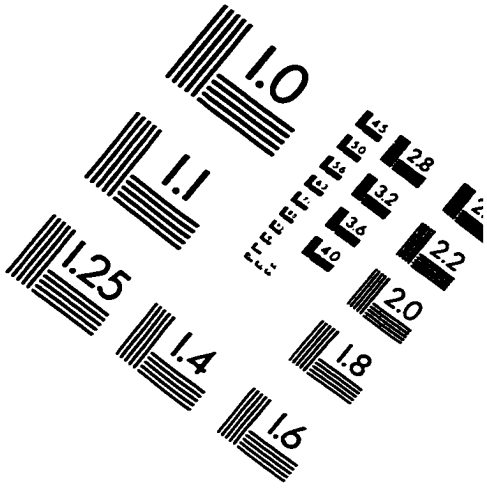

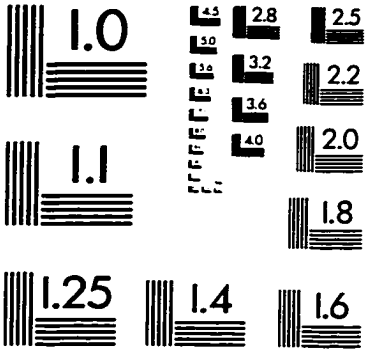

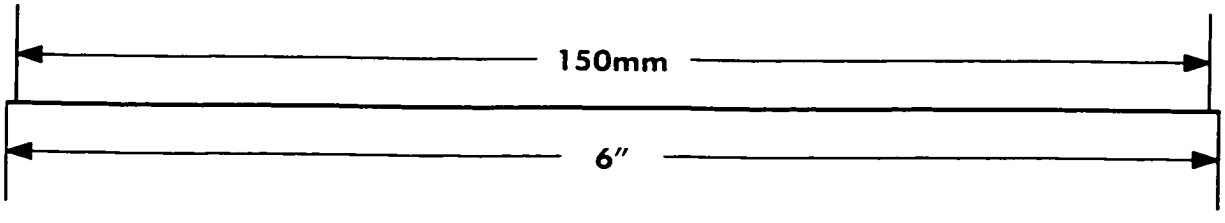

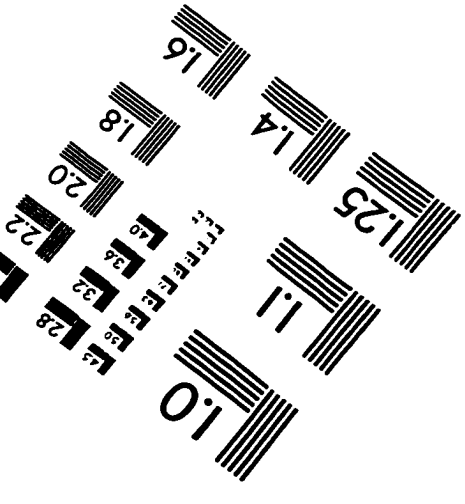

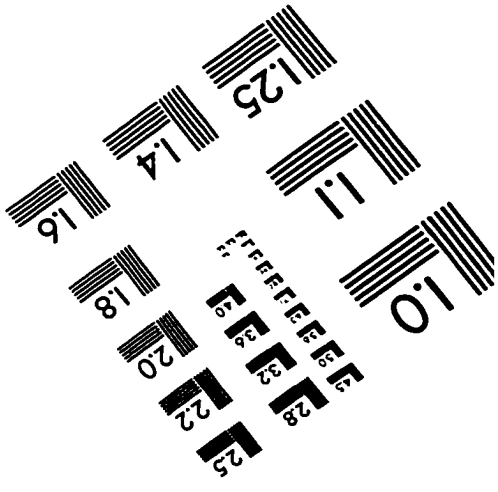

APPLIED IMAGE, Inc
1653 East Main Street
Rochester, NY 14609 USA
Phone: 716/482-0300
Fax: 716/288-5989